



TALLINN UNIVERSITY OF TECHNOLOGY

SCHOOL OF ENGINEERING

Department of Electrical Power Engineering and Mechatronics

**DEVELOPMENT OF TEST BENCH FOR
PROPULSION MOTOR OF SELF-DRIVING CAR
ISEAUTO**

**ISEJUHTIVA SÕIDUKI ISEAUTO VEOMOOTORI
KATSESTENDI VÄLJATÖÖTAMINE**

MASTER THESIS

Üliõpilane: Ihsan Ata Durgun

Üliõpilaskood: 184503MAHM

Juhendaja: Prof. Anton Rassõlkin

Tallinn 2020

AUTHOR'S DECLARATION

Hereby I declare, that I have written this thesis independently.

No academic degree has been applied for based on this material. All works, major viewpoints and data of the other authors used in this thesis have been referenced.

"....." 20.....

Author:

/signature /

Thesis is in accordance with terms and requirements

"....." 20....

Supervisor:

/signature/

Accepted for defense

"....."20... .

Chairman of theses defence commission: Prof. Mart Tamre

/name and signature/

Non-exclusive Licence for Publication and Reproduction of Graduation Thesis¹

I, Ihsan Ata Durgun (name of the author) (date of birth: 27.07.1994) hereby

1. grant Tallinn University of Technology (TalTech) a non-exclusive license for my thesis Development of Test Bench for Propulsion Drive of Self-Driving Car ISEAUTO,

(title of the graduation thesis)

supervised by

Prof. Anton Rassõlkin,

(Supervisor's name)

1.1 reproduced for the purposes of preservation and electronic publication, incl. to be entered in the digital collection of TalTech library until expiry of the term of copyright;

1.2 published via the web of TalTech, incl. to be entered in the digital collection of TalTech library until expiry of the term of copyright.

1.3 I am aware that the author also retains the rights specified in clause 1 of this license.

2. I confirm that granting the non-exclusive license does not infringe third persons' intellectual property rights, the rights arising from the Personal Data Protection Act or rights arising from other legislation.

¹ *Non-exclusive Licence for Publication and Reproduction of Graduation Thesis is not valid during the validity period of restriction on access, except the university's right to reproduce the thesis only for preservation purposes.*

_____ *(signature)*

_____ *(date)*

Department of Electrical Power Engineering and Mechatronics

THESIS TASK

Student: Ihsan Ata Durgun 184503MAHM (name, student code)

Study programme, MAHM, Mechatronics Master (code and title)

main speciality:

Supervisor(s): Professor Anton Rassõlkin, 620 3305 (position, name, phone)

Thesis topic:

(in English) Development of Test Bench for Propulsion Motor of Self-Driving Car

ISEAUTO

(in Estonian) Isejuhtiva Sõiduki ISEAUTO Veomootori Katsesendi Väljtöötamine

Thesis main objectives:

1. Mounting the electric motor on test bench.
2. Manufacturing the resolver.
3. Designing/selecting clutch.
4. Performing tests on the electric motor.
5. Designing/selecting gear system.

Thesis tasks and time schedule:

No	Task description	Deadline
1.	Understanding the problem.	30.09.2019
2.	Reorganizing the laboratory and the test bench for the motor and test equipments	01.10.2019
3.	Designing mounting parts.	14.10.2019
4.	Manufacturing mounting parts with 3D printer to check their dimensions.	21.10.2019
5.	Preparing technical drawings to manufacture mounting parts.	23.10.2019
6.	Manufacturing mounting parts.	05.11.2019
7.	Designing Clutch.	25.01.2020
8.	Performing Tests.	28.02.2020
9.	Selecting/Designing Gear System.	31.03.2020

Language: English **Deadline for submission of thesis:** ".....".....201....a

Student: Ihsan Ata Durgun ".....".....201....a

/signature/

Supervisor: Prof. Anton Rassõlkin "....."201....a
/signature/

Head of study programme: Prof. Mart Tamre "....."201.a
/signature/

Terms of thesis closed defence and/or restricted access conditions to be formulated on the reverse side

CONTENTS

PREFACE	9
List of abbreviations and symbols	10
1.Introduction to Background.....	11
2.1. Literature Review	14
2. Literature Review.....	14
2.1.1.Test Benches	14
2.1.2.Reduction Gearbox	16
2.1.3.Gear Types.....	16
2.1.4.Gearbox Types of EVs.....	16
2.1.5.Original RG of the EM	17
2.1.6.The Parameter Effect Gear Ratio	18
2.1.7.Clutches.....	20
2.2.Comparison of ISEAUTO and Similar SDCs	20
2.3.Methodology	21
2.3.1.Problems to Solve	21
2.3.2.Solution Methods	22
3.TEST BENCH	25
3.1.Torsional Vibrations of a Shaft System with Parallel Misalignment	25
3.2.Designing Mounting Parts.....	29
3.2.1.Rear Mounting Part.....	29
3.2.2.Front Mounting Part.....	30
3.3.Manufacturing Operation of the Resolver.....	30
4.Reduction Gearbox.....	32
4.1. Selecting Design Parameters	32
4.2.Designing the RG	33
4.3.Stress Analyses of the Designed Parts	42
4.3.1.Stress Analyses of the Designed Pinions/Gears	42
4.3.2.Stress Analyses of the Designed Shafts.....	43
5.Efficiency of the RG.....	44
5.1.Power Losses of an RG.....	44
5.1.1.Tooth Friction Losses	44
5.1.2.Bearing Losses.....	47
5.1.3.Lubricant Losses	54
5.1.4.Shaft Sealing Losses.....	55
5.1.5.Total Losses of a Triple-stage RG Losses	55
6.Clutche.....	59

7. Conclusion	60
LIST OF REFERENCES	64
APPENDICES	67
A.1.The Solid Model and the Actual Rear Mounting Part	67
A.2.Stress Analysis of Rear Mounting Part.....	68
A.3.Safety Analysis of Rear Mounting Part	69
A.4.The Solid Model and the Actual Front Mounting Part	70
A.5.Stress Analysis of Front Mounting Part.....	71
A.6.Safety Analysis of Front Mounting Part	72
A.7.The Solid Model and the Manufactured Resolver.....	73
A.8.BOM Drawing of the Rear Mounting Part	74
A.9.Assemble Drawing of the Rear Mounting Part	75
A.10.Technical Drawing of Rear Mounting Part	76
A.11.Technical Drawing of the Support Rib for Rear Mounting Part.....	77
A.12.Technical Drawing of the Bottom Plate of Rear Mounting Part	78
A.13.Technical Drawing of the Plate for Mounting Rear Mounting Part on TB	79
A.14.Technical Drawing of the Upper Plate of Rear Mounting Part	80
A.15.BOM Drawing of Front Mounting Part	81
A.16.Assemble Drawing of the Front Mounting Part.....	82
A.17.Technical Drawing of Front Mounting Part.....	83
A.18.Technical Drawing of the Front Plate Front Mounting Part	84
A.19.Technical Drawing of Bottom Plate of Front Mounting Part	85
A.20.Technical Drawing of First Support Rib of Front Mounting Part	86
A.21.Technical Drawing of Second Support Rib of Front Mounting Part	87
A.22.Technical Drawing of the Plate for Mounting Front Mounting Part on TB.....	88
A.23.Tables for Pinion and Gear Design	89
A.24.BOM Drawing of the RG	97
A.25.Technical Drawing of Right Body Part of the RG Page-1/3.....	98
A.26.Technical Drawing of Right Body Part of the RG Page-2/3.....	99
A.27.Technical Drawing of Right Body Part of the RG Page-3/3.....	100
A.28.Technical Drawing of Left Body Part of the RG Page-1/3.....	101
A.29.Technical Drawing of Left Body Part of the RG Page-2/3.....	102
A.30.Technical Drawing of Left Body Part of the RG Page-3/3.....	103
A.31.Technical Drawing of the First Pinion	104
A.32.Technical Drawing of the First Gear	105
A.33.Technical Drawing of the Second Gear	106
A.34.Technical Drawing of the Second Gear	107
A.35.Technical Drawing of the Third Pinion	108

A.36. Technical Drawing of the Second Gear	109
A.37. Technical Drawing of the First Shaft	110
A.38. Technical Drawing of Second Shaft	111
A.39. Technical Drawing of the Third Shaft	112
A.40. Technical Drawing of the Fourth Shaft	113
A.41. BOM Drawing of the RG	114
A.42. Stress Analyses of the First Pinion	115
A.43. Safety Analyses of the First Pinion	116
A.44. Stress Analyses of the First Gear	117
A.45. Safety Analyses of the First Gear	118
A.46. Stress Analyses of the Second Pinion	119
A.47. Safety Analyses of the Second Pinion	120
A.48. Stress Analyses of the Second Gear	121
A.49. Safety Analyses of the Second Gear	122
A.50. Stress Analyses of the Third Pinion	123
A.51. Safety Analyses of the Third Pinion	124
A.52. Stress Analyses of the Third Gear	125
A.53. Safety Analyses of the Third Pinion	126
A.54. Stress Analyses of the First Shaft	127
A.55. Safety Analyses of the First Shaft	128
A.56. Stress Analyses of the Second Shaft	129
A.57. Safety Analyses of the Second Shaft	130
A.58. Stress Analyses of the Third Shaft	131
A.59. Safety Analyses of the Third Shaft	132
A.60. Stress Analyses of the Fourth Shaft	133
A.61. Safety Analyses of the Fourth Shaft	134
A.62. Parameters of the First Gear Pair	135
A.63. Parameters of the Second Gear Pair	138
A.64. Parameters of the Third Gear Pair	141
A.65. Sommerfeld number – Coefficient of Friction Graph	144
A.66. Graphs, Tables, and Parameter Calculations for RG Efficiency Calculation	145
A.67. 3D-Model of the Clutch system	150
A.68. Photograph of the TB	151

PREFACE

The motivation of this thesis is Estonia's first self-driving car ISEAUTO. ISEAUTO is a self-driving car with 6 people maximum capacity. The purpose behind this design is to manufacture a driverless bus for transportation in the campus. Prof. Raivo Sell is the head of the project and the thesis is supervised by Prof. Anton Rassõlkin. ISEAUTO is powered by an electric motor like other self-driving cars. Mitsubishi's i-Miev electric car's electric motor is used to power ISEAUTO. A test bench is required for the motor to optimize the electric motor for ISEAUTO. The electric motor needs to be optimized because it was designed for a different vehicle and it was optimized due to the specifications of that car. It should be reoptimized due to ISEAUTO's specifications to run more efficiently. There are pre-made test benches on the market, but they are not suitable for this electric motor. There are two main reasons that a new test bench should design for the electric motor. The first one is mounting the electric motor on test bench. It does not have mounting locations for the test bench like industrial type electric motors. Test benches on the market are ideal for testing and tuning industrial electric drives. Industrial electric motors have test bench mounting locations under the motor and their bottom surface is straight which is suitable for pre-made test benches. Those electric motors reoptimized due to changes of the manufacturing process. On the other hand, this electric motor is designed for a vehicle. Electric motors for vehicles do not have standards and universal mounting locations for universal test benches. Commonly, the electric motor of a vehicle needed to tune for one time because it is not usual to disassemble it and use it on a different vehicle. The optimization of these electric motors is done by the company and they design test benches for those kinds of electric motors. Also, the bottom surface of the electric motor is circular, and it is not suitable for universal test benches. The second one is the rotor angle. The rotor of the electric motor should be parallel to the load motor, but the shape of the electric motor is circular, and it is not suitable to mount on universal test benches with correct angle. Moreover, there are four sub-objectives under the main objective to accomplish the thesis. They are mounting the electric motor on the test bench, manufacturing the resolver of the electric motor, designing/selecting a suitable clutch for the electric motor, and designing/selecting a new gear mechanism for the electric motor. These are necessary to run the electric motor on the test bench.

List of abbreviations and symbols

EV Electric vehicles

SDC Self-driving car

RG Reduction gearbox

EM Electric motor

TB Test bench

m Meter

mm Millimeter

s Second

min Minute

rad Radian

rev Revolution

deg Degree

W Watt

kW Kilowatt

N Newton

rpm Round per minute

MPa Megapascal

1. INTRODUCTION

The autonomous car has been in the headlines for a decade and continues to dominate auto headlines. The autonomous car has attracted the researchers, robotics communities and the automobile industries [1]. Currently, almost all car manufacturer brands and universities are designing their own self-driving cars (SDC). Also, TaiTech is designing its own SDC like other universities. The first generation of the SDC is already designed and working. Now, they are designing the second generation of it with better efficiency. For better efficiency, the optimization of the electric motor is required, and it needs a test bench (TB) to optimize it. "The Mitsubishi i-MiEV platform was used to test the software developed for object recognition and tune the controller used for propulsion. The propulsion system of Mitsubishi i-MiEV, designed as highway-capable mass production electric car, requires significant optimization. The size and parameters of the propulsion system should be verified and optimized, to provide a more stable and effective platform for future development steps of the project" [2].

The story of the driverless car is almost as old as the car itself [3]. It started with General Motors Highways and Horizons Futurama exhibition at New York in 1939. During 90s National Automated Highway System Research Program designed approach such as Personal Rapid Transport and Automated People Mover systems. In those systems vehicles would run without a driver on a special road which is designed for the vehicle. This special road designed to keep the vehicle on the road and run. Also, there would be special terminals for boarding and get off. This idea is like tram transportation without a driver. Today, there are some applications of those ideas such as airport shuttles and autonomous metros. SDC have a quite old history but they did not develop until the last decade. The main reason is the technology was not ready to develop controlled environments. In the beginning of the new millennium computer and network technologies opened the way of developing SDC. U.S. military organized several competitions for developing a SDC in 2004, 2005, and 2007. These competitions effected the industry and commercial companies started to build their own SDC.

Cars are a crucial part of modern human life. Cars shorten the traveling time from one place to another in a magnificent amount. Everyday millions of people are using them to go work. Unfortunately, traffic jams and car accidents are happening because of human failures. SDC can avoid those problems. SDC compared to ordinary vehicles, these vehicles are equipped with several extra sensors to compensate for a driver's requirement. Also, they can communicate by the help of these sensors. In that way, they can avoid car crashes and traffic jams. Another important problem caused by

normal cars is fossil fuel consumption. Fossil fuels are limited and one day humanity will run out of fossil fuels. Moreover, fossil fuel consumption causes carbon gas emissions. On the other hand, all SDC run by electric motor (EM) which is carbon gas emission free.

ISEAUTO is a first Estonian self-driving car developed in cooperation between TalTech and Silberauto AS. ISEAUTO is designed to serve as a bus in the campus. It's designed to travel around 10-20 km/h. The bus has 6 people maximum capacity. Nowadays, the second version of ISEAUTO is developing. New generation of it planned to be more efficient. In the first generation of it the EM used without tuning process, and the original RG of the EM used on it which is not optimal for ISEAUTO. A TB should be developed for the EM to optimized it for ISEAUTO. TB will be used for testing and tuning the EM. Test results will be used for tuning the EM due ISEAUTO's specifications. Furthermore, three more tasks should be done to develop a fully operating TB for the EM. They are, mounting the electric motor on the TB, manufacturing the resolver of the electric motor, designing/selecting a suitable clutch for the electric motor [4].

TB consist of measurement devices and the motor itself. The main purpose of the TB is to perform tests on the motor when it is assembled on it and support all other devices to perform tests. Also, it should handle the forces occur during performing test. These forces are the static forces caused by the weight of the equipment, and dynamic forces created by motor. Due to the, big forces applied on the TB it should designed rigidly. Moreover, during performing test vibration occurs by the motor. The TB should absorb vibrations. Otherwise, vibrations will cause noises on the test results. Also, the measurement equipment should be isolated from vibrations to avoid noises. That is why both the equipment and the motor should mount on the TB with anti-vibration mounting. Furthermore, the TB should satisfy job safety rules to protect the person who performs test on the TB. On the TB leak test, no load test, locked rotor test, temperature rise test, losses measurement test, torque speed characteristics test, current speed characteristics test, etc. can be performed. The motor efficiency can be increased by using the data obtained from those tests. Motor efficiency effects the lifetime of the motor. Lower efficiency motors have shorter lifetime than higher efficiency motors. For this reason, accurate testing is compulsory, and it can be achieved by developing a TB which satisfy these criterions [5].

There are pre-made universal TB on the market, but they are not suitable for i-Miev's EM. There are two main reasons why they are not suitable for the EM. The first one is the EM does not have TB mounting locations and flat bottom surface like industrial EMs.

Industrial EMs have regular shape such as flat bottom surface, and they have mounting locations for universal TBs on the bottom part. The reason why industrial EMs have regular shape and mounting location is they require preoptimization due to manufacturing plan changes. However, the EMs for vehicles have irregular shape and they do not have mounting locations. Also, the EM has circular body which is not suitable for universal TB. The second reason is the rotor angle. The rotor angle should be parallel to the load motor. Due to its circular body it cannot be assembled on the universal TB with correct rotor angle.

Mounting of the EM on the TB is compulsory to test the EM. Only holding stable the EM on the TB is not enough. Mounting parts should keep the EM on the TB with the correct rotor angle and they should protect the EM against vibrations. Otherwise, test result will not be accurate.

The EM cannot run without its resolver. The genuine resolver of the EM is missing and without it the EM cannot operate. EMs require a resolver to detect pole position of the electric motor and accurate rotational speed. The resolver is vital to run the EM and it should be manufactured and assembled on the EM.

A clutch is needed to connect the EM with a load motor to test it. On the TB the EM will relate to a load motor to perform load tests on it. The connection between the EM and the load motor is needed a clutch and belt connection. The load motor has its own clutch ready, but the EM does not have one. Firstly, the market will be searched to find a suitable clutch for the EM's rotor. If there is no suitable one in the market, then a suitable one will be designed.

A reduction gearbox (RG) is a device that allows the input speed to be lowered with the same or more output torque for a slower output speed requirement. The configuration of reduction gear consists of a series of rotating gears attached to an output shaft. The incoming high-speed movement from the wheel work is transmitted to the array of rotating gears in which the force or torque is modified. The number of gears used to mount the reduction gear depends on the application's speed specification. The reduction may have a single or two-stage reduction depending on the output speed required. The most critical sub-topic of the thesis is a new RG for the EM. RG is the key point to increase the efficiency of the EM. A new RG is needed to run the EM efficiently on ISEAUTO. The reason is I-Miev was designed to travel at max. 130km/h speed. On the other hand, ISEAUTO was designed to travel at max. 20km/h speed.

2. Literature Review

The purpose of this chapter to define problems, challenges, and methodology. Also, it includes information about theories, and topics are going to use to solve the problems. Moreover, it explains similar projects are done before, and why not other methodologies are not suitable. In section 2.1. is a short summary of the topic and supportive theories. Section 2.2. includes information about similar projects like ISEAUTO.

2.1. Overview

The aim of this chapter is giving an overview and summary of the topic. All information used in the thesis shortly explained under subtopics. Also, it provides references for important theories and to delineate terms. In section 2.1.1. TB is defined, and it explains why universal TBs are not suitable for the EM. In section 2.1.2. RG types, in section 2.1.3. gear types, and in section 2.1.4. gearbox types of electric vehicles (EV) are explained. Section 2.1.5. gives information about the original RG of the EM and explains its design by using the information in sections 2.1.2., 2.1.3., and 2.1.4. In section 2.1.6. the parameters effect the gear ratio of an RG are defined. The last section different types of clutches are explained.

2.1.1. Test Benches

TB is a rigid structure to hold together measurement & test devices, load motor, motor controller, and the test motor. Furthermore, it prevents all equipment from vibrations to avoid noises on test results. It should be rigid because both static and dynamic forces applied on the TB is high and it should have capable to handle it. The purpose of the TB is to perform tests on motors such as, the TB leak test, no load test, locked rotor test, temperature rise test, losses measurement test, torque speed characteristics test, current speed characteristics test, etc. These test results can be used to verify ideas, for tuning, or to optimize the EM for higher operating efficiency.

Universal test bench is a pre-made TB for EM by commercial companies. Mostly they used for industrial drives in manufacturing facilities for tuning operations. An EM should be tuned for better working efficiency. In this way, they play an influential role for decreasing energy consumption. They designed due to standards to increase the suitability of the TB for higher number of EMs. Mounting connections locations and dimensions are matching with industrial type EMs. One universal TB can be used for more than one EM [6], [21].

Custom Test Bench is designed for a single EM. They needed when the EM is not suitable to mount on universal TBs. This problem can be caused by the body shape of the EM, unmatched mounting connections or missing mounting locations [6], [21].

Comparison of Universal and Custom Test Bench Universal TBs are more practical compared to custom ones. There are many companies on the market is selling pre-made ones. On the other hand, custom TBs are having to be designed and manufactured. Universal TBs are more economical compared to custom TBs. In conclusion, due to being economical and less time-consuming universal TBs are better option against custom TBs. Custom test benches should be used in cases which the EM is not suitable to test on a universal TB.

Why I-Miev's EM is not suitable to test on universal test benches? Industrial EMs and EMs for vehicles are very similar in working principle but they have quite different body shape. Industrial EMs are designed to use in manufacturing processes such as running a conveyor belts, robots, CNC machines, etc. Their shapes are designed due to standards to increase the number of applicable tasks. They should be optimized for the tasks they are going to process. Otherwise, they will not work with their maximum efficiency and will increase electricity consumption cost. This is the main reason why universal TBs are designed for industrial type EMs. For example: the same EM can be used to run a conveyor belt, or a robot arm but both tasks require different optimization because their working speed, load, duty cycle, etc. are different. However, EMs for vehicles are designed for a single purpose which is running the vehicle. They are already optimized for the vehicle which they are going to use on. Also, their shapes are designed due to decrease the volume. In other words, their suitability for other applications is not a design criterion. Unmatched mounting locations is not the only reason why universal TBs are not suitable the EM. Also, its body shape is not suitable to perform test with correct rotor angle. The bottom surface of the EM is circular, and it has smaller diameter on the rear side and the diameter increases from the rear face to the front face. When it stays on a flat surface its rotor stays with an angle to the surface. It should stay parallel to the surface like the load motor. Otherwise, vibrations will cause noise on the test result.



Fig.1: I-Miev's EM on the TB.

2.1.2. Reduction Gearbox

Reduction gearbox is an instrument lowers the input speed of the motor with maintaining the same output torque. In RG, the gears connected to an output shaft. The high speed coming from the motor is transmitted to the rotating gears where the torque or motion is changed [8]. Reduction gearbox types:

Single stage reduction gearbox is made up of just one pair of gears. The incoming shaft of the engine drives a small gear known as a pinion. The velocity is adjusted by making the velocity reduction ratio proportional to the pinion and gear diameter. Usually single stage RGs have small gear ratios [8].

Double stage reduction gearbox is commonly used in very high-speed applications. The pinion is attached to the first reduction gear, an intermediate gear. Instead, with the aid of another shaft, the first reduction gear is attached to a low speed pinion. This pinion is connected directly on the propeller shaft to the second reduction gear. Usually double stage RGs have higher gear ratios than single stage RGs [8].

2.1.3. Gear Types

A gear is a rotating machine part having cut teeth, which mesh with another toothed part to transmit torque [8]. Gears are mounted on rotatable shafts and the teeth are mounted on another shaft to match. Gears transmit torque and motion from one part of a machine to another [9]. Gear types:

Spur gear the most frequently used spur gears. The teeth are aligned in parallel direction to the gear axis. A spur gear is designed for meshing on a parallel shaft with another spur gear. Only radial loads on gear shafts are imposed by spur gears. Due to the tendency to maximize rolling and minimize sliding, the shape is easy to manufacture and is an efficient way to transmit power between two gear teeth. Spur gear efficiency is around 90 percent [9].

Helical gear is like spur gears except for the positioning of the teeth at an angle to the rotational gear axis. This angle, called helix angle. Helical gears are stronger than comparable size spur gears and operate more quietly. Efficiency of helical gears are less than spur gears [9].

Bevel gear is like spur gears, except for the conical shape. Bevel gears are used for the transfer of motion between two non-parallel shafts. Two shafts that are connected by bevel gears at an angle of 90 °. Bevel gears work around 90% efficiency [9].

2.1.4. Gearbox Types of EVs

Transmission is a key component in vehicles, its main function is to transmit power from the engine to the wheels, it converts torque and engine speed so that the vehicle

performance requisites are achieved [10].

Single speed transmission Single speed transmission is the most used mechanism for both the simplicity of the design and the impressive performance of the EM over combustion engines. High torque and the ability to deliver constant power within a wide range of speeds. For its price, it ensures great driving performance [10].

Two speed transmission Two speed transmission ensures higher wheel torque at low revolution per minute than single speed transmission. EM torque is decreases with the size of the motor. Also, acceleration and gradeability increases. Moreover, the second gear provides a higher top speed. On the other hand, two speed transmissions are more expensive than single speed transmissions [10].

Continuously variable transmission Continuously variable transmissions have infinite number of gear ratios and the rare opportunity to change gear ratios without interrupting power flow. There are two variable pulleys connected with a belt. The gear ratio varies with the shift of pulley diameter. It allows the best possible speed across the entire driving range of the motor. This process increases the motor performance and efficiency. On the contrary, their design and manufacturing costs a lot and they are heavier than single/two speed transmissions [10].

2.1.5. The Original RG of the EM

It is a double stage type RG, so it consists of 4 gears. First gear is connected to the rotor of the EM. It is the biggest gear in the RG. Its diameter is 65mm, its width is 23,2 mm and it has 65 teeth. The second gear is the pinion gear of the first stage which is connect to the rotor. Its diameter is 55,9 mm, its width is 32.8 mm and it has 18 teeth. The third of is the connected to the pinion gear of the first stage (2nd gear). Its diameter is 93,9 mm, its width is 25,5 mm and it has 42 teeth. The last (4th gear) is the pinion gear of the second shaft which is connected to the drive shaft. Its diameter is 58.8 mm, its width is 27 mm and it has 25 teeth. All these measurements done by hand because the CAD file of the RG is impossible to find. The company does not share its CAD file to protect the privacy of their design. Gear ratio of the RG can be calculated by using the measurement mentioned above. Formula 2.1 for calculating gear ratio:

$$n = \frac{n_3}{n_4} * \frac{n_1}{n_2} \quad (2.1)$$

where n – gear ratio, constant,

n_1 – the number of teeth of 1st gear, constant,

n_2 – the number of teeth of 2nd gear, constant,

n_3 – the number of teeth of 3rd gear, constant

n_4 - the number of teeth of 4th gear, constant

As mentioned in the first paragraph teeth numbers of all gears are measured. The gear ratio of the RG can be calculated by using formula 1.11:

$$n = \frac{42}{25} * \frac{65}{18} = 6,066$$

The gear ratio of the RG is calculated 6.066 and it matches with the value is written on RG's user manual.

The general dimensions of the RG in length is 397 mm, in width is 300 mm, and in height is 300 mm. The total weight of RG is 19,3kg [11].

They used helical type gears on the RG. As mentioned before (Section 2.1.3.) spur gears work at higher efficiency than helical gears, but they used helical gears instead of spur gears. The reason is spur gears are not suitable for comfort driving because they cause a lot of vibrations and noise. Moreover, they are not good at working at high speeds. On the other hand, helical gears work quieter than spur gears and they vibrate less than spur gears. Furthermore, they are good at working at high speeds.

The working mechanism and design of the RG is simple just like other EVs gearboxes. It has only one gear selection which makes it single speed transmission type (Section 2.1.4.). The RG has three different working options. These are selector B, D, and C. The selector B is for downhill driving. It increases the regenerative braking to reduce the speed during going down from a hill. Selector D is for city driving. It has standard regenerative braking. Selector C is for comfortable driving. It has fewer regenerative braking for comfortable driving. Also, it works automatic and without a clutch. Furthermore, the RD locks the wheels in P mode by locking the park pinion [11].



Fig.2: The original RG of the EM.

2.1.6. The Parameters Effect Gear Ratio

Gear ratio depends on the maximum speed, the wheel radius, and the maximum motor speed, and the traction power between the road and the tires. A smaller motor speed

relative to the vehicle speed means a lower gear ratio, smaller size, and lower cost. On the other hand, a higher motor speed relative to the vehicle speed like in this case, it means a higher gear-ratio, larger size, and higher cost. Also, higher motor speed is desired in order to increase the power density of the motor. In Fig.6 shows speed-torque graph of the EM with different gear ratio size [2].

The vehicle speed can be calculated by using formula 2.2 (assuming no slip between the tires and):

$$v_{xT} = \omega_{wh} * r_{wh} \quad (2.2)$$

where v_{xT} - the vehicle speed, m/s,

ω_{wh} - the angular velocity of the wheel, rad/s,

r_{wh} - the radius of the wheel, m,

By using the vehicle speed and the tractive force the desired power rating of the electric motor can be calculated (formula 2.3):

$$P_{EM} = F_{TR} * v_{xT} = \omega_{wh} * T_{TR} \quad (2.3)$$

where v_{xT} - the vehicle speed, m/s,

ω_{wh} - the angular velocity of the wheel, rad/s,

P_{EM} - the desired power rating of the electric motor, W,

F_{TR} - the tractive force, N,

T_{TR} - the tractive torque, Nm,

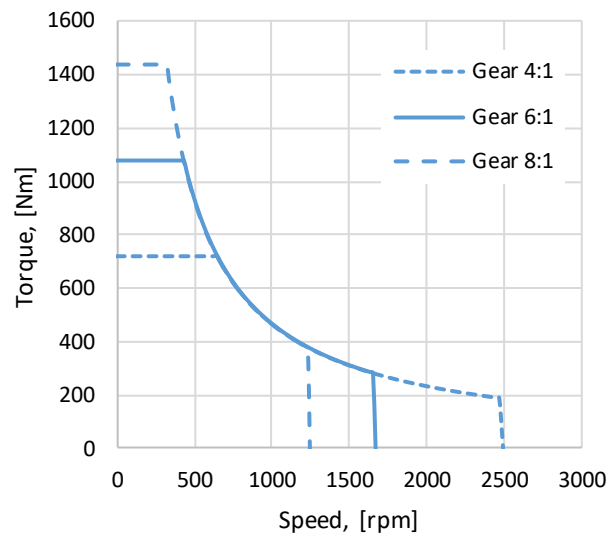


Fig.3: Theoretically calculated speed-torque graph for different gear ratios [2].

2.1.7. Clutches

The clutch is a mechanical component used to attach or separate the power source from the remaining parts of the power transmission network at the operator's convenience. There are four different type of classification for clutches [12].

Positive contact clutches accomplish the power transformation by interlocking of the jaws or teeth. Their key benefit is positive engagement, and they can transmit broad torque with no slip once coupled [12].

Friction clutches achieve the power transmission by using the friction between contact surfaces [12].

Electromagnetic clutches achieve the power transmission by using the magnetic field. Their advantage is rapid response time, easier to control, and smoother starts and stops [12].

Fluid clutches and couplings achieve the power transmission by using the hydraulic pressure. Their advantage is smooth starts and absorbs shock [12].

2.2. Comparison of ISEAUTO and Similar SDCs

The aim of this section is to research similar SDCs like ISEAUTO and learn their design methodology, challenges faced during development, the equipment they use, and most importantly EMs and RGs used on their design. Four similar SDCs are searched, they are The Navya Autonom Shuttle, WEpod, Olli, and EZ10. A table is prepared to demonstrate their specifications such as max. speed, EM type, general dimensions, AND gear ratio (Table 1.1).

Navya is a French company which designs and manufactures SDCs. Navya can carry maximum 15 passengers (11 seated, and 4 standing). WEpod is a self-driving car which designed by Technical University of Delft. It is designed to run public transportation in Wageningen University Campus and 8 km onwards to the railway station in the city of Ede. WEpod capacity is 6 people. Olli was designed by Local Motors company which is a USA company. Olli can carry maximum 8 people. EZ10 was designed and manufactured by Ligier which a French company is. EZ10 can carry up to 15 passengers [2], [13], [14], [15], [16].

In conclusion, due to similarities in the general dimensions, body shape, total weight, working purpose, working conditions, max. speed, and EM output ISEAUTO should have a similar RG like others. The reason is all those factors shows that they have similar load to carry at similar speed with similar drag force. As mentioned before the design criterions of an RG is reducing speed from a higher value to desired low value at specific load. On Table 2.1 shows that Olli has 9,59:1 gear ration. On the other hand, ISEAUTO's

current RG has 6,066:1 gear ratio which is smaller compared to other SDCs. The new RG should have higher gear ratio like others.

Table 2.1 Comparison of ISEAUTO and other self-driving busses [13], [14], [15], [16], [17].

Name	Max Speed [km/h]	Propulsion Motor		General Dimensions			Gear Ratio
		Type	Power [kW]	Length [mm]	Height [mm]	Width [mm]	
EZ10	45	IM	4	4000	2750	2000	Single Gear
Navya	25	IM	15	4750	2650	2110	N/A
Olli	40	PMSM	30	3945	2637	2041	9,51:1
WEpod	40	N/A	N/A	3930	2750	1990	N/A
ISEAUTO	20	PMSM	25	3500	2300	1300	6,066:1

2.3. Methodology

In this section the problems will be explained, and how they will be solved. In section 2.3.1. the problems will be defined. In section 2.3.2. solution methods will be explained.

2.3.1. Problems to Solve

The aim of the thesis is to develop a TB for I-Miev's EM, and there are several problems are needed to be solved to succeed it. Easiest way to solve this problem is buying a pre-made universal TB from a commercial company, but they are not suitable. A new suitable TB for the EM should be developed from the beginning by considering its criterions such as correct rotor angle and suitable mounting locations. Also, a motor controller, a load motor, a cooling system for the EM, an AC/DC converter, and DC power supply should be selected to develop a fully working TB. A motor controller is needed to run the EM motor and monitor its parameters during testing. Also, a load motor is required to run load test on the EM. The load motor must have higher output than the EM to handle the power out put of the EM. Otherwise, the load motor cannot handle the power output and it will be broken. The load motor needs a frequency converter to control during load test. The final instrument requires by the TB is an RG. A new RG should be designed to perform tests and to run ISEAUTO. The current RG of the ISEAUTO is not suitable and a new one should design due to ISEAUTO's maximum speed.

Tasks should be completed to run the EM First sub-problem is mounting the EM on the TB. The EM should be stay rigid on the TB to perform test on it, and it can be accomplished by designing suitable mounting parts for the EM. Holding the motor rigidly is not enough. They should prevent the EM form vibrations during testing. Otherwise, vibrations will create noise on test results, and it will decrease the accuracy of the test results. Another sub-problem is the original resolver of the EM is missing and it should be remanufactured to run the electric motor. Third sub-problem is a clutch is needed to connect the EM with a load motor to perform load test on the EM.

2.3.2. Solution Methods

Firstly, to develop a custom TB for the EM, there should be a bench to assemble the EM, the load motor, the RG, controller, and test instruments. There is a custom-made bench in the university in the EMG lab (NRG-001). This bench is suitable to assemble all equipment including the EM. It has a rigid body and huge space for assemble parts on it. After selecting the bench required instruments should be selected. The first instrument is motor controller. Sevcon-GEN4 Size 8 is selected as motor controller [18]. Both Sevcon and the EM needs a cooling system to get rid of the unwanted heat. The actual coolant system of the I-Miev is decided to use as a coolant system to cool down motor controller and the EM. Also, the control of the cooling pump will be controlled by Sevcon. A load motor is necessary to perform load tests. Dutchi motors DM1 225M6 model (59,8 kW) is selected as the load motor which has higher output than the EM [19]. Magna Power TSD800-18 model (15 kW, maximum voltage output is 800V) is selected as DC voltage source to run the system [20]. ACS880 is selected as frequency converter for controlling the load motor. The schematic of the developed TB can be seen in Fig.4.

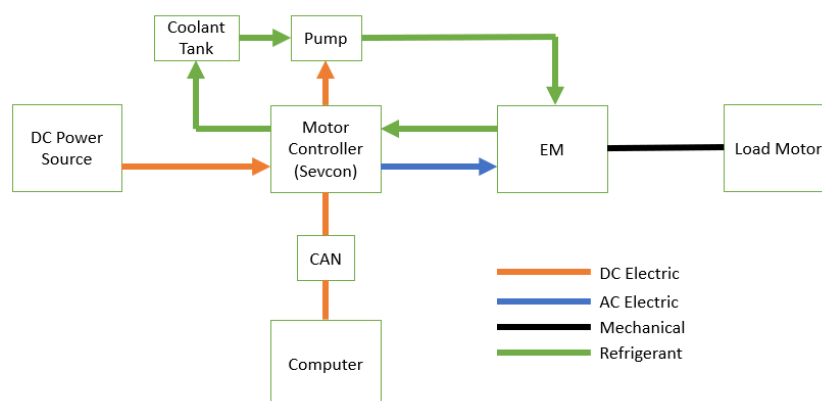


Fig.4: The schematic of the developed TB.

Solution methods for solving tasks. The body of the EM is analyzed and figured out that there are two suitable mounting locations for assembling mounting parts. One of them is in front of the EM, near to its rotor. There are three holes with 11,7mm holes

with teeth. These holes are designed to mount to motor on I-Miev, but in this case they are free to use. The second one is in the rear side of the EM. There is a small L shape frame with a 13,7mm blind hole in the middle. The purpose of this hole is assembling the EM on the car too. Again, in this case its free to use it for assembling mounting part. Except these two locations there are no possible way to assemble the EM on the TB. After deciding the mounting locations, the position of the EM on the TB should be decided. Assembling the RG, mounting parts, correct rotor angle, and connection of the EM and the load motor are the criterions of the positioning and it was decided to position the EM like in Fig.1. After deciding the position and assemble locations, the mounting parts should be designed and manufactured. Mounting parts should prevent the EM from vibrations to avoid noise on test results, and they should handle both the static forces and dynamic forces created by the EM. First, they are going to design on a CAD software by taking measurements on the TB and the EM. These designs will be analyzed that they can handle the forces or not. If they are suitable then they will be manufactured.

Another one is the connection of the EM and the load motor. A clutch is required to connect them and perform load tests on the EM. A clutch design will be made by Andres Petritshenko who is another student of TalTech. The design parameters, and the explanation of the design is in section 6.

The final task is designing a suitable RG for ISEAUTO's parameters. ISEAUTO is planned to travel at 20 km/h by using 0,285 m radius tires. Also, the electric motor is planned to run at 3000 rpm. Due to those parameters' smallest, safest and most efficient RG will be designed. All gears, shafts, bearings, and lubricant design methods and equations are in section 4. The safety of the parts will be checked by using stress analyze software. All technical drawings and the stress analyze results will be in appendix section. Moreover, an equation will be prepared to calculate the efficiency of the designed RG. The preparation steps and the calculation of the RG's efficiency are in section 5.

Challenges of tasks. The purpose of this section is to explain the factors that are cause the solution to become harder or take more time to solve them. The first challenge is the CAD files of the EM and RG are missing. The reason is this RG and EM were designed to accomplish one purpose which is running I-Miev. They do not have a purpose like industrial type EMs and RGs which can be used for more than one tasks. Mitsubishi does not share the CAD files of the RG and the EM to protect their copyright. On the other hand, CAD files and other technical documentation of the industrial EMs and RGs are can be requested. By using those technical documentation, they can be used in industrial tasks. Also, they can be reused in another application. Furthermore, missing CAD files are created a challenge on designing mounting parts. If the CAD files wasn't missing, on a CAD software the solid model of the EM can be put on the developed TB and by

using reference lines of both the EM and the TB body of the mounting parts could be easily designed. Now, the mounting parts can be designed by putting EM on the TB and taking measurements which is more time consuming, least accurate and harder compared designing them on a CAD software. The second challenge is the body shape of the EM. The body of the EM is circular, and its diameter increases from the rear face to front face like an irregular cone. This creates a challenge on both designing mounting parts and assembling the EM with the correct rotor angle. The rotor angle should be parallel to the load, otherwise additional vibration will occur on the EM during testing. Moreover, the irregular shape of the body makes taking measurements harder because more reference points, measurement instruments and measurements are required. Another challenge is lack of information about the EM and the RG. There is only basic information of about them and assembling & disassembling manuals. Detailed information of them kept by Mitsubishi due to protection of copyrights. This makes the RG and the EM like a black box model.

3. TEST BENCH

The purpose of this section is to explain how the TB is developed. In section 3.1. the results of parallel misalignment of rotors is explained. Section 3.1. was about design of the mounting parts. Section 3.2. covers the manufacturing process of the resolver.

3.1. Torsional Vibrations of a Shaft System with Parallel Misalignment

The aim of this chapter is explaining the results of parallel misalignment of rotors. As mention in section 2.1 before, the rotor angle of the EM and the load motor should be parallel. Otherwise, the parallel misalignment will cause additional vibration and it will create a noise on the test results.

The shaft coupling is shown in Fig.5. There are two conditions in the system. First one is the couplings between two shafts are elastic and the second one is shafts are rigid. B is a point at which shaft D is connected to coupling C, and point B is linked to both shaft D and coupling C when the shaft mechanism is rotating. There is a misalignment (r_1) between shaft D and shaft E. The rotation of shaft E will rotate point B. Shaft D and E are aligned which means point B will rotate around the common center of shafts D and E. When there is a misalignment, point B only rotates around the center line of shaft D. Shaft E is fixed with coupling, so an elastic deformation is produced in coupling C because of the misalignment. This elastic deformation will produce a force on shaft D & E. Displacement of point B on shaft D can be calculated by using formula 3.1 and 3.2 [21].

$$x = r * \sin(\theta + \varphi) \quad (3.1)$$

$$y = r_1 + r * \cos(\theta + \varphi) \quad (3.2)$$

where x - the displacement of point B on x-axis, m,

y - the displacement of point B on y-axis, m,

r - the distance from point B to OD, m,

r_1 - misalignment, m,

θ - the rotation angle, deg,

φ - the angle between y-axis and point B, deg.

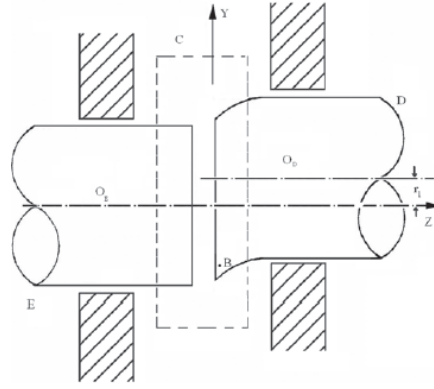


Fig.5: Misalignment of two rotors [21].

As shown in Fig.6 the movement of point B at coupling C relative to shaft E will be B'. Formula 3.3 and 3.4 represent the displacement of point B' at coupling C relative to shaft E [21].

$$x' = r * \sin(\theta + \varphi) \quad (3.3)$$

$$y' = r * \cos(\theta + \varphi) \quad (3.4)$$

where x' - the displacement of point B on x-axis, m,

y' - the displacement of point B on y-axis, m,

r - the distance from point B to OE, m,

θ - the rotation angle, deg,

φ - the angle between y-axis and point B', deg.

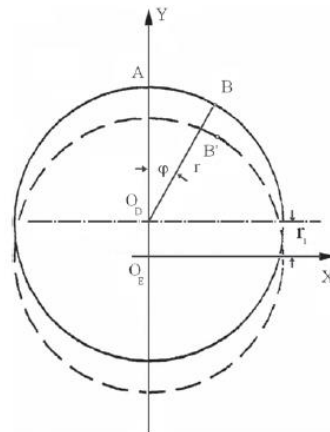


Fig.6: The trail of points B & B' [21].

The elastic deformation of coupling C can be calculated by using formula 3.5 and 3.6 [21].

$$\Delta x = x' - x = r * \sin(\theta + \varphi) - r * \sin(\theta + \varphi) = 0 \quad (3.5)$$

$$\Delta y = y' - y = r_1 + r * \cos(\theta + \varphi) - r * \cos(\theta + \varphi) = r_1 \quad (3.6)$$

where Δx - the elastic deformation on x-axis, m,

Δy - the elastic deformation on y-axis, m,

r - the distance from point B' to OE, m,

r_1 - misalignment, m,

θ - rotation angle, deg,

φ - the angle between y-axis and point B', deg.

As shown in Fig.7 the extra force will occur at point B can be calculated by using formula 3.7 and 3.8 [21].

$$F_x = k\Delta x = 0 \quad (3.7)$$

$$F_y = k\Delta y = -k * r_1 \quad (3.8)$$

where F_x - the force created by misalignment occur at point B on x-axis, N,

F_y - the force created by misalignment occur at point B on y-axis, N,

k - the elastic coefficient, N/m,

r_1 - misalignment, m,

Δx - the elastic deformation on x-axis, m,

Δy - the elastic deformation on y-axis, m.

This extra force will create a moment to the center of the shaft D which can be calculated by using formula 3.9 [21].

$$M_D = F_y * r * \sin(\theta + \varphi) \quad (3.9)$$

where M_D - The moment created by the extra force, Nm,

r - the distance from point B to OD, m,

θ - the rotation angle, deg,

φ - the angle between y-axis and point B, deg,

F_y - the force created by misalignment occur at point B on y-axis, N.

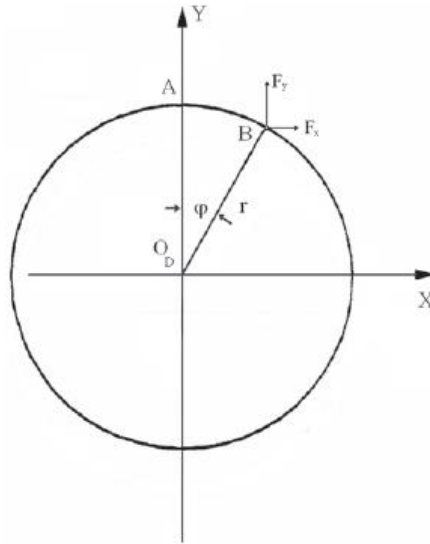


Fig.7: The moment on shaft D which is created by misalignment [21].

The torsional angle can be calculated by using formula 3.10 [21].

$$\theta = \Omega * t + \Delta\theta \quad (3.10)$$

where θ – the torsional angle, deg,

t - time, s,

Ω – the average angular velocity of shaft D, rad/s

$\Delta\theta$ – the initial torsional angle, deg.

The moment equation can be rewritten as formula 3.11 [21].

$$M_D = F_y * r * \sin(\Omega * t + \varphi + \Delta\theta) = -k * r_1 * \sin(\Omega * t + \varphi + \Delta\theta) \quad (3.11)$$

where Ω – the average angular velocity of shaft D, rad/s

t - time, s,

θ – the torsional angle, deg,

$\Delta\theta$ – the initial torsional angle, deg.

r - the distance from point B to OD, m,

F_y - the force created by misalignment occur at point B on y-axis, N,

In conclusion, misalignment in rotor angle will cause an extra force on rotor in radial axis. This force will affect test results and maybe even worsen it will break the rotor of the EM. The selected bench is suitable to assemble the EM in the correct rotor angle with the help of two custom designed mounting parts.

3.2. Designing Mounting Parts

The EM should be mount on the TB properly. Two mounting parts need to be designed for mounting the EM on the TB, one is for the front side of the EM and second one is for the rear side. There are three design criterions, they are holding the rotor with the correct rotor angle, handle all forces, and prevent the EM from vibrations. Firstly, their solid models will be designed by using Inventor CAD software. Their length and hole dimensions will be suitable for ISO standards. After their solid design is completed, their static analyses will be done by using Inventor's stress analyze feature. Von Mises Stress method will apply on the analyze. Mounting parts should satisfy at least 1,20 safety factors. Otherwise, an optimization process will be done on them to increase their strength. Their solid models are missing due to copyrights. That is why the dimensions of them will taking by cutting solid materials and filling the empty spaces between the mounting locations. After finalizing them, dimensions will be measured by using caliper, and angle protractor. Also, the EM should stay in a correct rotor angle. Parallelism of the angle between rotor and the surface will be checked by a spirit level. Taking measurements by hand is not so accurate and cause dimensional problems. First, they will manufacture by a 3D-printer as plastic to avoid scrap parts. Their suitability will be checked by using plastic models as a reference. If their prototypes are suitable then their actual models will be manufactured with St-37 steel. Also, the technical drawings of both mounting parts will draw due to ISO standards. These drawings are necessary for manufacturing process, and for checking quality control.

3.2.1. Rear Mounting Part

The general dimensions of the rear mounting part are 74,6 mm in length, 159,9 mm in width, and 70,9 mm in height. The angle between the upper and lower part is 61 deg. Its material is St-37 and its total weight is 0,854 kg (the solid model and the actual part can be seen on appendix section A.1). There were two different manufacturing process defined. The first one is machined it one piece from a rectangular prism. The second one is divided into 4 parts and cut them from a metal sheet, then assemble with welding. The first manufacturing process is stronger than the second one because assembling with welding decreases material strength. On the other hand, the second manufacturing process is cheaper than the second one because machining a rectangular prism will consume more raw material and cutting tools. Both models analyzed with different metal sheet thicknesses. In conclusion, due to the test results and economy factor second manufacturing process with 6 mm metal sheet thickness selected. In stress analyze it can handle 10000 N force with minimum 1.22 safety factor which is enough to handle all forces will occur on the mounting part (test results can be seen on appendix section no:3). Also, a second metal plate which matches with the lower metal plate of the

mounting part manufactured too. The mounting part on the top of the TB and the identical metal plate under the TB fixed with three M10 hex bolts with nuts. Washers and spring washers used to avoid auto-blocking of bolts. Moreover, a rectangular prism rubber used to correct the rotor angle by increasing the height of the EM on the rear side. Rubber selected as height increasing part to damp vibrations. In the end, it assembled the EM with the hole on the upper plate.

3.2.2. Front Mounting Part

First, the same design criterions, manufacturing process, and analyze technique is used on front mounting part which were previously on rear mounting part. The general dimensions of the rear mounting part are 110,1 mm in length, 133,1 mm in width, and 127,3mm in height. The angle between the upper and lower part is 61deg. Its material is St-37 and its total weight is 1,122 kg (the solid model and the actual part can be seen on appendix section no:4). Sheet metal thickness selected as 6 mm just like rear mounting part. In stress analyze it can handle 300 Nm torque with minimum 1.32 safety factor which is enough to handle all forces will occur on the mounting part (test results can be seen on appendix section no:6). Also, a second metal plate which matches with the lower metal plate of the mounting part manufactured too. The mounting part on the top of the TB and the identical metal plate under the TB fixed with four M10 hex bolts with nuts. Washers and spring washers used to avoid auto-blocking of bolts. In the end, it assembled the EM with the three holes in front of the EM.

3.3. Manufacturing Operation of the Resolver

The resolver of the EM planned to machine on a 3-axis CNC milling machine in the university. Programming of the manufacturing process prepared by using Siemens NX CAD/CAM software. Resolver manufactured from a St-37 cylindrical blank material with 80 mm diameter and 30 mm in length. The general dimension of the resolver is 23,2 mm in height and 59,4 mm in diameter. The weight of the resolver is 0,214 kg. After the manufacturing process the quality of the part checked. The manufacture resolver passed the quality control test, all dimensions are in the tolerances. In the end, the new resolver assembled on the EM. After the assemble operation, the EM run for testing the resolver. The EM run without a failure with the new resolver. The solid model of the resolver and the manufactured resolver can be seen on appendices section (A.7). Technical drawings with ISO standards of the resolver will be prepared and added on the appendices section.

In conclusion, the mounting parts to assemble the EM on the TB are designed, their 3D solid model and technical drawings prepared, their stress analysis done, and they manufactured. Their technical drawings, photos of 3D model/manufactured one and,

the results of stress analysis are in appendix section. Their suitability checked on a stress analyze software (Inventor is used) and they are enough durable to use them to assemble the EM. Due to the test results they can handle the weight of the EM and the vibrations will occur during testing. After the manufacturing process the EM is mounted on the TB. The EM still needs a resolver to run on the TB. Also, the resolver of the EM is manufactured then assembled on the EM. Photos of the manufactured resolver and its 3D model are in appendix section.

4. Reduction Gearbox

The purpose of this section is to explain the design methodology of the RG. As mentioned before the main purpose of the TB testing the EM and optimizing the SDC by using obtained test data. EMs are more efficient than internal combustion engines, but they still have significant power losses in RG. Designing a new RG for the SDC will increase its efficiency in critical amount.

4.1. Selecting Design Parameters

There are four parameters should be defined before start designing an RG. They are the total mass (m , kg), tire radius (r , m), desired velocity (v , m/s), and motor speed (w , rad/s). The motor speed is the most critical parameter because the motor speed effects the efficiency of the vehicle in a crucial amount. All motors have a maximum torque speed, and they run at maximum efficiency at this speed. The parameters of both I-Miev and ISEAUTO are given in Table 4.1.

Table 4.1 The parameters of ISEAUTO and I-Miev [22].

Parameters	I-Miev	ISEAUTO
Passenger Mass (kg)	80x4=320	80x6=480
Vehicle Mass (kg)	1080	1080
Tire Radius (m)	0,285	0,285
Vehicle Speed (m/s)	36,11	5,56

The maximum torque speed of the EM can be calculated by using formula 4.1 [8].

$$v = \frac{r*w}{n} \quad (4.1)$$

where v - Vehicle speed, m/s,

r - Tire Radius, m,

w - Motor speed, rad/s,

n - Gear ratio, constant.

The required gear ratio can be found by using formula 4.1. The maximum torque speed (n) is 314,16 rad/s which is converted from 3000 rpm (the maximum torque speed of the EM is checked from I-Miev manual), vehicle speed (v) is 20 km/h which is 5,56 in m/s, and tire radius is 0,285 m. The required gear ratio (n) is calculated 16,1 [11].

4.2. Designing the RG

In the previous section the required gear ratio (n) was calculated 16,1, and this value can be achieved with a triple-stage RD. Total parts of a two stage RG are 6 gears, 4 shafts, 8 bearings, and a body.

Pinion and gear design. Determining the dimensional parameters of the gears requires module (m) to be defined. There are two ways to define module. The first one is selecting a number between 1 to 10, and second one is there are some equations based on standards. Using a standard equation is selected to define module. Lewis form factor (Y), transmitted torque (MT), and bending stress (σ_{b1}). The desired gear ratio (n) of the first stage is 2,55, and pressure angle of the gears (α) is 20 deg selected. Firstly, minimum number of teeth to avoid interference should be calculated, which can be calculated by using formula 4.2 [12].

$$Z_1 = \frac{2}{\sin^2(\alpha)} \quad (4.2)$$

where Z_1 – The number of teeth of the pinion, constant,

α – Pressure Angle, deg (=20),

The number of teeth of the pinion (Z_1) is calculated 18. The teeth number of the first gear can be calculated by using formula 4.3 [8].

$$Z_2 = n * Z_1 \quad (4.3)$$

where Z_2 – The number of teeth of the gear, constant,

Z_1 – The number of teeth of the pinion, constant (=18),

n – Gear ratio, constant (=2.55).

The number of teeth of the gear (Z_2) is calculated 46. Another necessary parameter to calculate module (m) is transmitted torque which can be calculated by using formula 4.4 [33].

$$P = \frac{2 * \pi * N * M_T}{60} \quad (4.4)$$

where P – Power of the motor, W (=25000),

N – Rotational speed of the pinion, rpm (=3000),

M_T – Transmitted torque, Nm.

The transmitted torque (MT) is calculated 79,58 Nm. Next step is calculating Lewis form factor (Y) of both pinion and gear. Either it can be selected by using standard tables or there are equations based on standards. In this design the equation method is selected

which's equation is formula 4.5 [8].

$$Y = \pi * \left(0,154 - \frac{0,912}{Z_n}\right) \quad (4.5)$$

where Y – Lewis form factor, constant,

Z_n – The number of teeth of the pinion/gear, constant (=18, 173).

Lewis form factor is calculated for the pinion (Y1) 0,33, and for the gear (Y2) 0,42. All the required parameters to calculate module (m) are defined. Module (m) can be calculated by using formula 4.6 [8].

$$m = \sqrt[3]{\frac{M_T * k_0}{\sigma_{b1} * Y_1 * Z_1}} \quad (4.6)$$

where m – Module of the gear, mm,

M_T – Transmitted torque, Nmm (=79580),

k_0 – Safety factor for transmitted torque, constant (=1,25),

σ_{b1} – Bending stress of the pinion's material, MPa (=400),

Z_1 – The number of teeth of the pinion, constant (=18),

Y_n – Lewis form factor, constant (=0,33).

The module (m) is calculated 3,49 mm. After defining the module, geometric parameters of the gear and pinion can be calculated. First equation is for calculating the pitch circle diameter which is shown as formula 4.7. This RG is designing for a vehicle and its gears should be helical. The helix angle is selected 30 deg. It is selected larger to decrease the tooth contact surface area to increase efficiency [12].

$$d = Z * m \quad (4.7)$$

where d – The pitch circle diameter, mm,

m – Module of the gear, mm (=3,49),

Z – Number of teeth, constant (=18, 46),

The pitch circle diameter of the pinion (d1), and the gears (d2) is respectively 62,82 mm, and 160,54 mm. The center distance between the pinion and the gear (a) can be calculated by using formula 4.8 [12].

$$a = \frac{d_1 + d_2}{2 * \cos(\psi)} \quad (4.8)$$

where a – The center distance of the pinion and the gear, mm,

d_1 – The pitch circle diameter of the pinion, mm (=62,82),

d_2 – The pitch circle diameter of the gear, mm (=160,54).

ψ – Helix angle, deg (=30),

The center distance (a) of the pinion and the gear is calculated 128,96 mm. The next geometric parameter is face width (b) which can be calculated by using formula 4.9. The face width is calculated by multiplying module (m) value with a number between 8 to 12. 9 is selected to decrease the material cost of both the pinion and the gear [12].

$$b = 9 * m \quad (4.9)$$

where b – Face width, mm,

m – Module, mm (=3,49).

The face width of the gears (b) is calculated 31,41 mm which is changed to 32 mm to standardize them. After defining the dimensional parameters, calculations continue with the force analysis to determine the forces acting on the gears. These force values are used to prepare stress analysis for both the gear and the pinion which can be seen in appendix section A.42-61. There are three different forces acting on the gear, they are tangential force (F_t , formula 4.10), radial force (F_r , formula 4.11), and axial force (F_a , formula 4.12) [12].

$$F_t = \frac{2 * M_T}{d} \quad (4.10)$$

where F_t – Tangential force, N,

M_T – Transmitted torque, Nmm (=79580),

d – The pitch circle diameter, mm (=62,82).

$$F_r = F_t * \frac{\tan(\alpha)}{\cos(\psi)} \quad (4.11)$$

where F_r – Radial force, N,

F_t – Tangential force, N (=2533,59),

α – Pressure angle, deg (=20),

ψ – Helix angle, deg (=30),

$$F_a = F_t * \tan(\psi) \quad (4.12)$$

where F_a – Axial force, N,

F_t – Tangential force, N (=2533,59),

ψ – Helix angle, deg (=30),

The tangential force (F_t), the radial force (F_r), and the axial force (F_a) are calculated respectively 2533,59 N, 1064,81 N, 1462,77 N. The next step is checking the strength of both the pinion, and the gear. Beam strength of the gear (S_{bn}) should be higher than effective load (F_{eff}) for satisfying the safety criteria. Beam strength be calculated by

using formula 4.13, and effective load can calculate by using formula 4.14 [12].

$$S_{bn} = m * b * \sigma_b * Y_n \quad (4.13)$$

where S_{bn} – Beam strength, N,
 σ_b – Bending stress, MPa (= 124,18),
 b – Face width, mm (=32),
 m – Module, mm (=3,49),
 Y_n – Lewis form factor, constant (=0,33, 0,42).

$$F_{eff} = \frac{C_s * F_t}{C_v} \quad (4.14)$$

where F_{eff} – Beam strength, N,
 F_t – Tangential force, N (=2533,59),
 C_s – Service factor, constant (=1),
 C_v – Velocity factor, constant (=0,72).

Service factor (C_s) in beam strength formula (formula 4.15) can be selected from the table in appendix section table A.26.1 Velocity factor (C_v) can be calculated by using formula 4.15. Velocity factor requires the pitch line velocity (v) which can be calculated by using formula 4.16 [12].

$$C_v = \frac{5,6}{5,6 + \sqrt{v}} \quad (4.15)$$

where C_v – Velocity factor, constant,
 v – The pitch line velocity, m/s (=9,74).

$$v = \frac{2 * \pi * N * d_n}{60 * 2} \quad (4.16)$$

where C_v – Velocity factor, constant,
 d_n – The pitch circle diameter, m (=0,062),
 N – Rotational speed of the pinion, rpm (=3000).

The pitch line velocity of the pinion (v_1) is calculated 9,74 m/s. The pitch line velocity of the pinion velocity factor (C_v) is calculated 0,72. Also, service factor (C_s) is selected 1 from the table. Another required parameter for calculating beam strength is bending stress on the tooth which can be calculated by using formula 4.17 [12].

$$\sigma_b = \frac{M_b * y}{I} \quad (4.17)$$

where σ_b – Bending stress, MPa,
 M_b – Bending moment, Nmm (=19888),

y – Vertical distance away from the neural axis, mm (=2,74).

I – Moment of inertia around the neural axis, mm⁴ (=438,84).

Bending moment (M_b), vertical distance away from the neural axis (y), and moment of inertia around the neural axis (I) must calculate to obtain bending stress value on the tooth. Bending moment can be calculated by using formula 4.18 [12].

$$M_b = F_t * h \quad (4.18)$$

where M_b – Bending moment, Nmm,

F_t – Tangential force, N (=2533,59),

h – Tooth length, mm (= 7,85).

Tooth length is selected 7,85mm from the figure in appendix section table A11.2 As mention before the pressure angle of all gears and pinions is selected 20 deg, and module (m) is calculated 3,49 mm. Due to the selected parameters the tooth length of all gears and pinions should be $2,25 * m$ which is equal to 7,85 mm. Finally, bending moment (M_b) is calculated 19888 Nmm. Also, moment of inertia (I) calculation should be done which can be calculated by using formula 4.19 [12].

$$I = \left(\frac{1}{12}\right) * b * t^3 \quad (4.19)$$

where I – Moment of inertia around the neural axis, mm⁴,

b – Face width, mm (=32),

t – Tooth thickness, mm (= 5,48).

Tooth thickness is selected 5,48mm from the figure in appendix section table A11.2. Moment of inertia (I) is calculated 438,84 mm⁴. Also, vertical distance away from the neural axis (y) is equal to half of the tooth length which is 2,74. Finally, bending stress (σ_b) is calculated 124,18 MPa. After bending stress calculation beam strength of both the pinion and the gear is calculated respectively 4576,58 N and 5824,74 N. Furthermore, effective load (F_{eff}) is calculated 3518,87 N. Both beam strength of the pinion and the gear is higher than effective load which means both are safe to use. Moreover, both should satisfy wear safety too. Wear strength (S_w) can be calculated by using formula 4.20 [12].

$$S_w = \frac{b * Q * d_1 * K}{\cos^2(\psi)} \quad (4.20)$$

where S_w – Wear strength, N,

b – Face width, mm (=32),

Q – The ratio factor, constant (=1,44),

d_1 – The pitch circle diameter of the pinion, mm (=62,82),

ψ – Helix angle, deg (=30),

K – The K factor, constant (=1,75).

Load stress factor and the ratio factor (Q) can be calculated by using formula 4.21, and 4.22 [12].

$$Q = \frac{2 \cdot Z_2}{Z_2 + Z_1} \quad (4.21)$$

where Q – The ratio factor, constant,

Z_1 – The number of teeth of the pinion, constant (=18),

Z_2 – The number of teeth of the gear, constant (=46),

The ratio factor (Q) is calculated 1,44.

$$K = \frac{\sigma_c^2 \cdot \sin(\alpha) \cos(\alpha) \cdot \left(\frac{1}{E_1} + \frac{1}{E_2}\right)}{1,4} \quad (4.22)$$

where K – Load stress factor, constant,

E_1 – Module of elasticity of the pinion, N/mm² (=30x10⁶),

E_2 – Module of elasticity of the gear, N/mm² (=30x10⁶),

α – Pressure angle, deg (=20),

σ_c – Surface endurance strength, MPa (=7569,75).

Module of elasticity (E_n) is selected from table A.26.3 as stainless-steel SS304 is selected as material for the pinion, and SS420 is selected for the gear. Material of the pinion is selected weaker than the gear to reduce the maintenance cost of the RG. Furthermore, surface endurance strength (σ_c) can be calculated by using formula 4.23 [12].

$$\sigma_c^2 = \frac{1,4 \cdot F_t}{b \cdot Q \cdot \sin(\alpha) \cos(\alpha) \cdot \left(\frac{1}{E_1} + \frac{1}{E_2}\right)} \quad (4.23)$$

where σ_c – Surface endurance strength, MPa,

E_1 – Modulus of elasticity of the pinion, N/mm² (=30x10⁶),

E_2 – Modulus of elasticity of the gear, N/mm² (=30x10⁶),

F_t – Tangential force, N (=2533,59),

α – Pressure angle, deg (=20),

Q – The ratio factor, constant (=1,44),

d – The pitch circle diameter, mm (=62,82),

b – Face width, mm (=32),

The force pressing the pinion and the gear (P) is called normal force (F_n). Tangential force is equals to normal force's x-axis component which is shown as formula 4.24. Moreover, radius of curvature of both the pinion and the gear (r_n) should be obtained to calculate surface endurance strength (σ_c), and it can be calculated by using formula 4.25 [12].

$$P = F_n = \frac{F_t}{\cos(\alpha)} \quad (4.24)$$

where P – The force pressing the pinion and the gear, N,

F_n – Normal force, N,

α – Pressure angle, deg (=20),

F_t – Tangential force, N (=2533,59).

The normal force (F_n) is calculated 2696,19 N, and surface endurance strength (σ_c) is calculated 9074,76. When the value of the surface endurance strength is written the K factor is calculated 1,26. Finally, the value of wear strength (S_w) is calculated 4874,08 N. Wear strength value is higher than effective load which means it's safe to use. Design parameters of the other pinions and gears are in table A.23.4 In appendix section A.23.

Shaft design. After designing the pinion and the gear the RG design continues with shaft design. In shaft design only one parameter must be done which diameter (d). Three criteria effect the size of the shaft diameter. They are tensile stress (σ_t), bending stress (σ_b), and torsional shear stress (τ). The shafts that are used in RGs have only torsional moment. Diameter calculation requires the maximum torsional moment value of the selected material which can be calculated by using formula 4.25 [12].

$$\tau_{max.} = \frac{0,5 * S_{yt}}{f} \quad (4.25)$$

where $\tau_{max.}$ – Maximum torsional shear stress, MPa,

S_{yt} – Yield Strength, MPa (=205),

f – Safety factor, constant (=1,25).

Maximum torsional shear stress ($\tau_{max.}$) is calculated 82 MPa. Stainless steel (SS304) is selected as material for longer product life and rigidity. Table for yield strength of stainless is in appendix section A.23 (table A.23.5). First, shaft design starts with the pinion of the first stage. Diameter of the shaft for pinions can be calculated by using formula 4.26 [12].

$$\tau = \frac{16 * M_T}{\pi * d^3} \quad (4.26)$$

Where τ_{max} . – Maximum torsional shear stress, MPa
 M_T – Transmitted torque, Nmm (=79580),
 d – The shaft diameter, mm.

Diameter of the shaft for first pinion is calculated 17,03 mm. 18 mm diameter is selected because 17 mm diameter it is not suitable for steel bar standard. Design parameters of the other shafts are shared as table A.23.6 In appendix section A.23.

Bearing selection starts with calculating the load on the bearings. In gear systems, the radial load on gear tooth effects bearings as axial load and the tangential force on gear tooth effects bearings as radial load. After defining the radial and axial load on bearings, X and Y factors of the dynamic load should be calculated. X is radial force factor and Y is axial load factor. A static load capacity (C0) is selected by the designer in the beginning of the design because selecting bearing from a manufacturers catalogue is based on trial and error. Static load factor can be selected from table A.23.8 in appendix section A.23. Next step is calculating the ratios of axial load/radial load, and axial load/static load capacity. "e" factor is selected from table A.23.7 in appendix section A.23 by using axial load/static load factor ratio. If the exact value on the table cannot be found, then interpolation should apply on it. After defining X and Y factors dynamic load (P) on the bearing can be calculated by using formula 4.27 [12].

$$P = X * F_a + Y * F_r \quad (4.27)$$

where P – Dynamic load, N,
 F_a – Axial force, N,
 F_r – Radial force, N,
 X – Radial load factor, constant,
 Y – Axial load factor, constant.

The next step is calculating dynamic load capacity which can be calculated by using the relationship between load and life. Load-life relationship is shown as formula 4.28 [12].

$$L_{10} = \left(\frac{C}{P}\right)^p = \frac{60 * N * L_{10h}}{10^6} \quad (4.28)$$

where L_{10} – Rated bearing life, in million revolutions,
 C – Dynamic load capacity, N,
 p – for ball bearings = 3,
 P – Dynamic load, N,
 N – Rotational speed, rpm,

L_{10h} – Rated bearing life, hour (=20000).

Rated bearing life (L_{10}) is calculated by using the second equality in formula 4.28. Rotational speed (N) and dynamic load are known, and rated bearing life (L_{10h}) is selected 20000 hours from table A.23.5. Dynamic load capacity (C) can be calculated from the first equality in formula 4.28. After calculating dynamic load capacity its suitability is checked from table A.23.9. If the calculated dynamic load capacity is bigger than the value on the table, the selected bearing is not suitable. This calculation method should apply until the calculated dynamic capacity becomes smaller than the value on the table. For optimal selection, the calculated dynamic load capacity should be smaller than the selected one but should be bigger than the one smaller size.

When this method applied for the first stage of the RG. The tangential force acts on the first pinion is 2533,59 N, and the radial force acts on the first pinion is 1064,81 N. The shaft diameter of the first pinion is 25 mm. The bearing with 25 mm inner diameter and 52 mm outer diameter one is selected which has 6950 N static load capacity. Ratio of axial load/radial load is calculated 0,42 and ratio of axial load/static load capacity is calculated 0,153. "e" factor is 0,322 calculated by applying interpolation. X and Y factors are selected respectively 0,56 and 1,362 because ratio of axial load/radial load is bigger than "e" factor. Otherwise, they would be respectively 1 and 0. Dynamic load (P) is calculated 2869,08 N. Rated bearing life (L_{10}) is calculated 3600 in million revolutions by using the second equality in formula 4.28. Finally, dynamic load capacity (C) is calculated 43972,06 N but the dynamic load capacity of the selected bearing is 14000 N. Same calculations should be repeated until the dynamic load capacity becomes smaller than the selected bearing. Results of the calculations are in table A.23.10 in appendix section A.23. First shaft diameter was calculated 25 mm but none of the bearings with 25 mm inner diameter is suitable. The shaft diameter is increased to 35 mm for suitable bearing.

Lubricant selection. RGs needs lubricant to work just like other gear transmission mechanisms. The required kinematic viscosity of the gear pairs should be calculated to select a suitable lubricant for the designed RG. The working temperature of the RG is expected to be around 40 degree Celsius like other gearboxes. Pitch line velocity of the slowest gear (v_p) should be calculated which can be calculated by using formula 4.29 [36].

$$v_p = \pi * N * d_2 \quad (4.29)$$

where v_p – Pitch line velocity, mm/min,

d_2 – The pitch line diameter of the gear, mm,

N – Rotational speed, rpm.

After calculating the pitch line velocity of the lowest speed gear, the required kinematic viscosity can be calculated by using formula 4.30 [36].

$$v_{40} = \frac{122210}{\sqrt{v_p}} \quad (4.30)$$

where v_{40} – Kinematic viscosity of the lubricant at 40-degree Celsius, mm/min,

v_p – Pitch line velocity, mm/min.

The third gear is the slowest which turns at 186 rpm speed. Its pitch line diameter is 290,7 mm. Its pitch line velocity is calculated 169866 mm/min. The required lubricant viscosity of the RG is found 295,91 mm²/s. ISO VG 320 Industrial lubricant is selected from table A.23.12 in appendix section A.23.

4.3. Stress Analyses of the Designed Parts

In the previous section gears, and shafts are designed due to formulas in lectures books and they will double-check with stress analysis.

4.3.1. Stress Analyses of the Designed Pinions/Gears

Pinions and gears are designed due to the results of calculation in the previous section. Inventor is used to draw pinions and gears. Technical drawings and the 3D models of pinions and gears are in appendix section A.24-41. Suitability of the designed pinions and gears should be checked for the last time by using a stress analysis software. Inventor is used to analyze stress on pinions and gears. The safety factor is selected 1,25, and Von Mises Stress method is selected as stress analyze method. Stress analyze requires resultant force applied on the tooth surface. Resultant force applied on tooth surface is created by tangential and radial forces. Resultant force applied on the tooth can be calculated by using formula 4.31 [12].

$$F = \sqrt{(F_t^2 + F_r^2)} \quad (4.31)$$

where F – Resultant force applied on the tooth, N,

F_t – Tangential force, N,

F_r – Radial force, N,

Resultant force applied on first pinion and, gear is calculated 2748,25 N. The lowest safety factor on the analyze is 8,01 for the first pinion and, 10,87 is for the first gear. On the next stage the resultant force is 5159,96 N. The lowest safety factor on the analyze is 7,62 for the second pinion and, 10,05 is for the second gear. Resultant force of the last stage is calculated 9578,77 N. The lowest safety factor on the analyze is 7,91 for the third pinion and, 11,07 is for the third gear. Stress analyze results are in appendix section A.42-61.

4.3.2. Stress Analyses of the Designed Shafts

Shafts are designed by using formula 4.25, and 4.26 in the previous section. Inventor CAD software is used to draw shafts. Technical drawings and the 3D models of pinions and gears are in appendix section A.24-41. Only torsional stress occurs on shafts in this mechanism. They can handle the torsional stress occurs on them and it tested via physical equation (formula 5.25, and 4.26). Also, they tested via a stress analyze software. Von Misses Stress Method is used on stress analyze to check their safety. Torque is applied on the first shaft is 79,58 Nm. The result of stress analyzes shows that the minimum safety factor is 15. On the second shaft torque becomes 202,93 Nm because of increasing gear diameter. The lowest safety factor in its test result is 15. 513,41 Nm Torque applies on the third shaft, and 9,55 is the lowest safety factor on its test result. On the last shaft applied torque increases to 1283,53 Nm. Due to the test results its lowest safety factor is 4,93 In conclusion, safety of the designed shafts proved twice by using physical equations and stress analyze software.

In conclusion, the smallest possible RG was designed for the EM. In the beginning of the design criteria selection desired gear ratio was 16,1 but obtained gear ratio is 16,33. The reason why designed RG has bigger gear ratio is size. On every stage the lowest number of teeth is selected, and it caused big shifts. The result of the required number of teeth is always ended up with a fractional number and, a fractional number cannot be selected as number of teeth. This result hast to be shifted to one smaller integer or one bigger integer. For more accurate gear ratio size of the RG must be bigger. The aim of this project is increasing the efficiency of ISEAUTO and increasing the weight of the RG will result in worser efficiency than having less accurate gear ratio. Smallest suitable RG was designed. Design parameters of pinions, gears, shafts, and bearings are in appendix section A.23. Moreover, technical drawings of the RG are prepared, and they are in appendix section A.24-41.

All shafts, pinions, gears, and bearings designed/selected based on physical equation. Their suitability is checked analytically before and now they double checked with a stress analyze software which is Inventor. Von Misses Stress Method is selected as stress calculation method. Due to the analyze results all designed parts can handle the maximum power output of the EM. Their analyze results are in appendix section A.42-61. The RG is suitable for both testing the EM on the TB, and after complete tests on the EM it is suitable to use it on ISEAUTO.

5. Efficiency of the RG

The aim of this section is preparing a formula for calculating the efficiency of the designed RG. The power losses of an RG will be explained with their theoretical formulas.

5.1. Power Losses of an RG

The power losses in an RG dwell gear, bearing, seals, and auxiliary losses. Gear and bearing losses are separated into two different categories which are load and no-load losses. No-load losses are not depending on the torque. They appear with the rotation of the mechanism. No-load losses are lubricant losses due to the viscosity and density of the lubricant, internal design of the RD, and bearing no-load losses are rely upon arrangement, size, type, lubricant viscosity, and immersion depth. Load dependent losses take place in the contact point of the power transmitting elements. Load dependent losses are relying upon the transmitted torque, coefficient of friction, sliding velocity in the contact areas of the elements. Load dependent bearing losses are relying upon size, type, and rolling & sliding conditions, and lubricant type [9], [23].

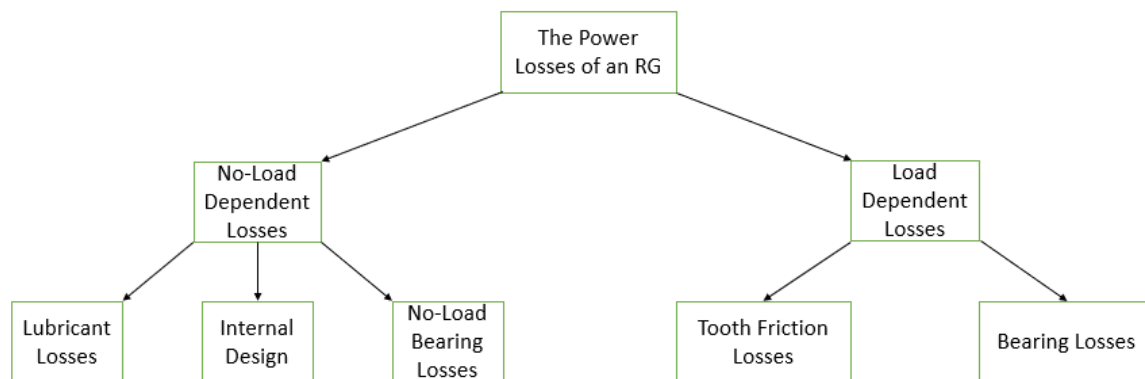


Fig.8: The power losses types of an RG.

5.1.1. Tooth Friction Losses

Tooth friction losses are the power losses between gear tooth. As mentioned on the previous section tooth friction losses are load dependent type power losses. The gear loss factor must be calculated accurately to obtain an accurate result. Gear loss factor evaluated by seeing the load transport forward the tooth connection. There is not a common accepted formula for the tooth friction losses. There are several different tooth friction losses formulas. All these formulas will be explained and one of them will be selected for the efficiency calculation [9], [23].

The first formula for calculating tooth friction losses is formula 5.1 and it developed by Ohlendorf. This equation is based on assuming a constant coefficient of friction which is the simplification of the problem. This equation is mostly valid for spur gears [23], [24].

$$P_{VZP} = P_{IN} * H_V * \mu_{mZ} \quad (5.1)$$

where P_{VZP} - Tooth friction loss, W,

P_{IN} - Input power, W,

H_V - Gear loss factor, constant,

μ_{mZ} - Average coefficient of friction, constant.

For calculating tooth friction loss (P_{vzp}) gear loss factor (H_v) should be calculated which can be calculated by using formula [23], [24].

$$H_V = (1 + n) * \frac{\pi}{Z_1} * \frac{1}{\cos(\beta_b)} * (1 - \epsilon_\alpha + \epsilon_1^2 + \epsilon_2^2) \quad (5.2)$$

where H_V - Gear loss factor, constant,

β_b - Base helix angle, rad,

ϵ_α - Transverse contact ratio, constant,

ϵ_1 - Addendum contact ratio, constant,

ϵ_2 - Dedendum contact ratio, constant,

n - Gear ratio, constant,

Z_1 - Number of teeth of gear number 1, constant.

Niemann and Winter came up with a different gear loss factor calculation which is formula 5.3. In this approach gear loss factor contemplate rigid load distribution [23], [25].

$$H_V = (1 + n) * \frac{\pi}{Z_1} * \frac{1}{\cos(\beta_b)} * \epsilon_\alpha * \left(\frac{1}{\epsilon_\alpha} - 1 + (2k_0^2 + k_0 + 1) * \epsilon_\alpha \right) \quad (5.3)$$

where H_V - Gear loss factor, constant,

β_b - Base helix angle, rad,

ϵ_α - Transverse contact ratio, constant,

k_0 - Gear geometry factor, constant,

n - Gear ratio, constant,

Z_1 - Number of teeth of gear number 1, constant.

Another one is founded by Buckingham which is shown in formula 5.4 [23], [26].

$$H_V = (1 + n) * \frac{\pi}{Z_1} * \frac{1}{\cos(\beta_b)} * \epsilon_\alpha * (2k_0^2 + k_0 + 1) \quad (5.4)$$

where H_V - Gear loss factor, constant,

β_b - Base helix angle, rad,

ϵ_α - Transverse contact ratio, constant,

k_0 - Gear geometry factor, constant,

n - Gear ratio, constant,

Z_1 - the Number of teeth of the pinion, constant.

Gear geometry factor (k_0) in both Niemann & Winter's and Buckingham's formulas can be calculated by using formula 5.5 [23].

$$k_0 = \frac{Z_1}{2\pi * H_V * n} * \left(\left(\left(\frac{r_{a2}}{r_{p2}} \right)^2 * \frac{1}{\cos(\alpha_t^2)} - 1 \right)^{\frac{1}{2}} - \tan(\alpha_t) \right) \quad (5.5)$$

where k_0 - Gear geometry factor, constant,

α_t - Transverse pressure angle, rad,

H_V - Gear loss factor, constant,

n - Gear ratio, constant,

r_{a2} - Tip radius of gear number 2, mm,

r_{p2} - Pitch radius of gear number 2, mm,

Z_1 - Number of teeth of gear number 1, constant.

The fourth one is (formula 5.6) based on the load distribution which is developed by Wimmer. The load distribution is dividing the total normal force by the length of the contact lines along the contact path. In this way the elastic effects of the load distribution can be calculated [23], [28].

$$H_V = \frac{1}{P_b} \int_0^b \int_A \frac{F_N(x,y)}{F_b} * \frac{V_g(x,y)}{V_b} * d_x d_y \quad (5.6)$$

where H_V - Gear loss factor, constant,

P_b - Base pitch, mm,

$F_N(x,y)$ - Normal force per length, N/mm,

$V_g(x,y)$ - Sliding Velocity, m/s,

F_b - Tooth normal force on transverse plane, N,

V_b - Base cylinder transverse tangential speed, m/s.

The load distribution can be calculated by using formula 5.7.

$$F_N(x,y) = \frac{F_b n}{L(x,y)} \quad (5.7)$$

where $F_N(x,y)$ - Normal force per length, N/mm,

F_{bn} – Tooth normal force, N,

$L(x, y)$ – Sum of the lengths of the lines of contact, mm.

The last one is the most recent gear pair efficiency calculation formula which is developed by Velex and Ville. In this formula the effects of profile modifications are included, but it has constant coefficient of friction like the previous formulas. Also, there is not pre-assumptions on the tooth load distribution [23] [27].

$$P_{VZP} = P_{IN} * \mu_{mZ} * (1 + n) * \frac{\pi}{Z_1} * \frac{1}{\cos(\beta_b)} * H_V * \Lambda(\mu) \quad (5.8)$$

where P_{VZP} - Tooth friction loss, W,

P_{IN} - Input power, W,

$\Lambda(\mu)$ - Efficiency parameter, constant,

β_b - Base helix angle, rad,

H_V - Gear loss factor, constant,

Z_1 - Number of teeth of gear number 1, constant,

μ_{mZ} - Average coefficient of friction, constant.

In Velex and Ville Method tooth friction loss calculation requires efficiency parameter ($\Lambda(\mu)$) which can be obtained by using formula 5.9 [23], [27].

$$\Lambda(\mu) = \frac{2k_0^2 + k_0 + 1}{1 - n * \left(\frac{\tan(\alpha_t) * (2k_0 - 1) - \frac{\pi}{Z_1} * H_V * (2k_0^2 + k_0 + 1)}{\cos(\beta_b)} \right)} \quad (5.9)$$

where $\Lambda(\mu)$ - Efficiency parameter, constant,

β_b - Base helix angle, rad,

H_V - Gear loss factor, constant,

n - Gear ratio, constant,

α_t - Transverse pressure angle, rad,

k_0 - Gear geometry factor, constant.

5.1.2. Bearing Losses

Another power loss in RD system is caused by bearings. The power losses in bearings divided into load dependent losses and no-load dependent losses. Load dependent bearing losses are depending on bearing size & type, rolling & sliding conditions, and lubricant type. On the other hand, no-load bearing losses are depending on bearing size & type, lubricant viscosity and immersion depth. Bearing friction was first explained by Petroff. Petroff's equation requires the assumption that the shaft is concentric, but it is

still giving accurate results for non-concentric shafts. Petroff's equation gives the frictional torque and by using frictional torque the power loss can be calculated.

Consider a vertical shaft rotating in a guide bearing. Assume that the bearing carries a very small load, the clearance space is filled with lubricant and lubricant leakage is negligible. No-load dependent bearing loss is caused by the lubricant. The shearing stress in the lubricant is equal to the velocity gradient times the viscosity which is shown in formula 5.10 [29].

$$\tau = \mu * \frac{U}{h} = \frac{2\pi * r * \mu * N}{c} \quad (5.10)$$

where τ – Sheer stress, MPa,

μ – Absolute viscosity, MPa*s

h – Film thickness, mm,

U – Surface velocity, m/s

c – Radial clearance, mm,

N – Rotational speed, rev/s.

After calculating the shearing stress in the lubricant is calculated then the required torque to shear the film can be calculated by using the formula 5.11 [29].

$$T = (\tau * A) * r = \left(\frac{2\pi * r * \mu * N}{c} \right) * (2\pi * r * l) * r = \frac{4\pi^2 * r^3 * l * \mu * N}{c} \quad (5.11)$$

where T – The required torque to shear the lubricant film, Nmm,

r – Radius of the lever arm, mm,

A – Area, mm²

l – Length of the bearing, mm,

μ – Absolute viscosity, MPa*s,

c – Radial clearance, mm,

N – Rotational speed, rev/s.

Load dependent bearing loss is depending on the coefficient of friction, input torque, and the radius of the shaft. The coefficient of friction is depending on the size and type of the bearing and it can be calculated by using formula 5.12 [29].

$$f = 2\pi^2 * \frac{\mu * N}{P} * \frac{r}{c} \quad (5.12)$$

where f – Coefficient of friction, constant,

P – Pressure, MPa,

- μ – Absolute viscosity, MPa*s,
- r – Radius of the lever arm, mm,
- c – Radial clearance, mm,
- N – Rotational speed, rev/s.

After calculating the coefficient of friction, the required torque to exceed the friction can be calculated by using formula 5.13 [29].

$$T = f * W * r = (f) * (2r * l * P) * (r) = 2r^2 * f * l * P \quad (5.13)$$

- where
- T – The required torque to exceed the friction force, Nmm,
 - f – Coefficient of friction, constant,
 - r – Radius of the lever arm, mm,
 - l – Length of the bearing, mm,
 - P – Pressure, MPa,
 - W – Load, N.

There is a second way to calculate coefficient of friction which is by using Sommerfeld number. Sommerfeld number is a dimensionless number which is used in design of bearings. Formula 5.14 is the formula of Sommerfeld number [29].

$$S = \left(\frac{r}{c}\right)^2 \frac{\mu * N}{P} \quad (5.14)$$

- where
- S – Sommerfeld number, constant,
 - P – Pressure, MPa,
 - μ – Absolute viscosity, MPa*s,
 - r – Radius of the lever arm, mm,
 - c – Radial clearance, mm,
 - N – Rotational speed, rev/s.

Formula 5.15 shows the relation between Sommerfeld number and coefficient of friction [29].

$$f * \frac{r}{c} = 2\pi^2 * \left(\frac{r}{c}\right)^2 \frac{\mu * N}{P} = 2\pi^2 * S \quad (5.15)$$

- where
- S – Sommerfeld number, constant,
 - P – Pressure, MPa,
 - μ – Absolute viscosity, MPa*s,

- r – Radius of the lever arm, mm,
- f – Coefficient of friction, constant,
- c – Radial clearance, mm,
- N – Rotational speed, rev/s.

Moreover, there is a graph for finding the coefficient of friction by using Sommerfeld number and l/d (the length of the bearing divided by the diameter of the bearing). The graph is in A.65.

Petroff's equation is not the only way to calculate the bearing losses. Also, there are formulas created by bearing manufacturer such as SKF. In the SKF model bearing losses are divided into four categories, they are rolling frictional moment, sliding frictional moment, frictional moment of seals, and frictional moment of drag losses. This model was developed by using advance computational models. Also, this model is valid for oil or grease lubricated bearings. This model should be applied to the all bearing in the system separately then their results added together. The total frictional moment can be calculated by using formula 5.16 [30].

$$M = M_{rr} + M_{sl} + M_{seal} + M_{drag} \quad (5.16)$$

- where
- M – Total frictional moment, Nmm,
 - M_{rr} – Rolling frictional moment, Nmm,
 - M_{sl} – Sliding frictional moment, Nmm,
 - M_{seal} – Frictional moment of seals, Nmm,
 - M_{drag} – Frictional moment of drag losses, Nmm.

The first loss of bearing is rolling frictional moment (M_{rr}) which can be calculated by using formula 5.17 [30].

$$M_{rr} = \phi_{ish} * \phi_{rs} * G_{rr} * (v * N)^{0.6} \quad (5.17)$$

- where
- M_{rr} – Rolling frictional moment, Nmm,
 - ϕ_{ish} – Inlet shear heating reduction factor, constant,
 - ϕ_{rs} – Kinematic replenishment/starvation reduction factor, constant,
 - G_{rr} – Variable depending on (table A.66.1):
 - The bearing type,
 - The bearing mean diameter d_m [mm] = $0,5(d+D)$
 - The radial load F_r [N]
 - The axial load F_a [N]

N – Rotational speed, rpm,

ν – Actual operating viscosity of the oil or the base oil of the grease, mm²/s.

Inlet shear heating reduction factor (ϕ_{ish}) and kinematic replenishment/starvation reduction factor (ϕ_{rs}) are required to calculate rolling frictional moment (M_{rr}) which can be calculated by using formula 5.18 and 5.19. Inlet shear heating reduction factor is a fraction of the oil which the ball of bearing passes through the contact area, a small amount of oil covers the ball of the surface like a film. Rest of the oil creates a reverse flow against the motion of the ball. This flow creates heat and it lowers the viscosity of the lubricant which reduces the film thickness on the ball. Rolling friction decreases with the decreasing thickness film. Kinematic replenishment/starvation reduction factor occurs when there is kinematic starvation in bearing's raceway. Kinematic starvation occurs when viscosity or speed is high. Lubricant starts to cannot fill the raceway of the bearing. Kinematic starvation decreases the film thickness and rolling friction [30].

$$\phi_{ish} = \frac{1}{1+1,84*10^{-9}*(N*d_m)^{1,28}*\nu^{0,64}} \quad (5.18)$$

where ϕ_{ish} – Inlet shear heating reduction factor, constant,

d_m – The bearing mean diameter = 0,5(d+D), mm,

N – Rotational speed, rev/min,

ν – Actual operating viscosity of the oil or the base oil of the grease, mm²/s.

Kinematic replenishment/starvation reduction factor can be calculated by using formula A.66.2 [30].

$$\phi_{rs} = \frac{1}{e^{\left[K_{rs}*\nu*n*(d+D)*\sqrt{\frac{K_z}{2(D-d)}} \right]}} \quad (5.19)$$

where ϕ_{rs} – Kinematic replenishment/starvation reduction factor, constant,

D – Bearing outside diameter, mm,

d – Bearing bore diameter, mm,

e – Base of natural logarithm, constant = 2.718,

K_{rs} – Replenishment/starvation constant, mm,

K_z – Bearing type related geometric constant, constant,

n – Rotational speed, rev/min,

ν – Actual operating viscosity of the oil or the base oil of the grease, mm²/s

Sliding frictional moment (M_{sl}) caused by the sliding action which can be calculated by using formula 5.20 [30].

$$M_{sl} = \mu_{sl} * G_{sl} \quad (5.20)$$

where M_{sl} – Sliding frictional moment, Nmm,

G_{sl} – Variable depending on (table A.66.1):

- The bearing type,
- The bearing mean diameter d_m [mm] = $0,5(d+D)$
- The radial load F_r [N]
- The axial load F_a [N]

Sliding frictional coefficient (μ_{sl}) in sliding frictional moment (M_{sl}) can be obtained by using formula 5.21 [30].

μ_{sl} – Sliding friction coefficient, constant.

$$\mu_{sl} = \phi_{bl} * \mu_{bl} + (1 - \phi_{bl}) * \mu_{EHL} \quad (5.21)$$

where μ_{sl} – Sliding friction coefficient, constant,

ϕ_{bl} – Weighting factor for the sliding friction coefficient, constant,

μ_{bl} – Constant depending on movement, constant:

- 0,12 for $n \neq 0$
- 0,15 for $n = 0$ (starting torque calculation).

μ_{EHL} – Sliding friction coefficient in full-film conditions, constant:

- 0,02 for cylindrical roller bearings.
- 0,002 for tapered roller bearings.
- 0,05 for lubrication with mineral oils.
- 0,04 for lubrication with synthetic oils.
- 0,1 for lubrication with transmission fluids.

Sliding frictional coefficient (μ_{sl}) calculation requires weighting factor for the sliding friction coefficient (ϕ_{bl}) value which can be calculated by using formula 5.22 [30].

$$\phi_{bl} = \frac{1}{e^{2,6*10^{-8}*(N*v)^{1,4}*d_m}} \quad (5.22)$$

where ϕ_{bl} – Weighting factor for the sliding friction coefficient, constant,

N – Rotational speed, rpm,

v – Actual operating viscosity of the oil or the base oil of the grease, mm^2/s ,

e – Base of natural logarithm, constant = 2.718,

d_m – The bearing mean diameter = $0,5(d+D)$, mm.

Frictional moment of seals (M_{seal}) is caused where bearings are fitted with contact

seals. Frictional moment of seals can be calculated by using formula 5.23. This formula can be applied on bearings which has seals on both sides [30].

$$M_{seal} = K_{S1} * d_s^\beta + K_{S2} \quad (5.23)$$

where M_{seal} – Frictional moment of seals, Nmm,

K_{S1} – Constant (table A.66.3), depending on:

- The seal types.
- The bearing type and size.

d_s – Seal counter-face diameter (the table in A.66.3), mm,

K_{S2} – Constant (table A.66.3), depending on:

- The seal types.
- The bearing type and size.

β – Exponent (table A.66.3), depending on:

- The seal types.
- The bearing types.

Drag losses (Mdrag) that occur when the bearing is rotating in an oil bath. Drag losses clout by bearing speed, oil viscosity, oil level, size and geometry of the oil reservoir. Drag losses for ball bearings can be calculated by using formula 5.24. Equation of the rolling element related constant (Kball) is formula 5.25 [30].

$$M_{drag} = 0,4 * V_M * K_{ball} * d_m^5 * N^2 + 1.093 * 10^{-7} * N^2 * d_m^3 * \left(\frac{N * d_m^2 * f_t}{v} \right)^{-1.379} * R_s \quad (5.24)$$

where M_{drag} – Frictional moment of drag losses, Nmm.

V_M – Drag loss factor (the graph in A7.4), constant,

d_m – The bearing mean diameter = $0,5(d+D)$, mm,

K_{ball} – The rolling element related constant, constant,

N – Rotational speed, rpm,

v – Actual operating viscosity of the oil or the base oil of the grease, mm^2/s ,

$$R_s = 0,36 * d_m^2 * (t - \sin(t)) * f_A$$

$$f_A = 0,05 * \frac{K_Z * (D+d)}{D-d}$$

$$f_t = \begin{cases} \sin(0,5 * t), & \text{when } 0 \leq t \leq \pi \\ 1, & \text{when } \pi < t < 2\pi \end{cases}$$

$$t = 2\cos^{-1} \left(\frac{0,6 * d_m - H}{0,6 * d_m} \right) \text{ when } H \geq 1,2d_m, \text{ use } H = 1,2d_m$$

$$K_{ball} = \frac{i_{rw} * K_z * (d+D)}{D-d} * 10^{-12} \quad (5.25)$$

where K_{ball} – The rolling element related constant, constant,
 D – Bearing outside diameter, mm,
 d – Bearing bore diameter, mm,
 i_{rw} – Number of ball rows, constant,
 K_z – Bearing type related geometric constant, constant.

5.1.3. Lubricant Losses

RGs requires lubricant to avoid friction and deformations on tooth connection. Lubricant losses occur when lubricant splash to the pinion which creates a drag torque on it. Lubricant losses depend on the rotational speed of the pinion, surface area of the pinion contacts with the lubricant, pitch diameter of the pinion, and density of the lubricant. The drag torque caused by lubricant can be calculated by using formula 5.26 [31], [32].

$$C_{drag} = \frac{1}{2} * \rho * \left(\frac{\pi * N}{30}\right)^2 * A * \left(\frac{d_1}{2}\right)^3 * C_m \quad (5.26)$$

where C_{drag} – Drag torque of the lubricant, Nm,
 ρ – The lubricant density, kg/m³,
 N – Rotational speed, rpm,
 A – Surface area of the pinion contacts with the lubricant, m²,
 d_1 – Pitch diameter of the pinion, m,
 C_m – Dimensionless drag torque coefficient, constant.

Dimensionless drag torque coefficient (C_m) can be calculated by using formula 5.27 [31], [32].

$$C_m = \left(\frac{2h}{d_1}\right)^{0,45} * \left(\frac{V_0}{d_1^3}\right)^{0,1} * Fr^{-0,6} * Re^{-0,21} \quad (5.27)$$

where C_m – Dimensionless drag torque coefficient, constant,
 h – Submerged depth of pinion, m,
 Fr – Froude number, constant,
 Re – Reynolds number, constant,
 d_1 – Pitch diameter of the pinion, m,
 V_0 – Lubricant volume, m³.

Reynolds number and Froude number can be calculated by using formula 5.28, and 5.29

[29].

$$Re = \frac{v * l}{\nu} \quad (5.28)$$

where Re – Reynolds number, constant,

ν – Kinematic viscosity, m^2/s ,

l – The cord width, m ,

v – Velocity of the fluid, m/s .

$$Fr = \frac{v}{\sqrt{g * l}} \quad (5.29)$$

where Fr – Froude number, constant,

g – Acceleration of gravity, m/s^2 ($=9,81$),

l – The cord width, m ,

v – Velocity of the fluid, m/s .

5.1.4. Shaft Sealing Losses

Shaft sealing losses are caused by the friction occur between the shaft and it is sealing.

Shaft sealing losses depend on the shaft diameter, and rotational speed of the shaft.

Shaft sealing losses can be calculated by using formula 5.30 [31], [12].

$$P_j = 7,69 * 10^{-6} * D^2 * N \quad (5.30)$$

where P_j – Shaft sealing power loss, W ,

D – Shaft diameter, mm ,

N – Rotational speed, rpm .

5.1.5. Total Losses of a Triple-Stage RG

The losses in an RG system are caused by tooth friction, bearing, lubricant and sealing.

There are three different tooth friction losses in a triple-stage RG caused by three gear

pairs. Also, there are four shaft sealing losses and, four bearing pairs losses. For

calculating the losses of bearings SKF model is selected because SKF model is an

improved version of Petroff's equation due to test results. The latest method is selected

for calculating tooth friction which is Velez and Ville method. Velez and Ville equation

gives better results where rigid load distribution just like RGs for EVs. After deciding

calculation methods, the total losses of a triple-stage RG can be written as formula 5.31.

(Frictional moment of bearings and drag torque formulas gives torque value and they

transformed to power value by multiplying the torque value with rotational speed and

dividing it by 95,488.)

$$P_{loss} = P_{VZP1} + P_{VZP2} + P_{VZP3} + ((2 * M_1 + C_{drag1}) * N_1 + (2 * M_2 + C_{drag2}) * N_2 + (2 * M_3 + C_{drag3}) * N_3 + 2 * M_4 * N_4) * \frac{1}{95,488} + P_{J1} + P_{J2} + P_{J3} + P_{J4} \quad (5.31)$$

where P_{loss} – Total power loss of the RD, W,

P_{VZP1} – Tooth friction loss of the first gear pair, W (=2702,82),

P_{VZP2} – Tooth friction loss of the second gear pair, W (=2454,44),

P_{VZP3} – Tooth friction loss of the third gear pair, W (=2159,15),

P_{J1} – Shaft sealing power loss of the first shaft, W (=28,26),

P_{J2} – Shaft sealing power loss of the second shaft, W (=18,33),

P_{J3} – Shaft sealing power loss of the third shaft, W (=10,82),

P_{J4} – Shaft sealing power loss of the fourth shaft, W (=6,04),

M_1 – The total frictional moment of the first bearing pair, Nm (=2,49),

M_2 – The total frictional moment of the second bearing pair, Nm (=2,77),

M_3 – The total frictional moment of the third bearing pair, Nm (=3,64),

M_4 – The total frictional moment of the fourth bearing pair, Nm (=3,97),

C_{drag1} – Drag torque of the lubricant acting on the first stage, Nm (=1,27),

C_{drag2} – Drag torque of the lubricant acting on the second stage, Nm (=1,34),

C_{drag3} – Drag torque of the lubricant acting on the third stage, Nm (=0,4),

N_1 – Rotational speed of the first shaft, rpm (=3000).

N_2 – Rotational speed of the second shaft, rpm (=1177).

N_3 – Rotational speed of third shaft, rpm (=465).

N_4 – Rotational speed of the fourth shaft, rpm (=186).

The efficiency of a system can be calculated by dividing the difference of input power and power losses to input power. The efficiency of a double-stage RD can be calculated by using formula 5.32.

$$\eta = \frac{P_{in} - P_{loss}}{P_{in}} * [100\%] \quad (5.32)$$

where η – Efficiency of the RD, presentence (=69,14),

P_{loss} – Total power loss of the RD, W (=7713,89),

P_{in} – Input power, W (=25000).

Explanation of the calculation. The calculation starts with selecting the tooth friction losses. Velex and Ville method is selected for calculating tooth friction losses. First, for calculating tooth friction loss (P_{VZP}) gear loss factor (Hv) should be calculated. Niemann and Winter method is selected for calculating gear loss factor because Niemann and Winter method is more suitable for rigid load distribution and for this RG load always near to be rigid because the bus will travel at constant low speed. For calculating gear loss factor gear geometry factor should be selected from table A.23.11 in appendix section A.23. Gear loss factor is calculated by using formula 5.3. Also, efficiency parameter ($\Lambda(\mu)$) should be calculated to find tooth friction loss which can be calculated by using formula 5.9. After calculating efficiency parameter, and gear loss factor tooth friction loss calculated by using formula 5.8.

The next step is calculating bearing losses. SKF developed a formula to calculate bearing losses by improving Petroff's equation due to test results. This method is selected to calculate bearing losses which is formula 5.16. For calculating the total frictional moment (M) in the bearing rolling frictional moment (M_{rr}), sliding frictional moment (M_{sl}), frictional moment of seals (M_{seal}), and frictional moment of drag losses (M_{drag}) should be calculated. First, calculation starts with rolling frictional moment which can be calculated by using formula 5.17. For calculating the rolling frictional moment variable depending on the bearing type (G_{rr}), inlet shear heating reduction factor (ϕ_{ish}), and kinematic replenishment/starvation reduction factor (ϕ_{rs}) should be calculated. They can be calculated by using formula respectively 5.18 and 5.19. Variable depending on the bearing type can be calculated by using the table A.66.1 in appendix section A.66. Geometric constants for rolling frictional moments (R1, R2) can be selected from table A.66.6. Geometry constant (Kz) can be selected from table A.66.2. After calculating them the rolling frictional moment can be calculated. The next loss is sliding frictional moment which can be calculated by using formula 5.20. Sliding frictional coefficient (μ_{sl}) should be calculated from the formula 5.21, and variable depending on the bearing type (G_{sl}) should be defined to calculate sliding frictional moment which can be calculated respectively from table A.66.1. Also, geometric constants for rolling frictional moments (S1, S2) can be selected from table A.66.6. Another loss is frictional moment of seals which can be calculated by using formula 5.19. For calculating frictional moment of seals constants depending on the seal type (Ks1, Ks2), and exponent depending on the seal type (β) should be selected from table A.66.3. The last frictional loss type in bearings is caused by drag force (formula 5.20). For calculating drag losses drag loss factor should be selected from table A.66.4. The last operation is adding all the four losses, and it will give the total losses in the bearing. All parameters and calculation results for bearing losses are in appendix section A.66.

Another step is calculating the lubricant losses. Calculation of the drag torque of the lubricant requires parameters such as density of the lubricant (ρ), rotational speed (N), the pitch diameter of the pinion (d_1), and surface area of the pinion contacts with the lubricant (A). Lubricant selection was made on the previous section and ISO VG 320 was selected. The density of the lubricant is found 897,4 kg/m³ from its data sheet. Pitch diameter of the pinion and rotational speed are known and surface area is calculated by using the 3D-solid model of the RG. The last required parameter is dimensionless drag torque coefficient (C_m). For calculating the coefficient submerged depth of pinion (h), lubricant volume (V_0), Reynolds number (Re), Froude number (Fr), and pitch diameter of the pinion (d_1). Reynolds number and Froude number can be calculated by using formula 5.28, and 5.29. Depth of pinion and lubricant volume can be calculated by using 3D-solid model of the RG.

The last loss is shaft sealing losses. It can be calculated by only multiplying the square of the shaft diameter (D), rotational speed (N), and $7,69 \cdot 10^{-6}$ (formula 5.30).

In conclusion, all the loss in the RG is added up in a single formula. The efficiency of the designed RG is calculated 69,14% by using the developed formula. In the market RGs designed by well known companies have only 10% efficiency loss on every stage. The designed RG has triple-stage and it has 30,84% efficiency loss which is close enough to the ones in the market. It has an advantage against the pre-made ones. For lower electricity consumption accurate gear ratio is necessary. The desired gear ratio is 16,1 which is hard to find a suitable one in the market. In other words, it will increase the efficiency of ISEAUTO higher than the pre-made ones.

6. Clutch

The EM is ready for single testing, but it needs to connect with the load motor to perform load tests. A clutch should design to connect them. Another student of TalTech Andres Petrishenko was designed a suitable clutch for the TB. It is a friction clutch design which based on two pulleys connected to shafts of EM and load motor connected with a toothed belt. The design parameters are same as the RG. The power output of the EM is 25 kW at 3000 rpm speed. The transmission ratio is selected 3:1 because the maximum rotational speed of the load motor is 1000 rpm. The load motor is an industrial type and it has a wedge on its shaft to assemble pulley, but the EM is designed to use on car, and it has straight shaft with teeth to connected with the RG. The suitable pulleys are found on the market and ordered. The pulley on the load motor is fixed with the help of the wedge. The pulley on the EM is fixed with plate covers the back side of the pulley and connect to the EM from the front side. There are 6 screw holes in front of the EM to connect with the RG, but these holes are free to use when the EM is assembled on the TB. Photos of the 3D solid model are in appendix section A.67.



Fig.9: The clutch system (the load motor is on the left).

7. Conclusion

In conclusion, the TB is prepared as planned. A suitable TB for the electric motor is designed which satisfies the criteria in the second chapter which is correct rotor angle. In the beginning the background information is searched. Due to the research results a custom design TB is necessary to perform accurate test on the electric motor. Premade TB are not suitable because the EM is not suitable to assemble at every TBs. The EM is designed to run an electric vehicle and suitability to assemble it on pre-made TBs is not a design criterion. Also, the irregular shape of the body creates a challenge on assembling the EM at correct rotor angle. The results of inaccurate rotor angle are mentioned in the third section. A bench is selected to assemble all instruments and the EM on it. Mounting parts are designed to assemble the EM with correct rotor angle and they prevent the EM from vibrations. After manufacturing the mounting parts, the EM is assembled on the TB with correct rotor angle. The next step was selecting/designing other instruments. Sevcon Gen4 is selected as motor controller for more precise control and obtaining data. Dutchi motors DM1 225M6 model (59,8 kW) is selected as the load motor. The reason is the EM has 25 kW power output and the load motor should have higher power output to compensate the power output of the test motor. Otherwise, the test motor will burn the load motor. ACS880 is selected as frequency converter for controlling the load motor. Magna Power TSD800-18 model (15 kW, maximum voltage output is 800V) is selected as DC voltage source to power the EM. Sevcon and the EM need water cooling system to get rid of unwanted heat. The coolant pump and tank of I-Miev is assembled on the TB to run coolant in the EM and Sevcon. Also, Sevcon is used to control the coolant pump (During quarantine the coolant pump of I-Miev is broken and could not order a new one. Instead of original pump, another cooling system is assembled to the TB which designed by another student of TalTech for thesis project. The cooling system has a radiator and a pump which controls with a potentiometer). After completed the cooling system the load motor and the EM need to connect with a clutch. A frictional clutch is designed to connect them. Moreover, a metal sheet is designed for protection because the EM is not industrial type EM and it does not have wedge on it to fix a pulley on it. This metal sheet is connected to the free holes which locate is in front of the EM. In this way, the pulley cannot disassemble and hurt anyone (Clutch is designed by another student, not author's design. All drawings and technical information belong to Andres Petritshenko). Now, the TB is ready to perform tests on the EM. Another step of the project is to design/select a suitable RG for ISEAUTO and the TB to achieve the purpose of the paper. The original RG of the EM is disassembled and analyzed. It's a double-stage RG with 6,066 gear ratio. I-Miev was designed to travel at maximum 130 km/h speed. On the other hand, ISEAUTO was designed to travel at maximum 20 km/h speed. Both have the same tire diameter which is 0,285

m. The desired gear ratio is calculated 16,1 for ISEAUTO's specifications. Theoretically and practically the smallest number of teeth is selected to decrease the size and weight of the RG. Moreover, weight reduction optimization is made on gears. Their width thickness is reduced by 10% without effecting teeth, and holes cut on gears. In the end of design process the obtained gear ratio was 16,32. Also, shafts and bearings are selected due to ISO standards (Bearings are selected from SKF catalogue). Furthermore, a cover box is designed to assemble all gears. On design safety, long product life, less manufacturing cost, and light weight considered. All gears, shafts, and bearings designed based on physical formulas then checked by stress analyze results. 3D solid model, technical drawings and analyze results of parts are in appendix section. A formula is prepared to calculate the efficiency of the RG. All losses in a RG is searched and found out there are two type of losses. The first one is load dependent losses such as tooth friction and bearing. On the other hand, there are no-load dependent losses such as lubricant losses and no-load bearing losses. For every type of losses different methods are searched to find the most suitable ones for RGs. Velex and Ville method is selected because their equation gives better results where rigid force distribution occurs. For calculating bearing losses two methods are found. First one is Petroff's equation which is based on conditions. These conditions are ideal conditions and in RG, conditions are not ideal. On the other hand, SKF created a method for calculating bearing losses by using steps of equation based on test results. SKF's method has different constants for different type of bearings to increase the accuracy of the equation. SKF's method is selected for calculating all bearing losses because it is more suitable for RG condition than Petroff's equation. For calculating lubricant and shaft sealing losses only one equation was founded, and they are used in the total efficiency calculation without comparing with another method. After selecting methods for calculating losses, all of them added together in a single equation by changing their unit in Watt. In the end, the efficiency of the RG is calculated 69,14%. The designed RG works efficient as the ones in the market. The pre-made RGs have 10% efficiency loss which is around %30 for a triple-stage RG. Finally, the aim of the thesis is achieved, the TB works and the efficiency of ISEAUTO is increased with the new RG. Also, the TB can be used for further research and developments of ISEAUTO. The test bench is built in TalTech University and, locates in room NRG-001.

7. Järeldus

Kokkuvõttes võib öelda, et katsestend on valmistatud plaani järgi. Elektrimootorile on kavandatud sobiv katsestend, mis vastab teise peatüki kriteeriumidele, milleks on rootori õige nurk. Esiteks otsitakse taustteavet. Uurimistulemuste jaoks on vaja elektrimootoriga täpse katse tegemiseks kohandatud disaini katsestendi. Eeltöödeldud katsestendid ei sobi selleks, kuna elektrimootor ei sobi kokku panemiseks igas katsestendis. Elektrimootor on elektrisõiduki käitamiseks ette nähtud ja selle kokkupaneku jaoks eelnevalt valmistatud katsestendi sobivus pole projekteerimiskriteerium. Samuti korpuse ebaharilik kuju tekitab raskusi elektrimootori õige rootori nurga all kokkupanekule. Ebatäpse rootori nurga tulemused on meenutatud kolmandas osas. Kõigi instrumentide ja seal asuva elektrimootori kokkupanekuks valitakse katsestendi. Paigaldusosad on loodud rootori õige nurga all elektrimootori kokkupanekuks ja need takistavad elektrimootori vibratsiooni. Pärast paigaldusosade valmistamist elektrimootor monteeritakse katsestendile rootori õige nurga all. Järgmine samm oli teiste instrumentide valimine/kujundamine. Täpsemaks juhtimiseks ja andmete saamiseks on valitud Sevcon Gen4 mootori kontrolleriks. Koormusmootoriks on valitud Dutchi motors DM1 225M6 (59,8 kW). Sellise mootori valiku põhjus on see, et elektrimootoril on 25 kW väljundvõimsus ja testmootori väljundi kompenseerimiseks koormusmootoril peaks olema suurem võimsus. Vastasel juhul katsemootor põletab koormusmootori. Sagedusmuunduriks on valitud ACS880 koormusmootori juhtimise jaoks. Elektrimootori toiteks kasutatakse alalisvoolu pingeallikana Magna Power TSD800-18 mudelit (15 kW, maksimaalne väljundvõimsus on 800 V). Sevcon ja elektrimootor vajavad vesijahutussüsteemi soovimatust kuumusest vabanemiseks. I-Mievi jahutusvedeliku pump ja paak on katsestendile kokku pandud jahutusvedeliku juhtimiseks elektrimootoris ja Sevconis. Jahutusvedeliku pumba juhtimiseks kasutatakse Sevconit. I-Mievi jahutusvedeliku pump läks karantiini ajal katki ja uut ei olnud võimalik tellida. Algse pumba asemel on katsestendile kokku pandud veel üks jahutussüsteem, mille on kavandanud teine TalTech'i lõputöö projekti osaleja. Jahutussüsteemil on radiaator ja pump, mida juhitakse potentsiomeetriga. Pärast jahutussüsteemi valmimist peab koormusmootori ja elektrimootori siduriga ühendama. Nende ühendamiseks on ette nähtud hõõrdesidur. Metallplekk on ette nähtud kaitseks, kuna elektrimootor ei ole tööstuslikku tüüpi elektrimootor ja sellel ei ole rihmaratta kinnitamiseks kiilu. See metallplekk on ühendatud vabade aukudega, mis asuvad elektrimootori ees. Sel viisil ei saa rihmaratas lahti võtta ega vigastada kedagi. (Siduri konstrueeris teine tudeng, see ei ole autori projekt. Kõik joonised ja tehniline teave kuuluval Andres Petritshenkole). Nüüd on katsestend valmis elektrimootoriga katseid tegema. Veel üks projekti samm paberi eesmärgi saavutamiseks on ISEAUTO jaoks sobiva reduktorkäigukasti ja katsestendi kavandamine/valimine. Elektrimootori

originaal reduktorkäigukast on lahti võetud ja analüüsitud. See on kaheastmeline reduktor, mille ülekandearv on 6,066. I-Miev oli maksimaalse kiirusega 130 km/h liikumiseks mõeldud. Teisest küljest ISEAUTO oli maksimaalsel kiirusel 20 km / h liikumiseks mõeldud. Mõlemal on sama rehvi läbimõõt, mis on 0,285 m. ISEAUTO spetsifikatsioonide järgi on soovitud ülekandearv arvutatud 16,1. Teoreetiliselt ja praktiliselt reduktsioonikäigukasti suuruse ja kaalu vähendamiseks valitakse väikseim hammaste arv. Käikudel optimeeritakse kaalu vähendamine. Nende laiuse paksust vähendatakse 10% nende habrasuse tõttu. Projekteerimisprotsessi lõpuks oli saavutatud ülekandearv 16,32. Võllid ja laagrid valitakse vastavalt ISO standarditele (Laagrid valitakse SKF kataloogist). Kattekest on mõeldud kõigi käikude kokkupanekuks. Projekteerimisohutuse osas kaaluti toote pikka kasutusiga, väiksemaid tootmiskulusid ja kergust. Kõik hammasrattad, võllid ja laagrid olid konstrueeritud füüsikaliste valemite alusel ja neid kontrolliti stressianalüüsi tulemuste abil. 3D-mudel, tehnilised joonised ja osade analüüsitulemused on toodud lisa osas. Reduktsioonikäigukasti efektiivsuse arvutamiseks on koostatud valem. Otsiti välja ja leiti kõik reduktorkäigukastiga seotud kaod. Kahjusid oli kahte tüüpi. Esimene neist on koormusest sõltuvad kaod, näiteks hammaste hõõrdumine ja kulumine. Teisest küljest puuduvad koormusest sõltuvad kaod, näiteks määrdeainekaod ja kandevõimetuse kaod. Igat tüüpi kadude jaoks otsiti erinevaid meetodeid, et leida reduktorkäigukastile kõige sobivamad. Valiti Velexi ja Ville'i meetod, kuna nende võrrand annab parema tulemuse jäika jõu jaotuse korral. Laagrikadude arvutamiseks leiti kaks meetodit. Esimene on Petroffi võrrand, mis põhineb tingimustel. Need tingimused on ideaalsed, ning reduktoriga tingimused pole ideaalsed. Teisest küljest SKF lõi meetodi laagrikao arvutamiseks, kasutades katsetulemustel põhinevaid võrrandi astmeid. Võrrandi täpsuse suurendamiseks SKF meetodil on erinevate tüüpi laagrite jaoks erinevad konstandid. Kõigi laagrikao arvutamiseks valiti SKF-i meetod, kuna see sobib paremini reduktorile, kui Petroffi võrrand. Määrdeainete ja võllide tihenduskaotuste arvutamiseks leiti ainult üks võrrand ja seda kasutati kogu efektiivsuse arvutamisega ilma teise meetodiga võrdlemiseta. Pärast kadude arvutamise meetodite valimist, neid kõik pandi ühte võrrandisse, muutes ühikuid vattideks. Projekteeritud reduktorkäigukasti efektiivsus arvutati välja töötatud valemi abil. Redutseeritud käigukasti kasuteguriks arvutati 69,14%. See konstrueeritud reduktorkäigukast töötab sama tõhusalt kui turul olevad. Eelnevalt valmistatud reduktorkäigukastidel on kasutegur 10%, mis on umbes 30% kolmeastmelise reduktoriga käigukasti puhul. Lõputöö eesmärk saavutatud, katsestend töötab ja uue reduktoriga ISEAUTO efektiivsus on suurenenud. Katsestendi saab kasutada ISEAUTO edasiseks uurimiseks ja arendustegevuseks. Katsestend oli ehitatud TalTechi ülikoolis ja asub ruumis NRG-001.

LIST OF REFERENCES

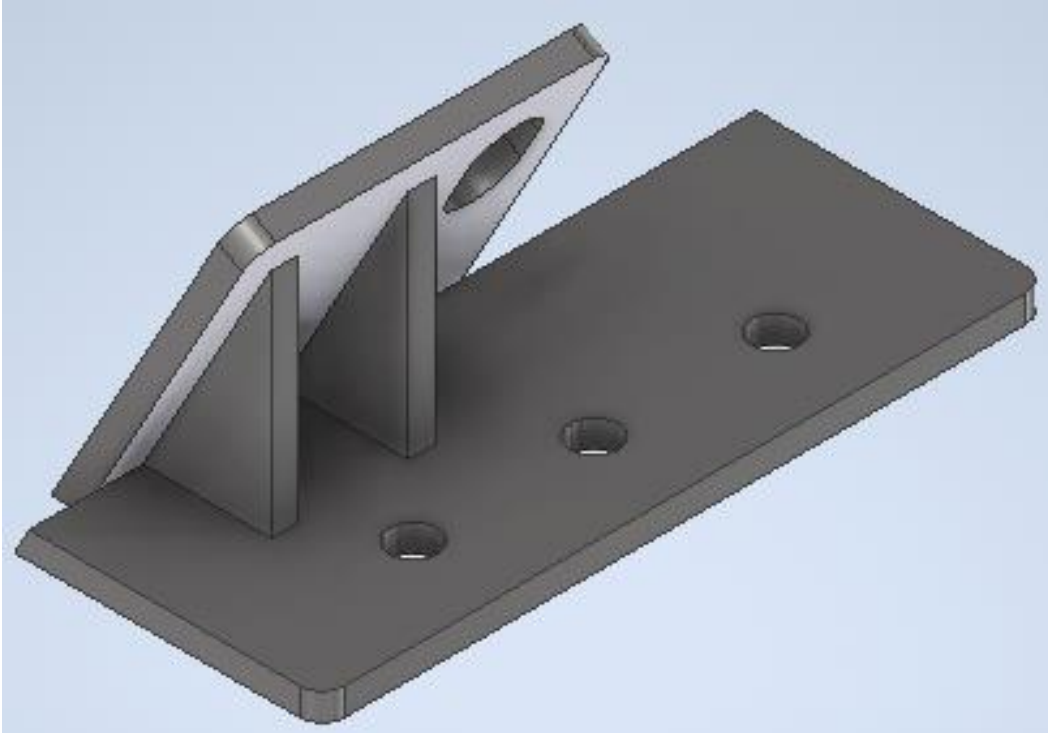
- [1] A. R. Fayjie, S. Hossain, D. Oualid, and D. J. Lee, "Driverless Car: Autonomous Driving Using Deep Reinforcement Learning in Urban Environment," 15th Int. Conf. Ubiquitous Robot UR, pp. 896-901, 2018.
- [2] A. Rassolkin, T. Vaimann, A. Kallaste, and R. Sell, " Propulsion Motor Drive Topology Selection for Further Development of ISEAUTO Self-Driving Car," IEEE 59th Annu. Int. Sci. Conf. Power Electr. Eng. Riga Tech. Univ., pp. 81-88, 2018.
- [3] R. P. Richner, " Autonomous Vehicles - The next Revolution in Mobility," PhD. Thesis, ETH Zurich, 2011.
- [4] R. Anton, S. Raivo, and L. Mario, "Development case study of first Estonian Self-driving car ISEAUTO," Electrical, Control and Communication Engineering, vol. 14, no. 2, 2018.
- [5] A. Lesuisse, "Development of a Motor Test Bench to Measure Electrical/Mechanical Parameters," 2017.
- [6] A. Rassõlkin, Research and Development of Trial Instrumentation for Electric Propulsion Motor Drives, PhD Thesis, Tallinn University of Technology, 2014.
- [7] Z. Hui, L. Cheng, and Z. Guojiang, "Design of a versatile test bench for hybrid electric vehicles," IEEE Veh. Power Propuls. Conf., pp. 3-6, 2008.
- [8] V. P. D. Reddy and Talasila Pranay Nag, "Design and Analysis of a Two Stage Reduction Gearbox, Master Thesis, VNR Vignana Jyothi Institute of Engineering & Technology, 2018.
- [9] M. Hinterstoißer, B.-R. Höhn, and K. Michaelis, "Optimization of Gearbox Efficiency," Goriva i Maz. časopis za Tribol. Teh. Pod. i Primjen. tekućih i plinovitih goriva i inženjerstvo izgaranja, vol. 48, no. 4, pp. 462-480, 2009.
Available at:
https://www.researchgate.net/publication/228628459_Optimization_of_gearbox_efficiency [Accessed: Feb. 25, 2020]
- [10] C. Daniel and P. Rodrigues, "Design of a high-speed transmission for an electric vehicle," 2018.
- [11] Mitsubishi Technical Support, "Data sheet of Mitsubishi i-Miev," 2011.
- [12] V. B. Bhandari, Design of Machine Elements, New York: McGraw-Hill, vol. 3rd, 2016.
- [13] Navya, "The Navya Autonom Shuttle," 2016.
- [14] J. W. Van Der Wiel, "Automated Shuttles on public roads: Lessons learned," 2016.
- [15] L. Motors, "Olli Safety Report," 2019.

- [16] Ligier, "An Introduction to EZ10," 2018. Transmission: A Review on Performances and Complexities," SAE Int. J. Altern. Powertrains, vol. 7, no. 2m, 2018.
- [17] R. Sell, M. Leier, A. Rassolkin, and J. P. Ernits, "Self-driving car ISEAUTO for research and education," 19th Int. Conf. Res. Educ. Mechatronics, REM 2018, no. August, pp. 111–116, 2018.
- Available at:
https://www.researchgate.net/publication/325683320_Self-driving_car_ISEAUTO_for_research_and_education [Accessed: Feb. 15, 2020]
 [Accessed: Feb. 19, 2020]
- [18] S. Simon, "Sevcon Gen4 Size 8 Application Reference Manual," 2011.
- [19] Dutchi Motor Technical Stuff, "Series DM1," 2008.
- Available at: <http://www.marathon-electric.ru/DM1.pdf> [Accessed: Jan. 23, 2020]
- [20] Magna-Power Technical Stuff, "TS Series," 2019.
- Available at: https://magna-power.com/assets/docs/html_ts/index-prodinfo.html#id2
 [Accessed: Jan. 23, 2020]
- [21] D. Huang, "Characteristics of torsional vibrations of a shaft system with parallel misalignment," Proc. Inst. Mech. Eng. Part C J. Mech. Eng. Sci., vol. 219, no. 11, pp. 1219–1224.
- [22] A. Rassolkin, L. Gevorkov, T. Vaimann, A. Kallaste, and R. Sell, "Calculation of the traction effort of ISEAUTO self-driving vehicle," 2018 25th Int. Work. Electr. Drives Optim. Control Electr. Drives, IWED 2018 - Proc, pp. 1–5, 2018.
- [23] C. M. C. G. Fernandes, P. M. T. Marques, R. C. Martins, and J. H. O. Seabra, "Influence of gear loss factor on the power loss prediction," Mech. Sci., vol. 6, no. 2, pp. 81–88, 2015.
- Available at: <https://www.mech-sci.net/6/81/2015/> [Accessed: Feb. 20, 2020]
- [24] H. Ohlendorf, "Verlustleistung und Erwärmung von Stirnrädern," PhD thesis, Dissertation TU München, Munich, 1958.
- [25] G. Niemann, and H. Winter, Band 2: Getriebe allgemein, Zahnradgetriebe - Grundlagen, Stirnradgetriebe, Munich: Springer , 1989.
- [26] E. Buckingham, Analytical Mechanics of Gears, New York: Dover Publications, 1959.
- Available at:
<https://ia801604.us.archive.org/9/items/in.ernet.dli.2015.212458/2015.212458.Analytical-Mechanics.pdf> [Accessed: Feb. 27, 2020]
- [27] J. D. De Gevigney, F. Ville, C. Changenet, and P. Velex, "Tooth friction losses in internal gears: Analytical formulation and applications to planetary gears," Proc. Inst. Mech. Eng. Part J J. Eng. Tribol., vol. 227, no. 5, pp. 476–485, 2013.

- [28] A. J. Wimmer, "Lastverluste von Stirnradverzahnungen", PhD thesis, Fakultät für Maschinenwesen der Technischen Universität München, Munich, 2006.
Available at: <https://archive.org/details/in.ernet.dli.2015.212458/page/n23/mode/2up>
- [29] R. G. Budynas and J. K. Nisbett, Mechanical Engineering Design, New York: McGraw-Hill, 2011.
Available at: <https://www.engineeringbookspdf.com/shigleys-mechanical-engineering-design/> [Accessed: Feb. 28, 2020]
- [30] SKF Technical Support, Rolling Bearings, Gothenburg, 2018.
Available at: <https://www.skf.com/binaries/307-299767/0901d1968065e9e7-The-SKF-model-for-calculating-the-frictional-movement.pdf> [Accessed: Feb. 28, 2020]
- [31] C. Changenet and M. Pasquier, "Power losses and heat exchange in reduction gears: Numerical and experimental results," VDI Berichte, vol. 2, no. 1665, pp. 603–613, 2002.
- [32] C. Changenet and A. Heckly, "Rendement et comportement thermique d'une boîte de vitesses à cinq rapports", 4th world congress on gearing and power transmission, Paris, 1999.
- [33] William D. Callister, Materials Science and Engineering: An Introduction, John Wiley & Sons, vol. 7th, 2007.
- [34] A. Rassölkin, A. Kallaste, and T. Vaimann, "Dynamic control system for electric motor drive testing on the test bench," Int. Conf. Compat. Power Electron. CPE 2015, pp. 252–257, 2015.
- [35] (ISO) International Standards Organisation, "Industrial Lubricant Classifications", vol. 1, no. 724, pp. 776–790, 2002.
- [36] R. Errichello, "Lubrication of Gears", Lubrication Engineering vol. 119, no. 2, pp. 187–189, 2010.

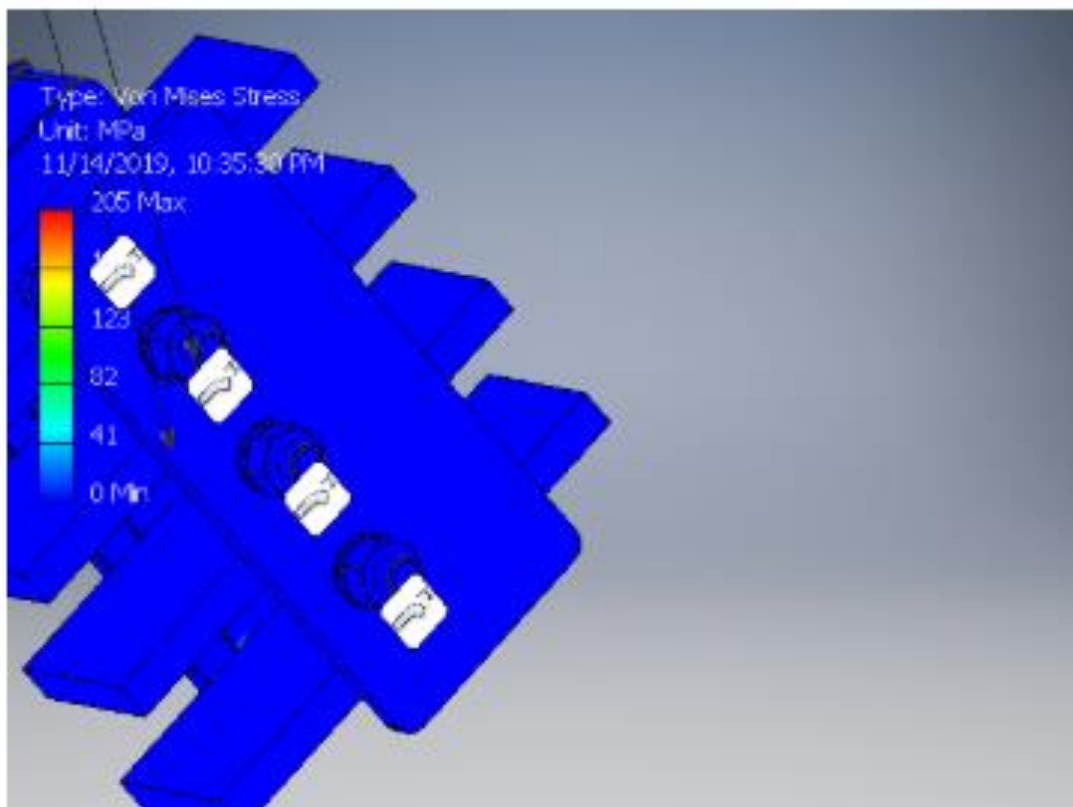
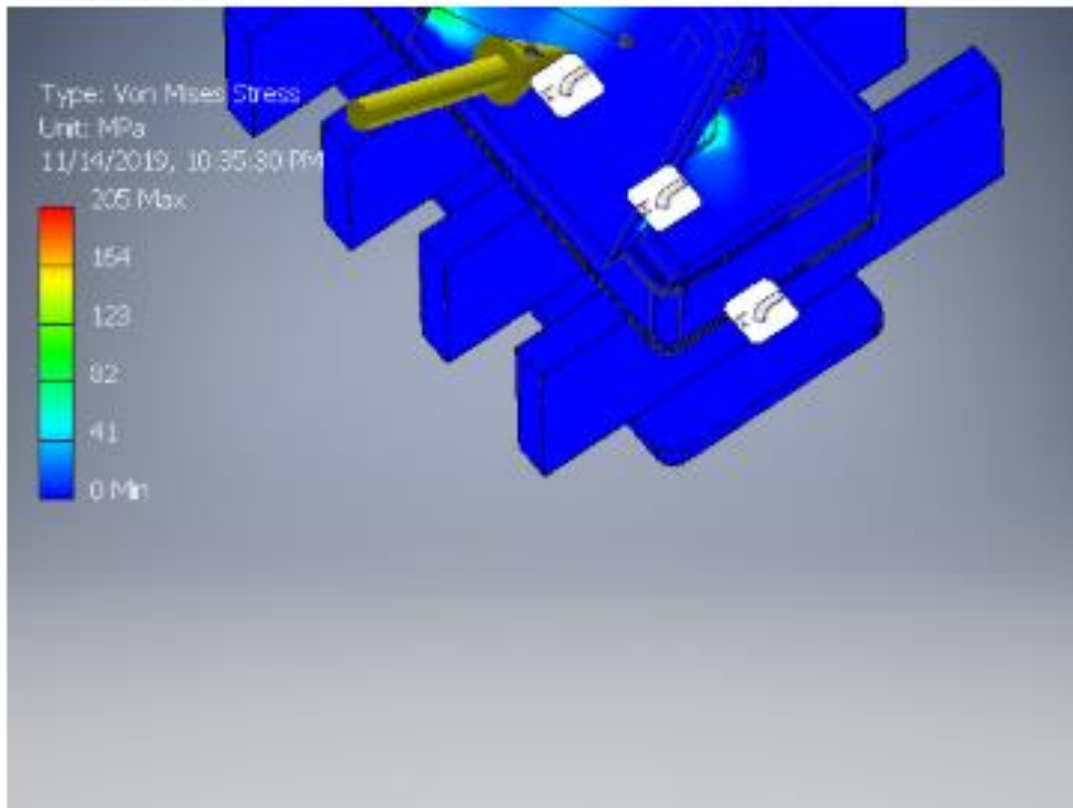
APPENDICES

A.1. The Solid Model and the Actual Rear Mounting Part



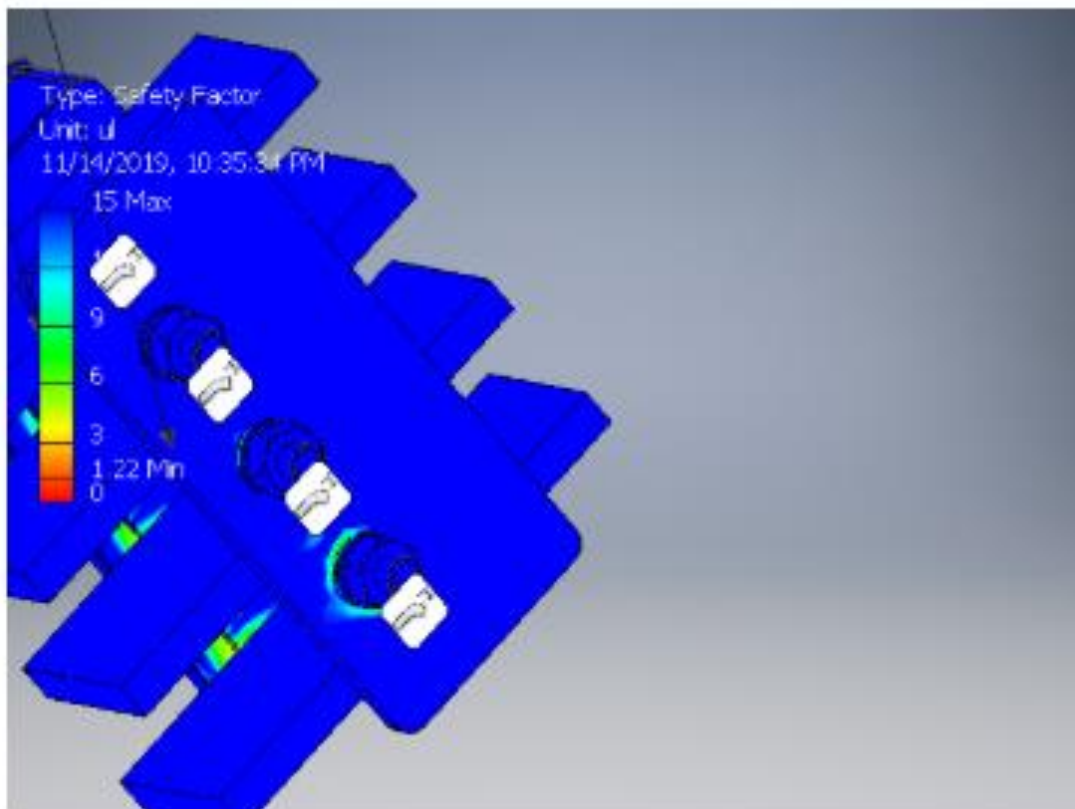
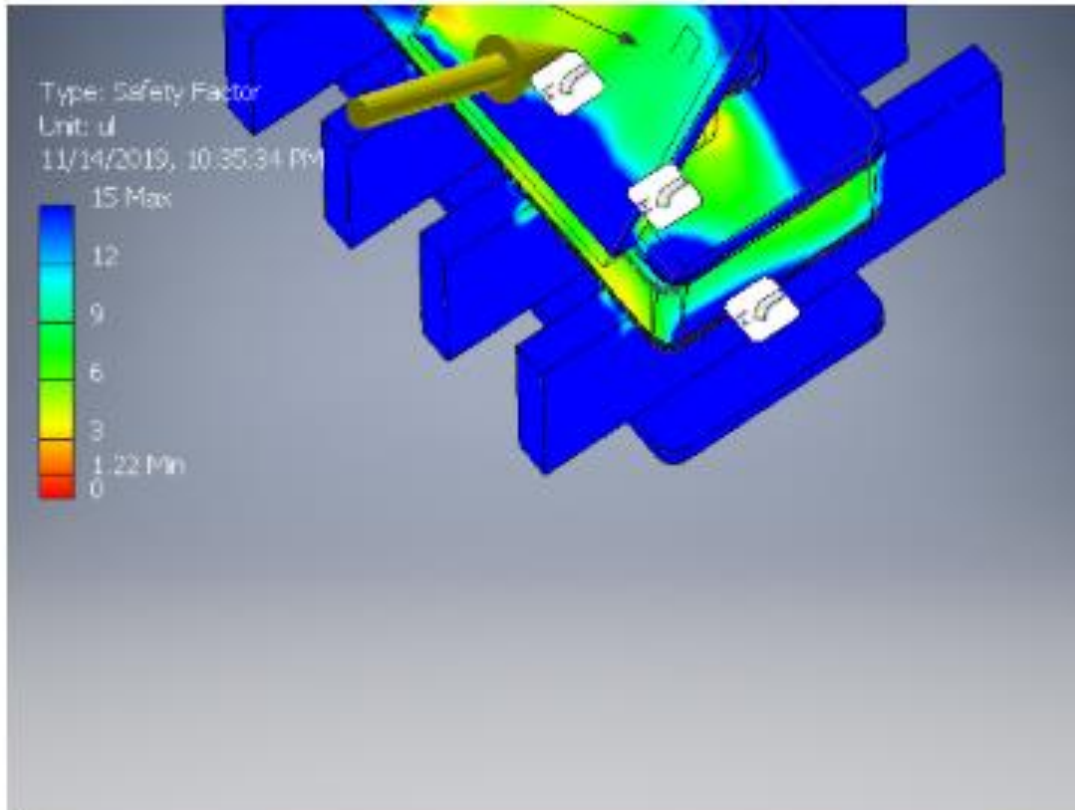
A.2. Stress Analysis of Rear Mounting Part

☐ Von Mises Stress

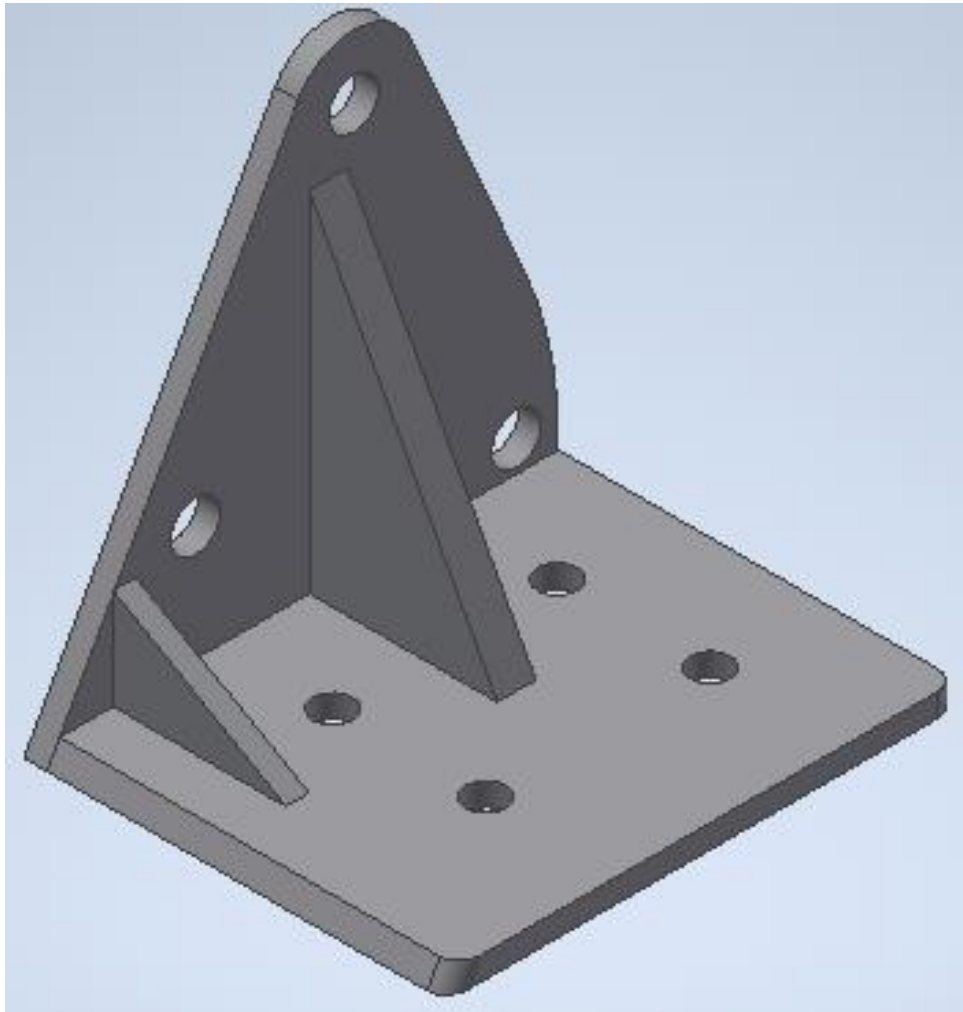


A.3. Safety Analysis of Rear Mounting Part

☐ Safety Factor

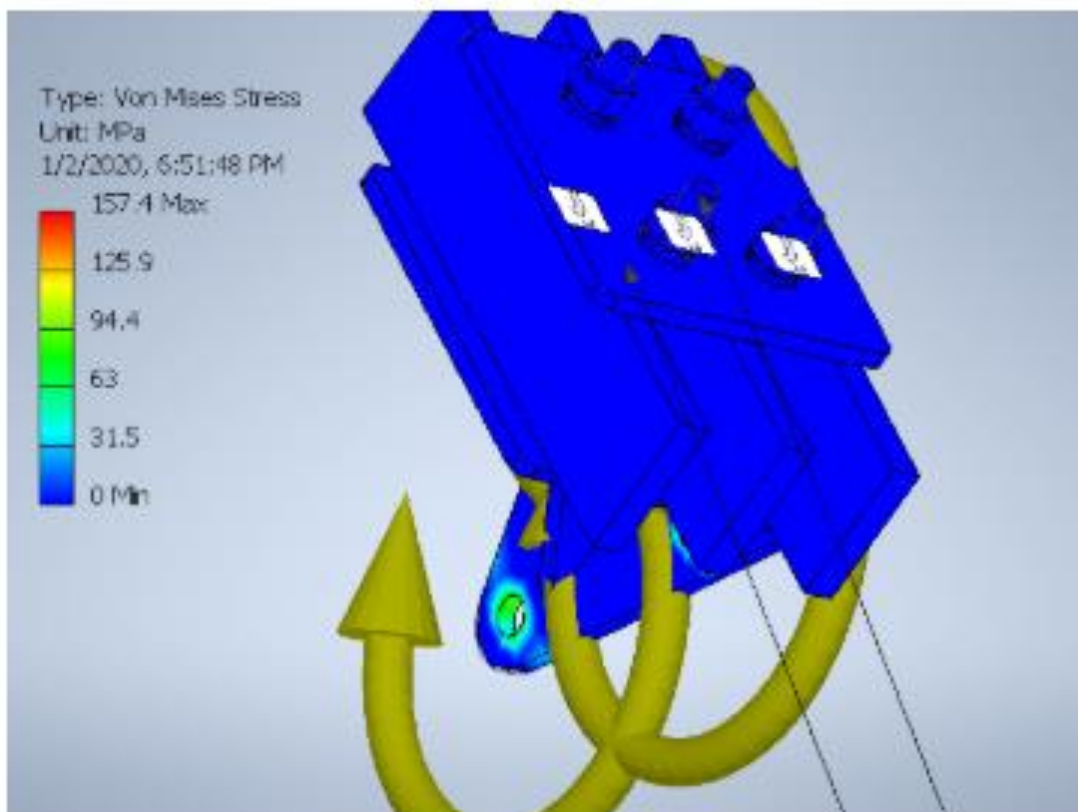
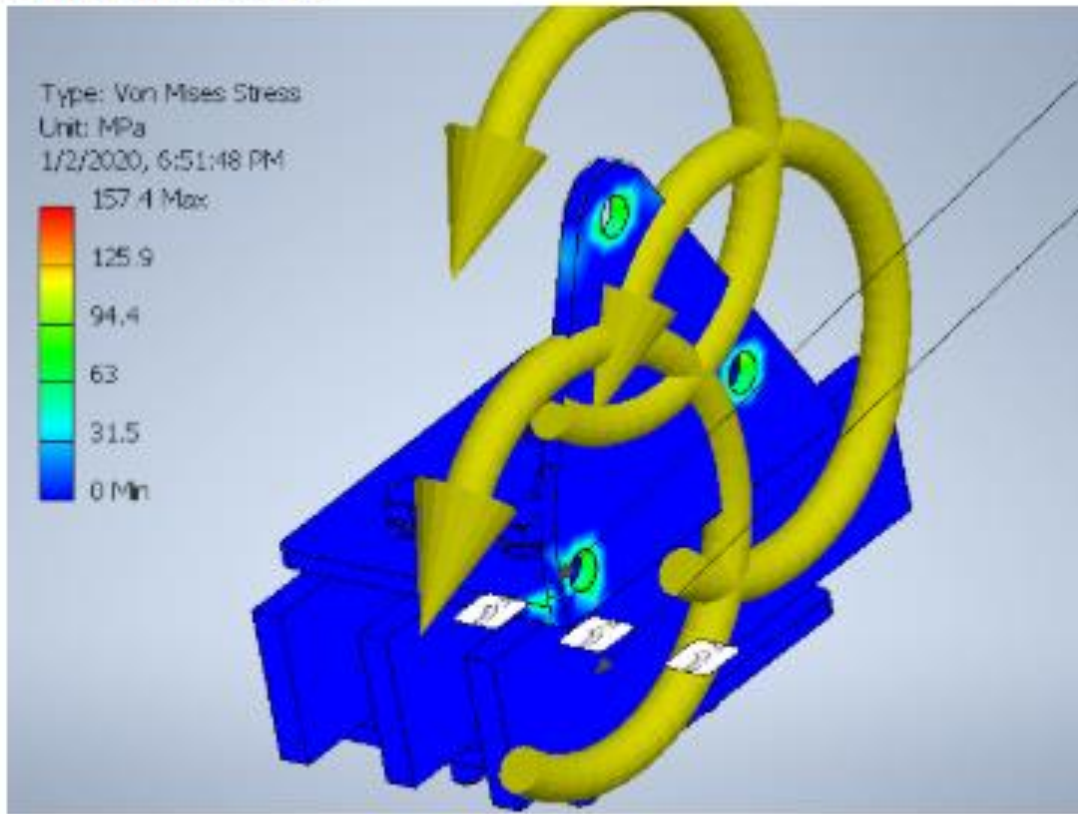


A.4. The Solid Model and the Actual Front Mounting Part



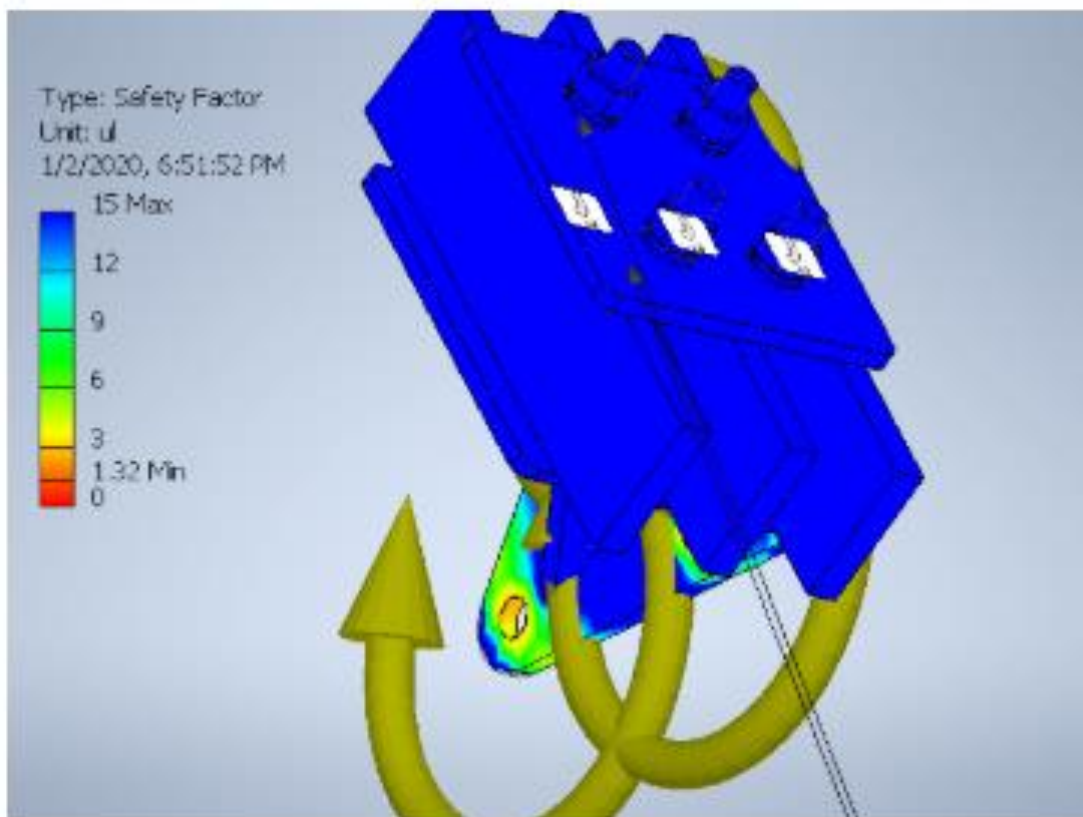
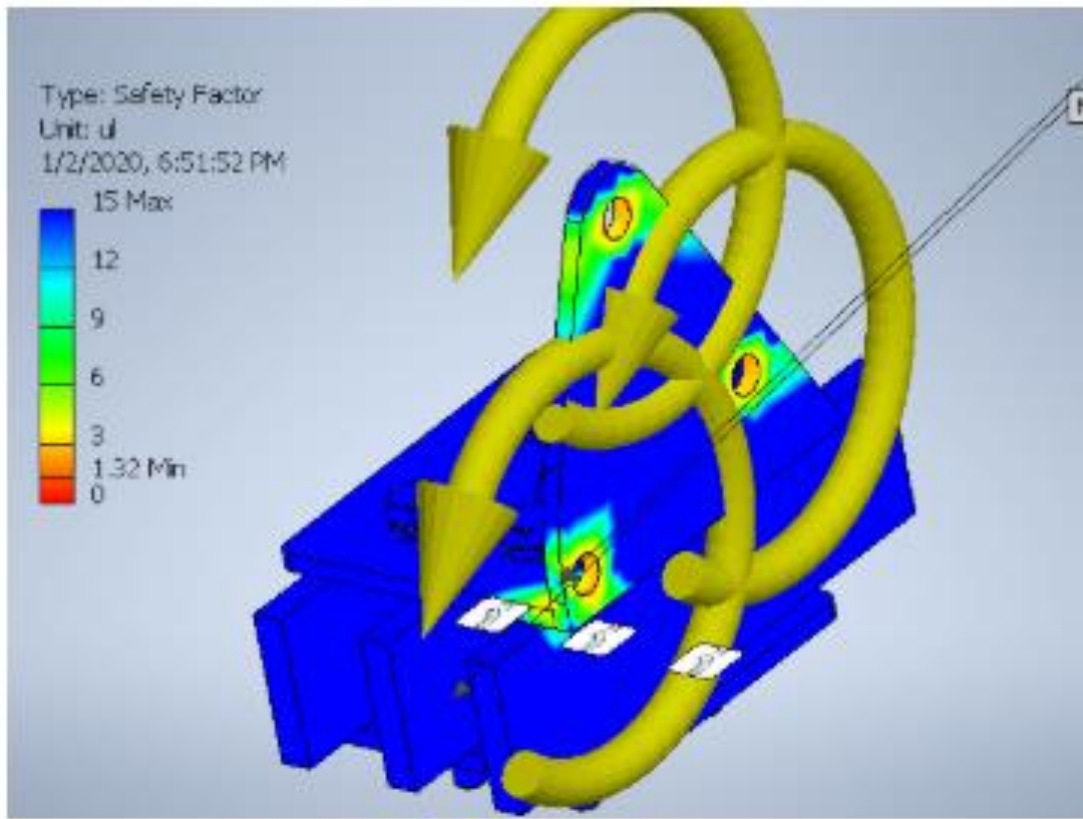
A.5. Stress Analysis of Front Mounting Part

☐ Von Mises Stress

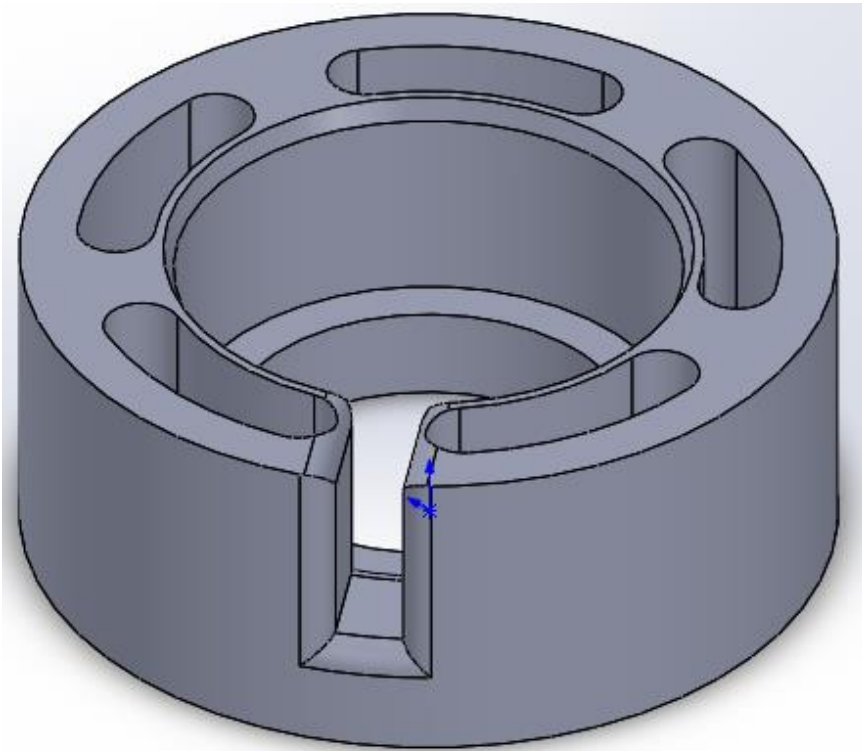


A.6. Safety Analysis of Front Mounting Part

☐ Safety Factor



A.7. The Solid Model and the Manufactured Resolver



A.8. BOM Drawing of the Rear Mounting Part

Part Number	Part Name	Quantity	Material
01	Hex Head Bolt M10x120	3	SS316
02	Spring Washer M10	6	SS316
03	Plain Waher M10	6	SS316
04	Rear Mounting Part	1	St37
05	Rubber Block	1	Si
06	Rear Mounting Bottom Plate for Mounting	1	St37
07	Nut M10	3	SS316

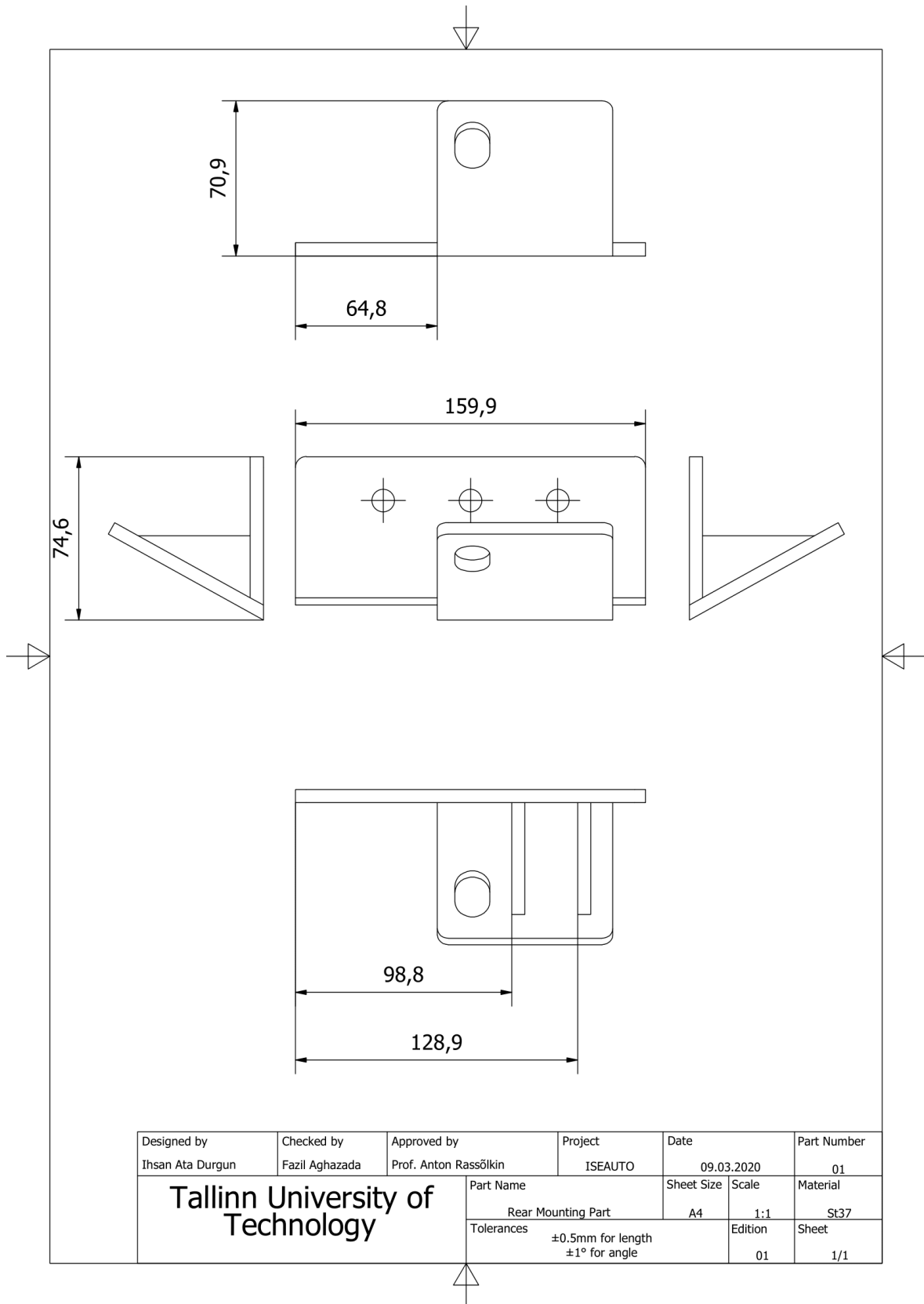
Designed by	Checked by	Approved by	Project	Date	Part Number	
Ihsan Ata Durgun	Fazil Aghazada	Prof. Anton Rassölkin	ISEAUTO	09.03.2020	-	
Tallinn University of Technology			Part Name	Sheet Size	Scale	Material
			Rear Mounting Part	A4	1:2	-
			Tolerances	-		Edition
				01	1/1	

A.9. Assemble Drawing of the Rear Mounting Part

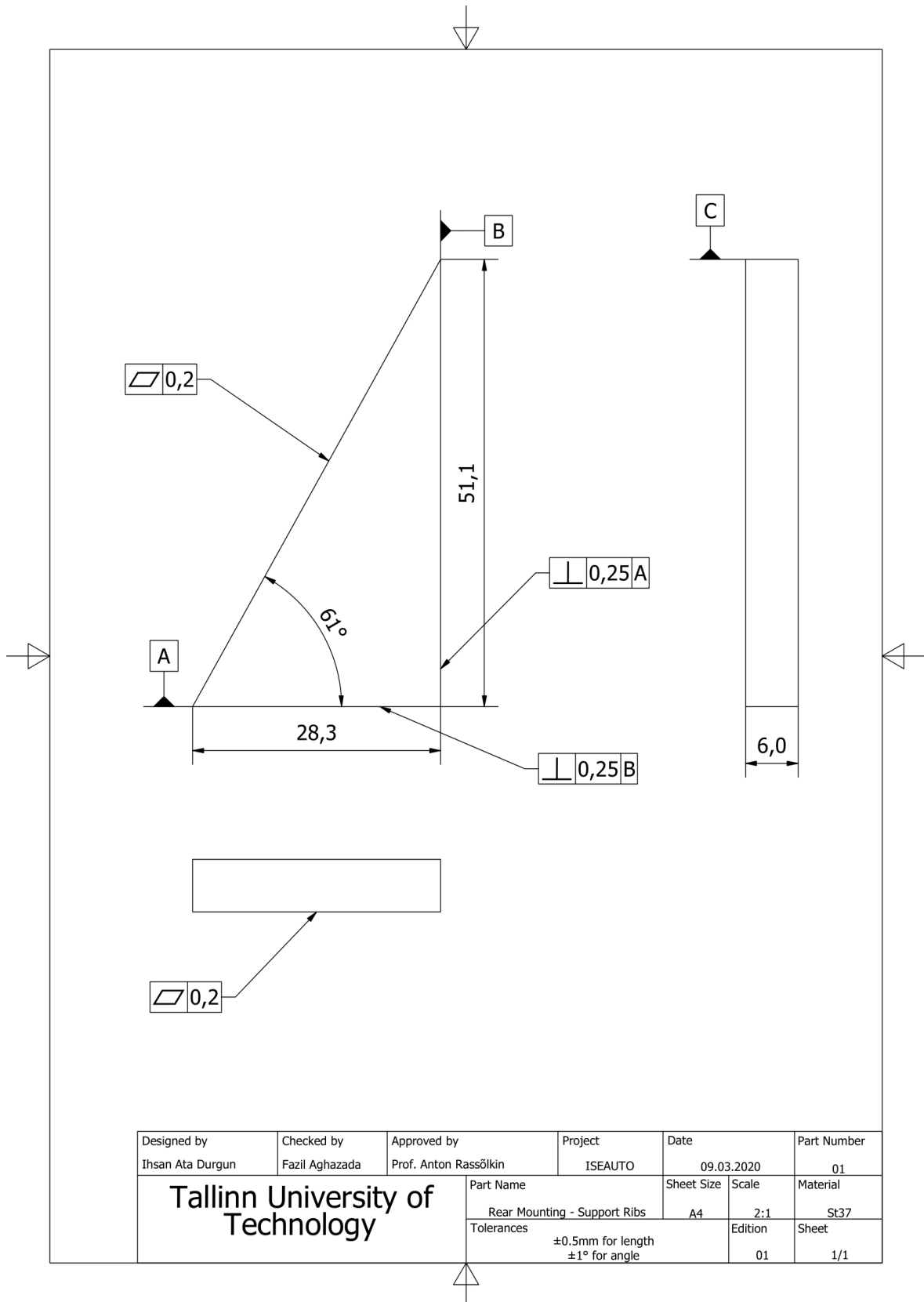
Part Number	Part Name	Quantity	Material
01	Rear Mounting - Support Ribs	2	S137
02	Rear Mounting Bottom Plate	1	S137
03	Rear Mounting Top Plate	1	S137

Designed by	Insan Ata Durgun	Checked by	Fazil Aghazada	Approved by	Prof. Anton Rassolkin	Project	ISEFAUTO	Date	09.03.2020	Part Number	-
Tallinn University of Technology		Part Name	Rear Mounting Part	Sheet Size	A4	Scale	1:1	Material	-	Edition	01
		Tolerances	-	Sheet	1/1						

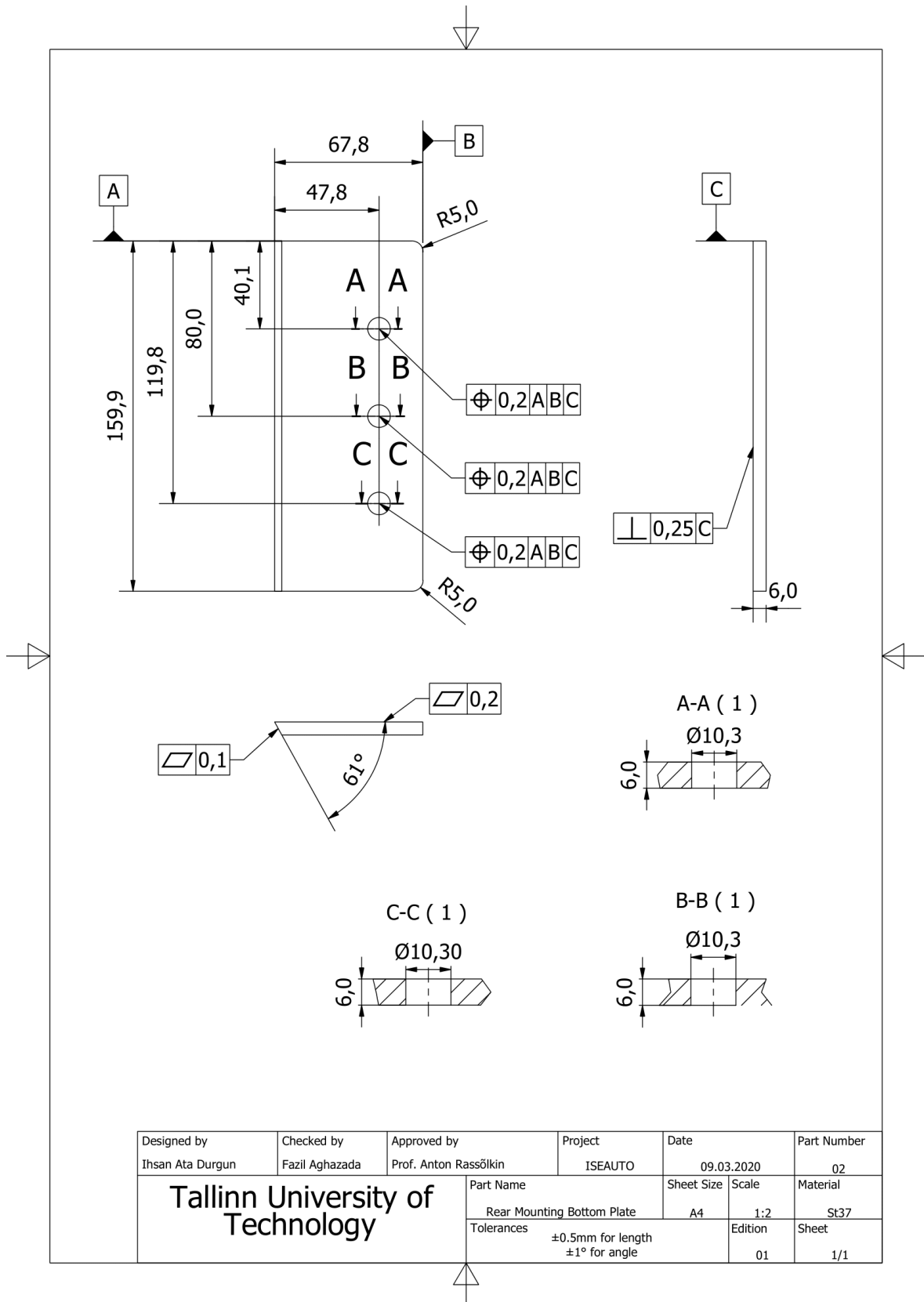
A.10. Technical Drawing of Rear Mounting Part



A.11. Technical Drawing of the Support Rib for Rear Mounting Part

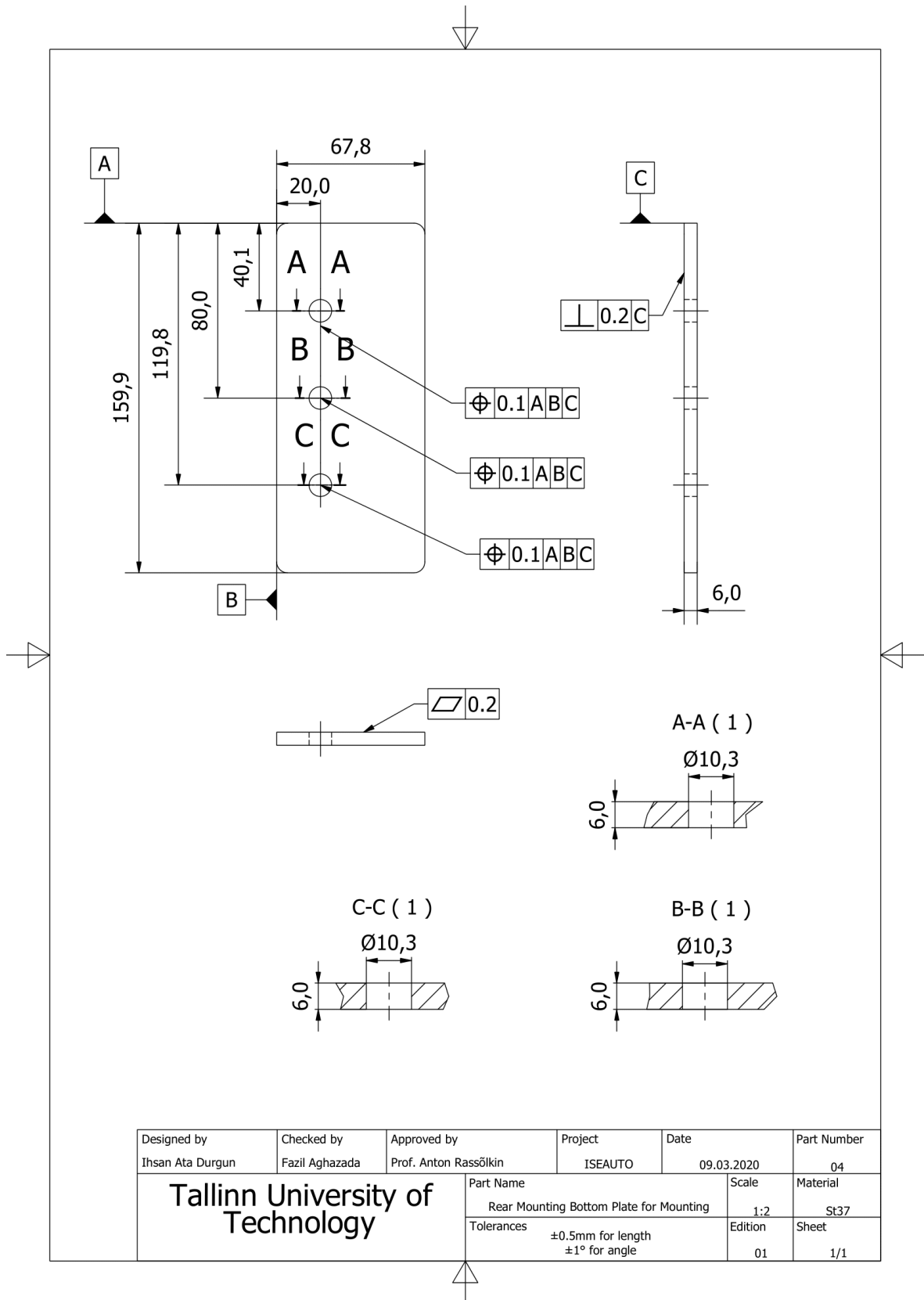


A.12. Technical Drawing of the Bottom Plate of Rear Mounting Part

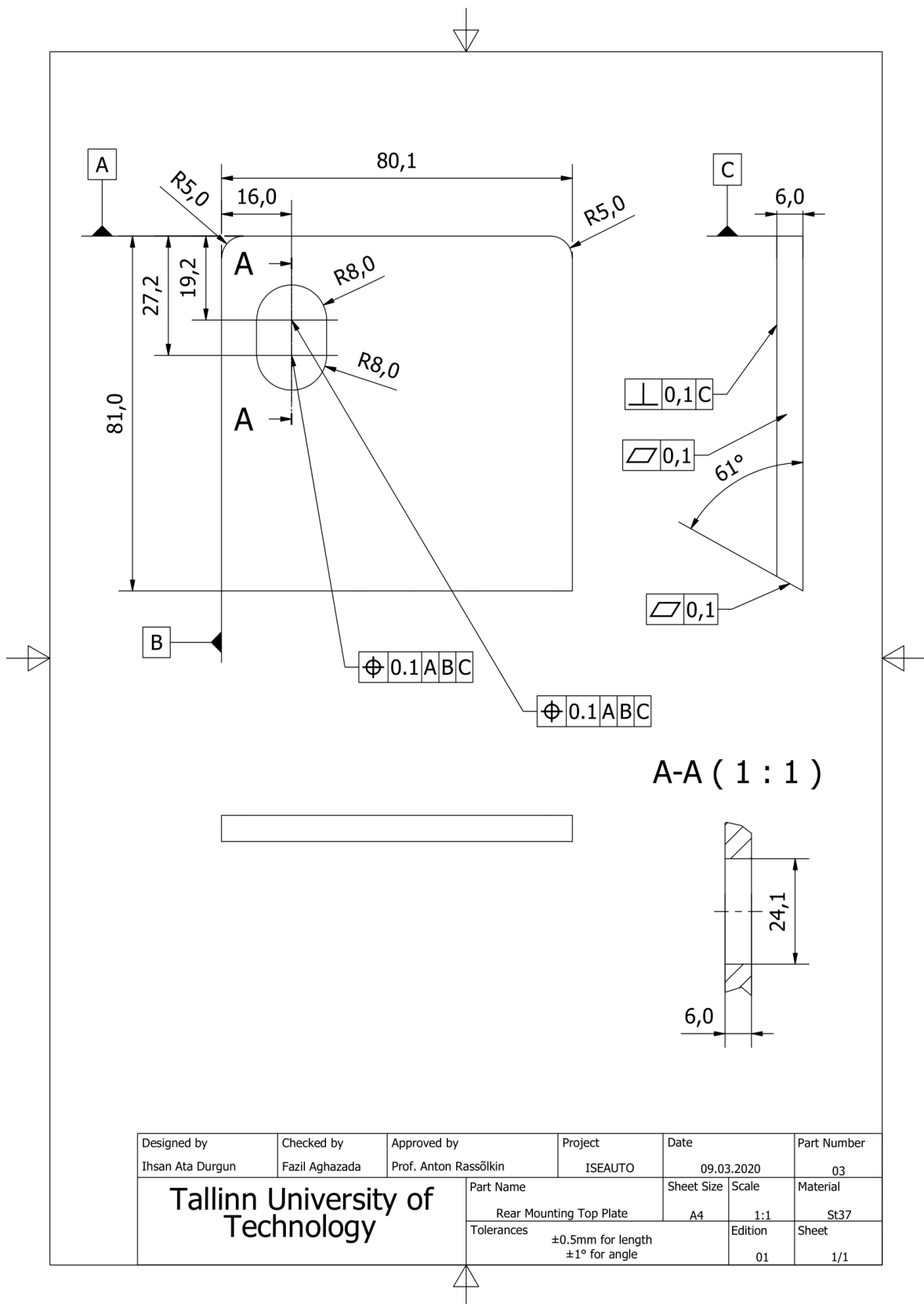


Designed by Ihsan Ata Durgun	Checked by Fazil Aghazada	Approved by Prof. Anton Rassõlkin	Project ISEAUTO	Date 09.03.2020	Part Number 02		
Tallinn University of Technology			Part Name Rear Mounting Bottom Plate	Sheet Size A4	Scale 1:2	Material St37	
			Tolerances ±0.5mm for length ±1° for angle			Edition 01	Sheet 1/1

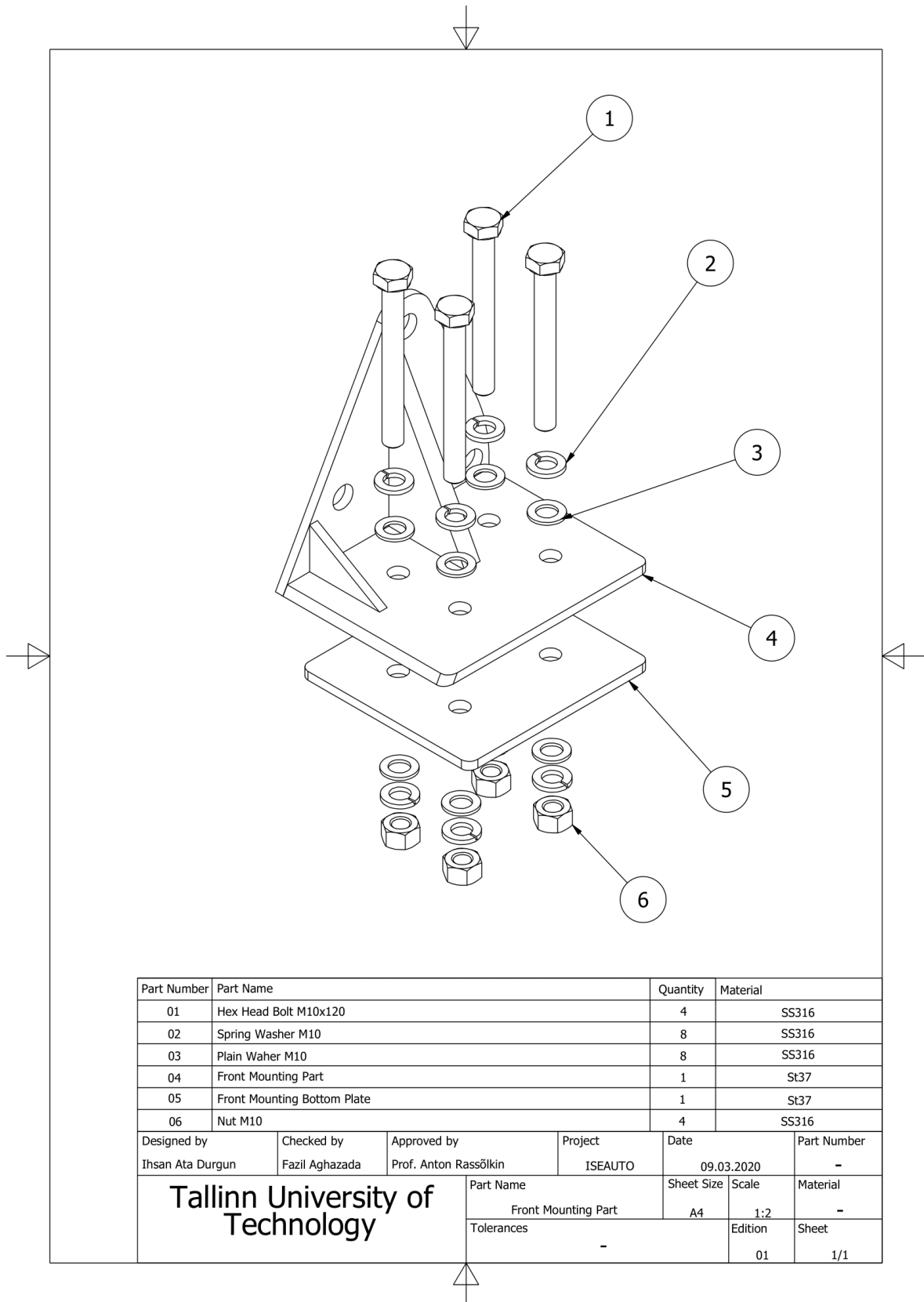
A.13. Technical Drawing of the Plate for Mounting Rear Mounting Part on TB



A.14. Technical Drawing of the Upper Plate of Rear Mounting Part



A.15. BOM Drawing of Front Mounting Part

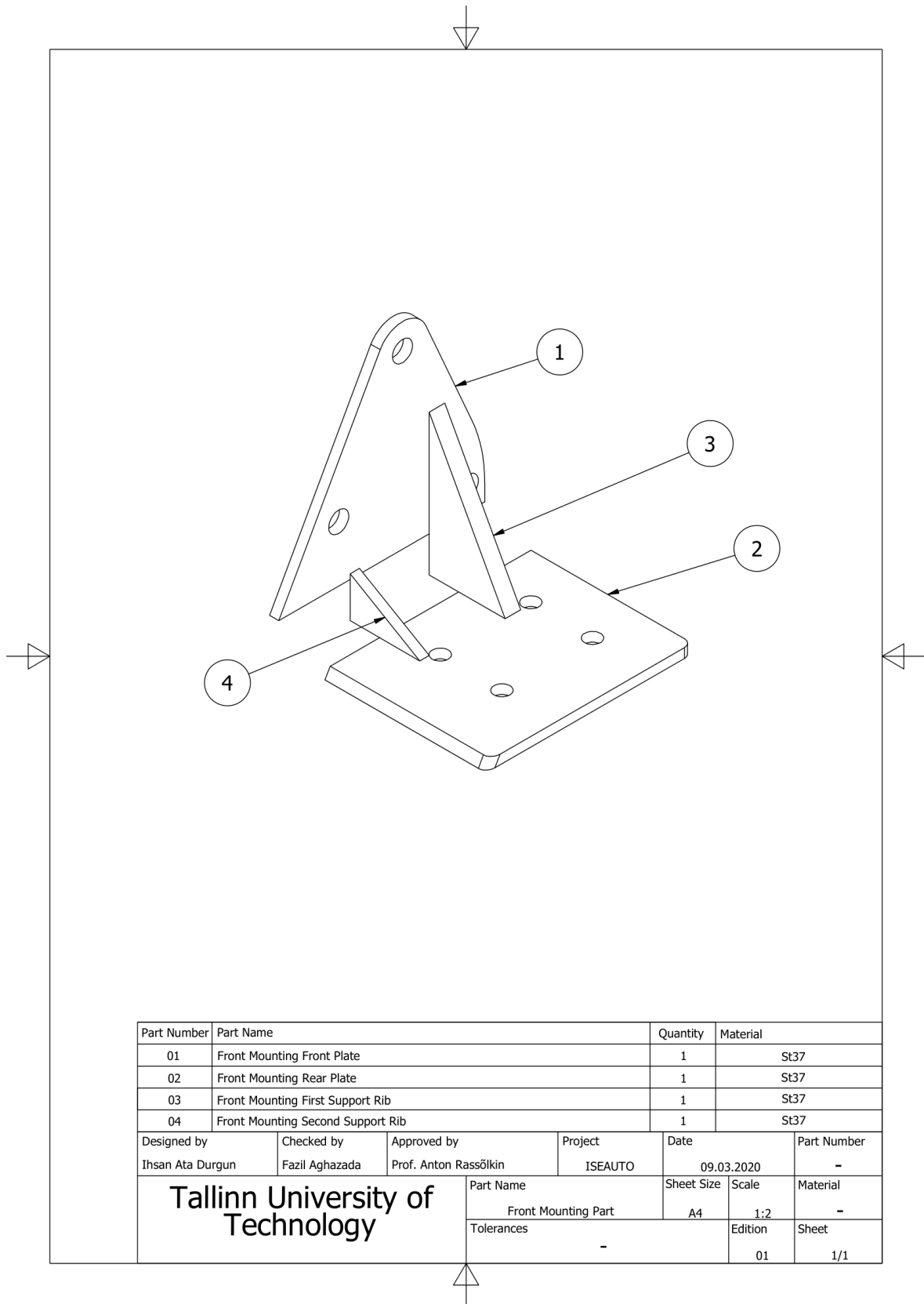


Part Number	Part Name	Quantity	Material
01	Hex Head Bolt M10x120	4	SS316
02	Spring Washer M10	8	SS316
03	Plain Washer M10	8	SS316
04	Front Mounting Part	1	St37
05	Front Mounting Bottom Plate	1	St37
06	Nut M10	4	SS316

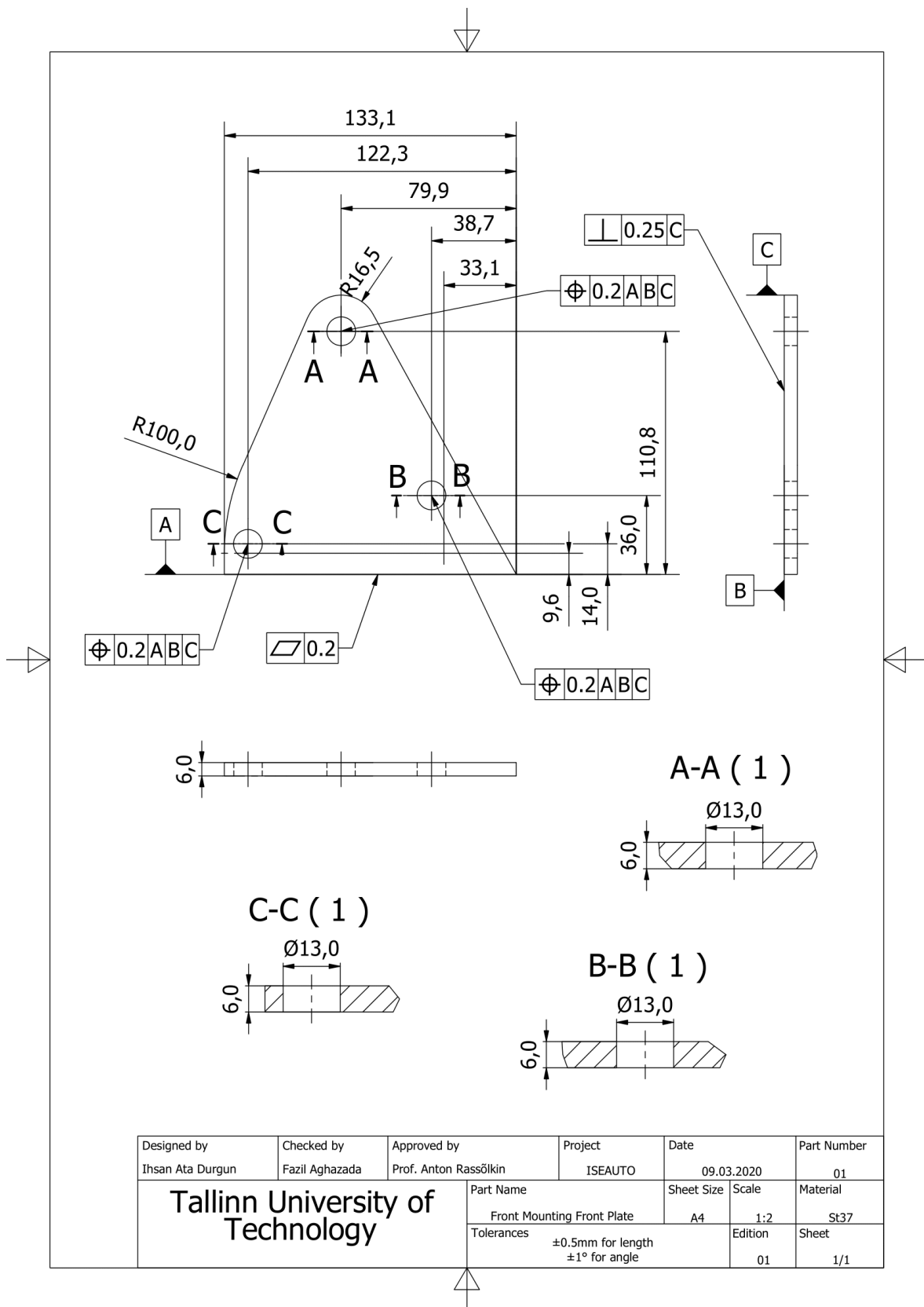
Designed by	Checked by	Approved by	Project	Date	Part Number
Ihsan Ata Durgun	Fazil Aghazada	Prof. Anton Rassõlkin	ISEAUTO	09.03.2020	-

Tallinn University of Technology	Part Name	Sheet Size	Scale	Material
	Front Mounting Part	A4	1:2	-
	Tolerances	-		Edition
				01
				1/1

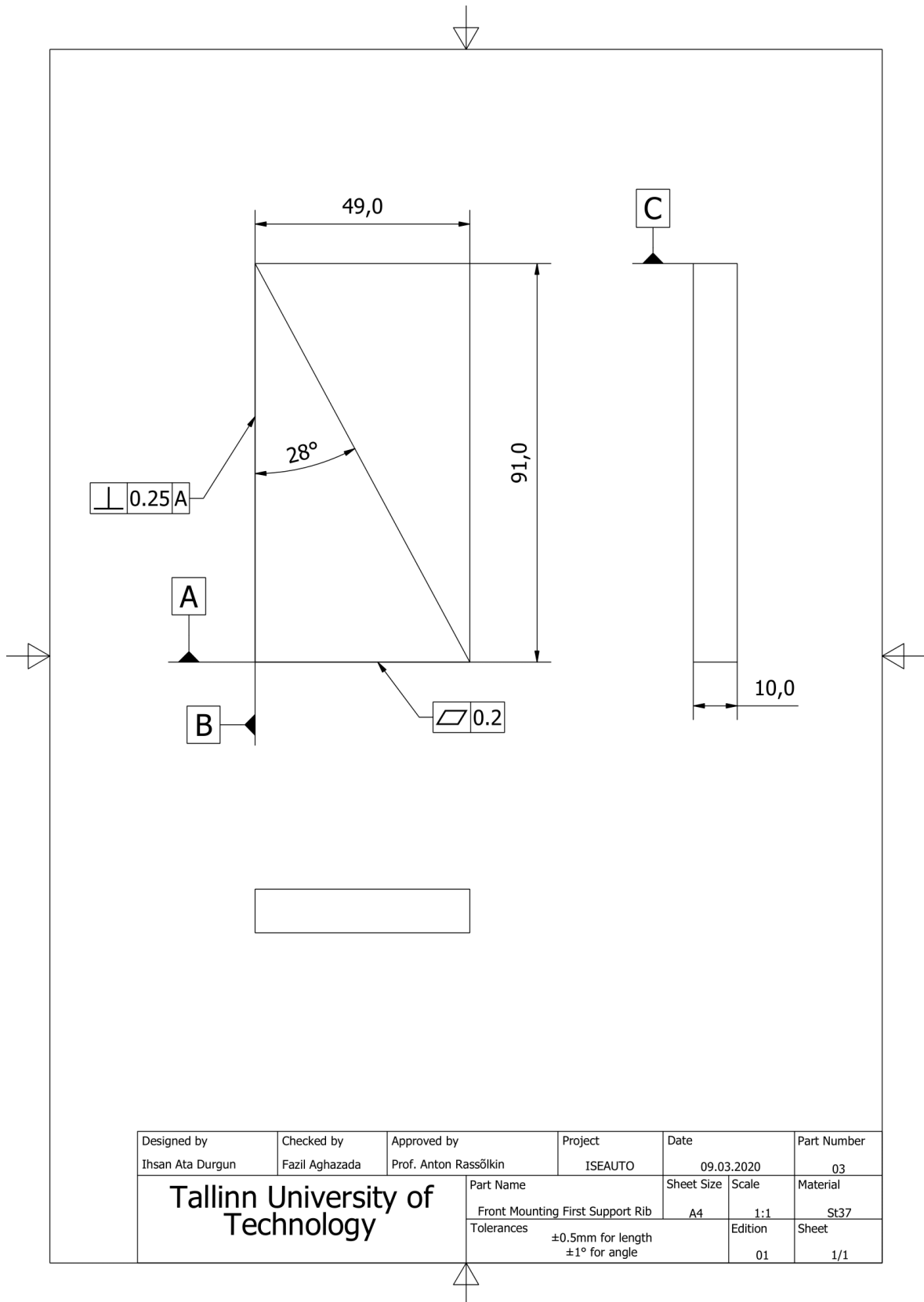
A.16. Assemble Drawing of the Front Mounting Part



A.18. Technical Drawing of the Front Plate Front Mounting Part

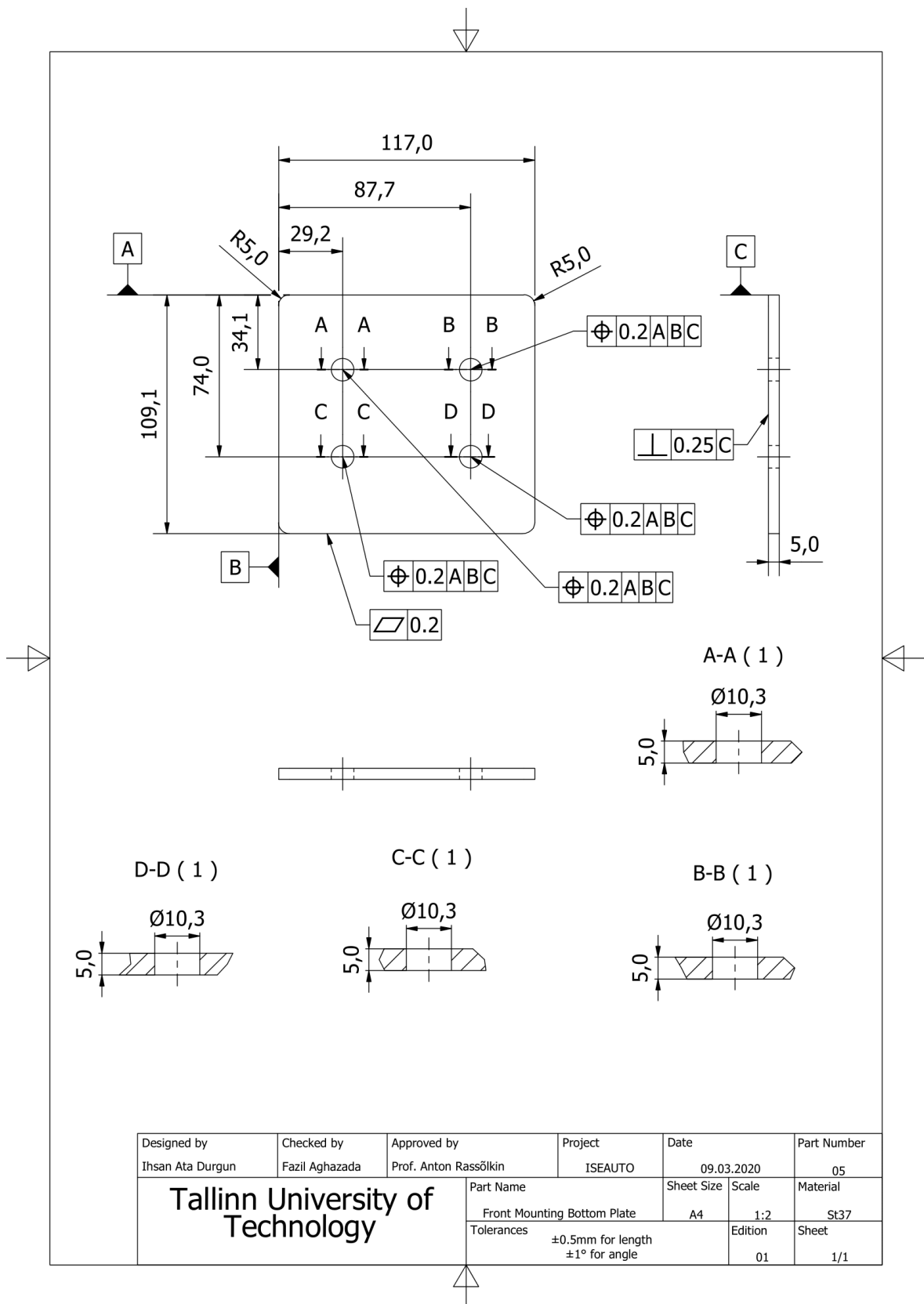


A.20. Technical Drawing of First Support Rib of Front Mounting Part



Designed by Ihsan Ata Durgun	Checked by Fazil Aghazada	Approved by Prof. Anton Rassõlkin	Project ISEAUTO	Date 09.03.2020	Part Number 03	
Tallinn University of Technology			Part Name Front Mounting First Support Rib	Sheet Size A4	Scale 1:1	Material St37
			Tolerances ±0.5mm for length ±1° for angle		Edition 01	Sheet 1/1

A.22. Technical Drawing of the Plate for Mounting Front Mounting Part on TB



Designed by Ihsan Ata Durgun	Checked by Fazil Aghazada	Approved by Prof. Anton Rassõlkin	Project ISEAUTO	Date 09.03.2020	Part Number 05	
Tallinn University of Technology			Part Name Front Mounting Bottom Plate	Sheet Size A4	Scale 1:2	Material St37
			Tolerances ±0.5mm for length ±1° for angle		Edition 01	Sheet 1/1

A.23. Tables for Pinion and Gear Design

Table A.23.1 Table for Service Factor (C_s) Selection [12]

<i>Working characteristics of Driving machine (Table 17.5)</i>	<i>Working characteristics of Driven machine (Table 17.6)</i>		
	<i>Uniform</i>	<i>Moderate shock</i>	<i>Heavy shock</i>
Uniform	1.00	1.25	1.75
Light shock	1.25	1.50	2.00
Medium shock	1.5	1.75	2.25

<i>Characteristic of operation</i>	<i>Driving machines</i>
Uniform	Electric motor, steam turbine, gas turbine
Light shock	Multi-cylinder internal combustion engine
Medium shock	Single cylinder internal combustion engine

<i>Characteristic of operation</i>	<i>Driven machines</i>
Uniform	Generator, belt conveyor, platform conveyor, light elevator, electric hoist, feed gears of machine tools, ventilators, turbo-blower, mixer for constant density material
Medium shock	Main drive to machine tool, heavy elevator, turning gears of crane, mine ventilator, mixer for variable density material, multi-cylinder piston pump, feed pump
Heavy shock	Press, shear, rubber dough mill, rolling mill drive, power shovel, heavy centrifuge, heavy feed pump, rotary drilling apparatus, briquette press, pug mill

Table A.23.2 Table for Defening Tooth Geometry Parameters Depend on Pressure Angle [12]

	<i>14.5° full depth system</i>	<i>20° full depth system</i>	<i>20° stub system</i>
Pressure angle	14.5°	20°	20°
Addendum	m	m	0.8 m
Dedendum	1.157 m	1.25 m	m
Clearance	0.157 m	0.25 m	0.2 m
Working depth	2 m	2 m	1.6 m
Whole depth	2.157 m	2.25 m	1.8 m
Tooth thickness	1.5708 m	1.5708 m	1.5708 m

Table A.23.3 Table for Material Selection [29]

Pinion Material	Pinion Modulus of Elasticity E_p , psi (MPa)*	Gear Material and Modulus of Elasticity E_g , lbf/in ² (MPa)*					
		Steel 30×10^6 (2×10^5)	Malleable Iron 25×10^6 (1.7×10^5)	Nodular Iron 24×10^6 (1.7×10^5)	Cast Iron 22×10^6 (1.5×10^5)	Aluminum Bronze 17.5×10^6 (1.2×10^5)	Tin Bronze 16×10^6 (1.1×10^5)
Steel	30×10^6 (2×10^5)	2300 (191)	2180 (181)	2160 (179)	2100 (174)	1950 (162)	1900 (158)
Malleable iron	25×10^6 (1.7×10^5)	2180 (181)	2090 (174)	2070 (172)	2020 (168)	1900 (158)	1850 (154)
Nodular iron	24×10^6 (1.7×10^5)	2160 (179)	2070 (172)	2050 (170)	2000 (166)	1880 (156)	1830 (152)
Cast iron	22×10^6 (1.5×10^5)	2100 (174)	2020 (168)	2000 (166)	1960 (163)	1850 (154)	1800 (149)
Aluminum bronze	17.5×10^6 (1.2×10^5)	1950 (162)	1900 (158)	1880 (156)	1850 (154)	1750 (145)	1700 (141)
Tin bronze	16×10^6 (1.1×10^5)	1900 (158)	1850 (154)	1830 (152)	1800 (149)	1700 (141)	1650 (137)

Table A.23.4 Table of Gear Parameters

Parameter (Symbol, Unit)	1 st -Stage	2 nd -Stage	3 rd -Stage
Gear ratio (n , constant)	2,55	2,53	2,5
Pressure angle (α , deg)	20	20	20
The number of teeth of the pinion (Z_1 , constant)	18	18	18
The number of teeth of the pinion (Z_2 , constant)	46	46	45
Power of the motor (P , W)	25000	-	-
Rotational speed of the pinion (N , rpm)	3000	1177	465
Transmitted torque (MT , Nm)	79,58	202,93	513,41
Lewis form factor of the pinion (Y_1 , constant)	0,33	0,33	0,33
Lewis form factor of the gear (Y_2 , constant)	0,42	0,42	0,42
Module (m , mm)	3,49	4,74	6,46
The pitch circle diameter of the pinion (d_1 , mm)	62,82	85,32	116,28
The pitch circle diameter of the gear (d_2 , mm)	160,54	218,04	290,7
The center distance of the pinion and the gear (a , mm)	128,96	175,15	234,97
Face width (b , mm)	32	43	58
Tangential force (F_t , N)	2533,59	4756,92	8830,58
Radial force (F_r , N)	1064,81	1999,22	3711,29
Axial force (F_a , N)	1462,77	2746,41	5098,34
Helix angle (ψ , deg)	30	30	30
Beam strength of the pinion (S_{b1} , N)	4576,58	8582,45	15941,47
Beam strength of the gear (S_{b2} , N)	5824,74	10923,12	20289,15
Bending stress (σ_b , MPa)	124,18	127,6	128,93
Service factor (C_s , constant)	1	1	1
Velocity factor (C_v , constant)	0,64	0,69	0,74
The pitch line velocity (v , m/s)	9,74	6,47	3,77
Bending moment (M_b , Nmm)	19888	50756	128396
Tooth length (h , mm)	7,85	10,67	14,54
Moment of inertia around the neural axis (I , mm ⁴)	438,84	1481,69	5054,11
Tooth thickness (t , mm)	5,48	7,45	10,15
Effective load (F_{eff} , N)	3958,73	6894,09	11933,22
Wear strength (S_w , N)	4874,08	9157,23	12948,94
The ratio factor (Q , constant)	1,44	1,44	1,44
Load stress factor (K , N/mm ²)	1,26	1,3	1,31
Module of elasticity of the pinion (E_1 , N/mm ²)	30×10^6	30×10^6	30×10^6
Module of elasticity of the gear (E_2 , N/mm ²)	30×10^6	30×10^6	30×10^6
Surface endurance strength (σ_c , MPa)	9074,76	9204,37	9249,52

Normal force (F_n , N)	2696,19	5062,21	9397,31
Radius of curvature of the pinion (r_1 , mm)	10,74	14,59	19,89
Radius of curvature of the gear (r_2 , mm)	27,45	37,29	49,71

Table A.23.5 Table of Yield Strength & Tensile Strength Values for Stainless Steel [33]

Yield Strength, Tensile Strength and Ductility Values for Stainless Steels			
Material	Yield Strength	Tensile Strength	% Elong.
	MPa (ksi)	MPa (ksi)	
Stainless Steel Alloy 304 Hot finished and annealed	205 (30) (min)	515 (75) (min)	40 (min)
Stainless Steel Alloy 304 Cold worked (1/4 Hard)	515 (75) (min)	860 (125) (min)	10 (min)
Stainless Steel Alloy 316 Hot finished and annealed	205 (30) (min)	515 (75) (min)	40 (min)
Stainless Steel Alloy 316 Cold drawn and annealed	310 (45) (min)	620 (90) (min)	30 (min)
Stainless Steel Alloy 405 Annealed	170 (25)	415 (60)	20
Stainless Steel Alloy 440A Annealed	415 (60)	725 (105)	20

Table A.22.6 Table of Shaft Parameters

Parameter (Symbol, Unit)	1 st -Shaft	2 nd -Shaft	3 rd -Shaft	4 th -Shaft
Maximum torsional shear stress (τ_{max} , MPa)	34,17	34,17	34,17	34,17
Yield Strength (S_y , MPa)	205	205	205	205
Safety factor (f , constant)	3	1,25	1,25	1,25
Transmitted torque (M_t , Nm)	79,58	202,93	513,41	1283,53
Shaft Diameter (d , mm)	35	45	55	60

Table A.23.7 Table of Bearing Life [30]

Guideline values of specification life for different machine types	
Machine type	Specification life Operating hours
Household machines, agricultural machines, instruments, technical equipment for medical use	300 ... 3 000
Machines used for short periods or intermittently: electric hand tools, lifting tackle in workshops, construction equipment and machines	3000 ... 8 000
Machines used for short periods or intermittently where high operational reliability is required: lifts (elevators), cranes for packaged goods or slings of drums, etc.	8 000 ... 12 000
Machines for use 8 hours a day, but not always fully utilized: gear drives for general purposes, electric motors for industrial use, rotary crushers	10 000 ... 25 000
Machines for use 8 hours a day and fully utilized: machine tools, woodworking machines, machines for the engineering industry, cranes for bulk materials, ventilator fans, conveyor belts, printing equipment, separators and centrifuges	20 000 ... 30 000
Machines for continuous 24-hour use: rolling mill gear units, medium-sized electrical machinery, compressors, mine hoists, pumps, textile machinery	40 000 ... 50 000
Wind energy machinery, this includes main shaft, yaw, pitching gearbox, generator bearings	30 000 ... 100 000
Water works machinery, rotary furnaces, cable stranding machines, propulsion machinery for ocean-going vessels	60 000 ... 100 000
Large electric machines, power generation plant, mine pumps, mine ventilator fans, tunnel shaft bearings for ocean-going vessels	100 000 ... 200 000

Table A.23.8 Table for X and Y Factors for Ball Bearings [12]

$\left(\frac{F_a}{C_0}\right)$	$\left(\frac{F_a}{F_r}\right) \leq e$		$\left(\frac{F_a}{F_r}\right) > e$		e
	X	Y	X	Y	
0.025	1	0	0.56	2.0	0.22
0.040	1	0	0.56	1.8	0.24
0.070	1	0	0.56	1.6	0.27
0.130	1	0	0.56	1.4	0.31
0.250	1	0	0.56	1.2	0.37
0.500	1	0	0.56	1.0	0.44

Table A.23.9 Table of Bearings Dimensions and Static/Dynamic Load Capacities [12]

Principal dimensions (mm)			Basic load ratings (N)		Designation
d	D	B	C	C_0	
10	19	5	1480	630	61800
	26	8	4620	1960	6000
	30	9	5070	2240	6200
	35	11	8060	3750	6300

<i>Principal dimensions (mm)</i>			<i>Basic load ratings (N)</i>		<i>Designation</i>
<i>d</i>	<i>D</i>	<i>B</i>	<i>C</i>	<i>C₀</i>	
12	21	5	1430	695	61801
	28	8	5070	2240	6001
	32	10	6890	3100	6201
	37	12	9750	4650	6301
15	24	5	1560	815	61802
	32	9	5590	2500	6002
	35	11	7800	3550	6202
	42	13	11400	5400	6302
17	26	5	1680	930	61803
	35	10	6050	2800	6003
	40	12	9560	4500	6202
	47	14	13500	6550	6303
	62	17	22900	11800	6403
20	32	7	2700	1500	61804
	42	8	7020	3400	16404
	42	12	9360	4500	6004
	47	14	12700	6200	6204
	52	15	15900	7800	6304
	72	19	30700	16600	6404
25	37	7	3120	1960	61805
	47	8	7610	4000	16005
	47	12	11200	5600	6005
	52	15	14000	6950	6205
	62	17	22500	11400	6305
	80	21	35800	19600	6405
30	42	7	3120	2080	61806
	55	9	11200	5850	16006
	55	13	13300	6800	6006
	62	16	19500	10000	6206
	72	19	28100	14600	6306
	90	23	43600	24000	6406
35	47	7	4030	3000	61807
	62	9	12400	6950	16007
	62	14	15900	8500	6007
	72	17	25500	13700	6207
	80	21	33200	18000	6307
	100	25	55300	31000	6407

<i>Principal dimensions (mm)</i>			<i>Basic load ratings (N)</i>		<i>Designation</i>
<i>d</i>	<i>D</i>	<i>B</i>	<i>C</i>	<i>C₀</i>	
40	52	7	4160	3350	61808
	68	9	13300	7800	16008
	68	15	16800	9300	6008
	80	18	30700	16600	6208
	90	23	41000	22400	6308
	110	27	63700	36500	6408
45	58	7	6050	3800	61809
	75	10	15600	9300	16009
	75	16	21200	12200	6009
	85	19	33200	18600	6209
	100	25	52700	30000	6309
	120	29	76100	45500	6409
50	65	7	6240	4250	61810
	80	10	16300	10000	16010
	80	16	21600	13200	6010
	90	20	35100	19600	6210
	110	27	61800	36000	6310
	130	31	87100	52000	6410
55	72	9	8320	5600	61811
	90	11	19500	12200	16011
	90	18	28100	17000	6011
	100	21	43600	25000	6211
	120	29	71500	41500	6311
	140	33	99500	63000	6411
60	78	10	8710	6100	61812
	95	11	19900	13200	16012
	95	18	29600	18300	6012
	110	22	47500	28000	6212
	130	31	81900	48000	6312
	150	35	108000	69500	6412
65	85	10	11700	8300	61813
	100	11	21200	14600	16013
	100	18	30700	19600	6013
	120	23	55900	34000	6213
	140	33	92300	56000	6313
	160	37	119000	78000	6413

Table A.23.10 Table of Bearing Parameters

Parameter (Symbol, Unit)	1 st -Bearing	2 nd -Bearing	3 rd -Bearing	4 th -Bearing
Rated bearing life (L_{10} , in mil. Rev.)	3600	1412,4	558	223,2
Dynamic load capacity (C, N)	52425,53	69658,14	93478,88	68560,67
P (for ball bearings = 3)	3	3	3	3
Dynamic load (P, N)	3420,65	6208,49	11354,52	11302,56
Rotational speed (N, rpm)	3000	1177	465	186
Rated bearing life (L_{10h} , hour)	20000	20000	20000	20000
Radial load (Fr, N)	2533,59	4756,92	8830,58	8830,58
Axial load (Fa, N)	1064,81	1999,22	3711,29	3711,29
Static load capacity (C0, N)	31000	45500	63000	69500
Ratio of axial load/radial load	0,42	0,42	0,42	0,42
Ratio of axial load/static load capacity	0,034	0,044	0,059	0,053
Radial load factor (X, constant)	0,56	0,56	0,56	0,56
Axial load factor (Y, constant)	1,88	1,773	1,727	1,713
e factor (e, constant)	0,232	0,244	0,251	0,253
Inner diameter of bearing (d, mm)	35	45	55	60
Outer diameter of bearing (D, mm)	100	120	140	150
Designation number of bearing	6407	6409	6411	6412

Table A.23.11 Table of Gear Geometry Factor (k_0) [29]

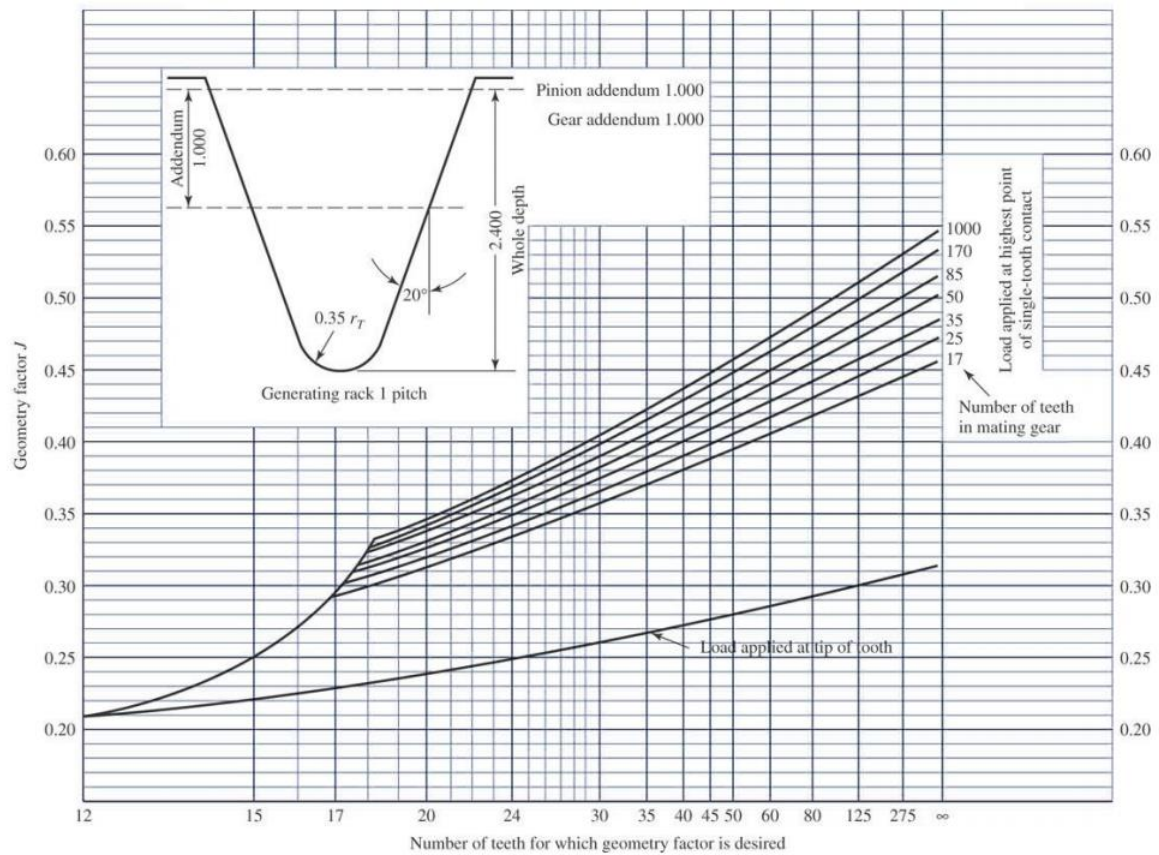
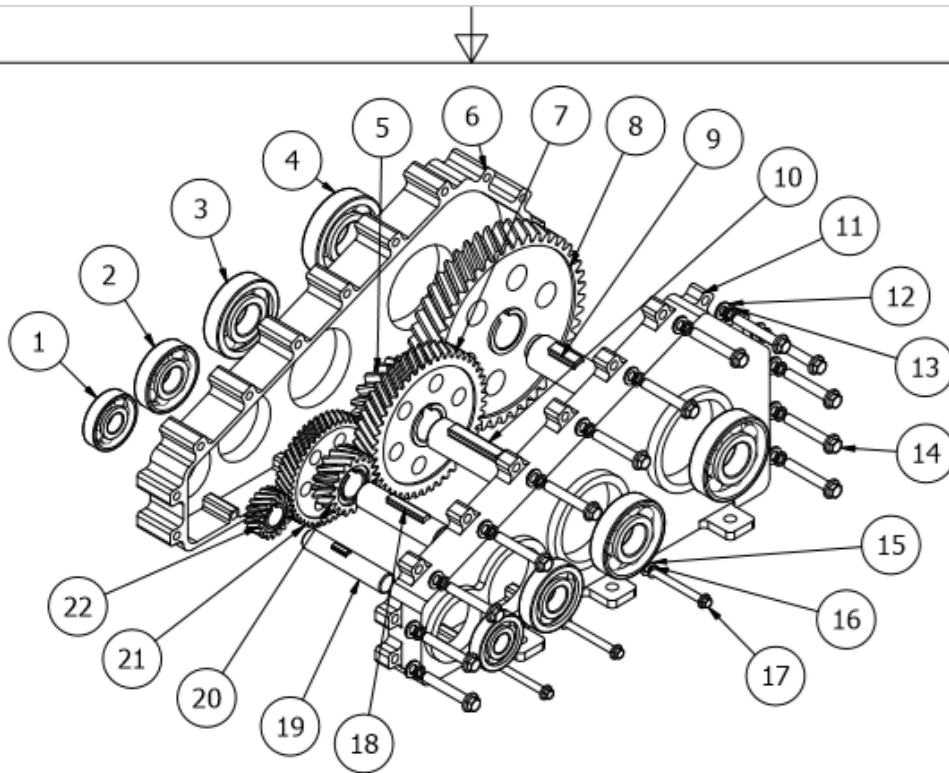


Table A.23.12 Table of Kinematic Viscosity of ISO Standard Industrial Lubricants [35]

		Viscosity System for Industrial Lubricants at 40°C		
Identification	Mid-Point mm ² /s, cSt	Min Kin Vis mm ² /s, cSt	Max Kin Vis mm ² /s, cSt	Approx SUS
ISO VG 2	2.2	1.98	2.42	32
ISO VG 3	3.2	2.88	3.52	36
ISO VG 5	4.6	4.14	5.06	40
ISO VG 7	6.8	6.12	7.48	50
ISO VG 10	10	9.00	11.0	60
ISO VG 15	15	13.5	16.5	75
ISO VG 22	22	19.8	24.2	105
ISO VG 32	32	28.8	35.2	150
ISO VG 46	46	41.4	50.6	215
ISO VG 68	68	61.2	74.8	315
ISO VG 100	100	90.0	110	465
ISO VG 150	150	135	165	700
ISO VG 220	220	198	242	1000
ISO VG 320	320	288	352	1500
ISO VG 460	460	412	506	2150
ISO VG 680	680	612	748	3150
ISO VG 1000	1000	900	1100	4650
ISO VG 1500	1500	1350	1650	7000

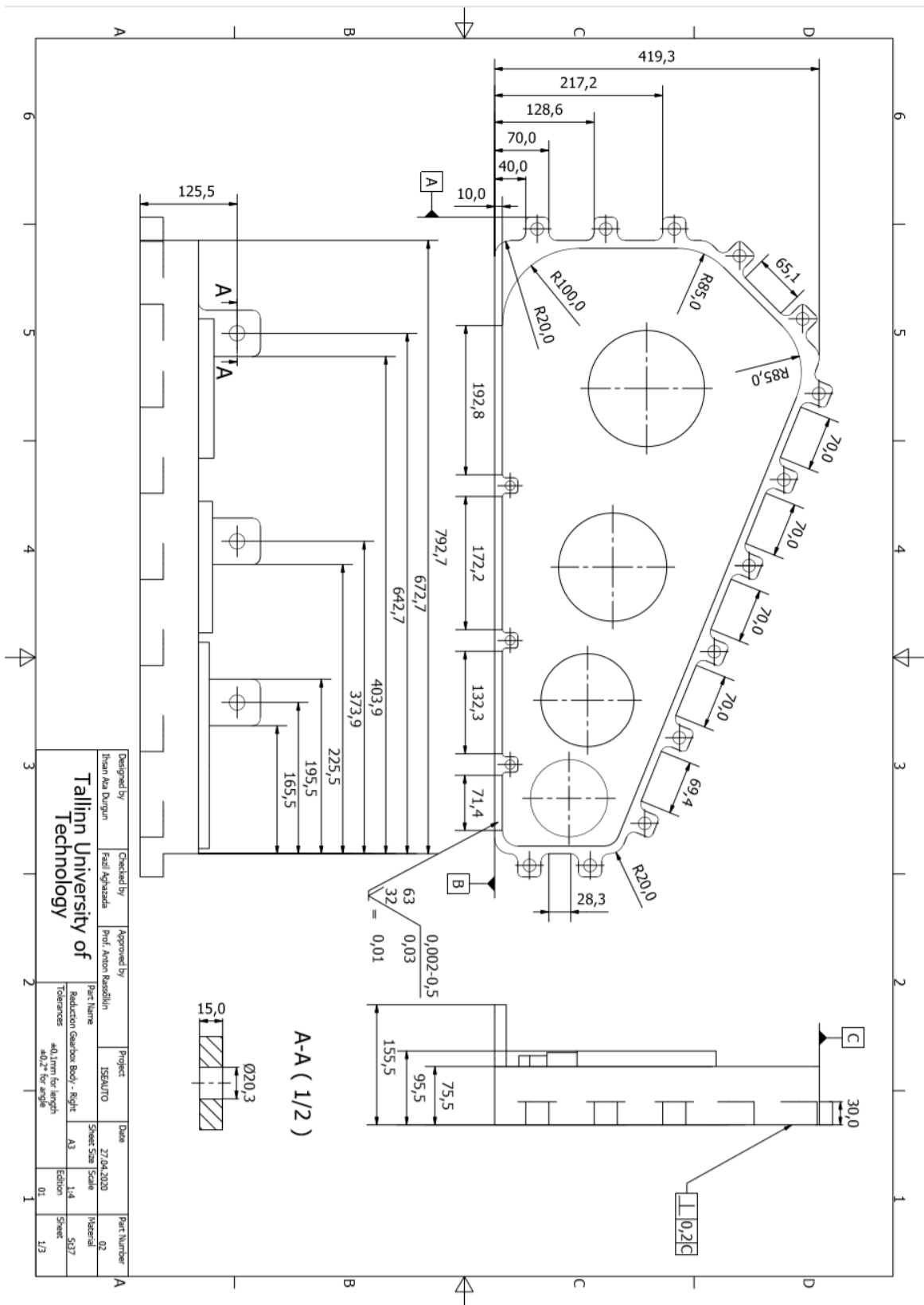
A.24. BOM Drawing of the RG



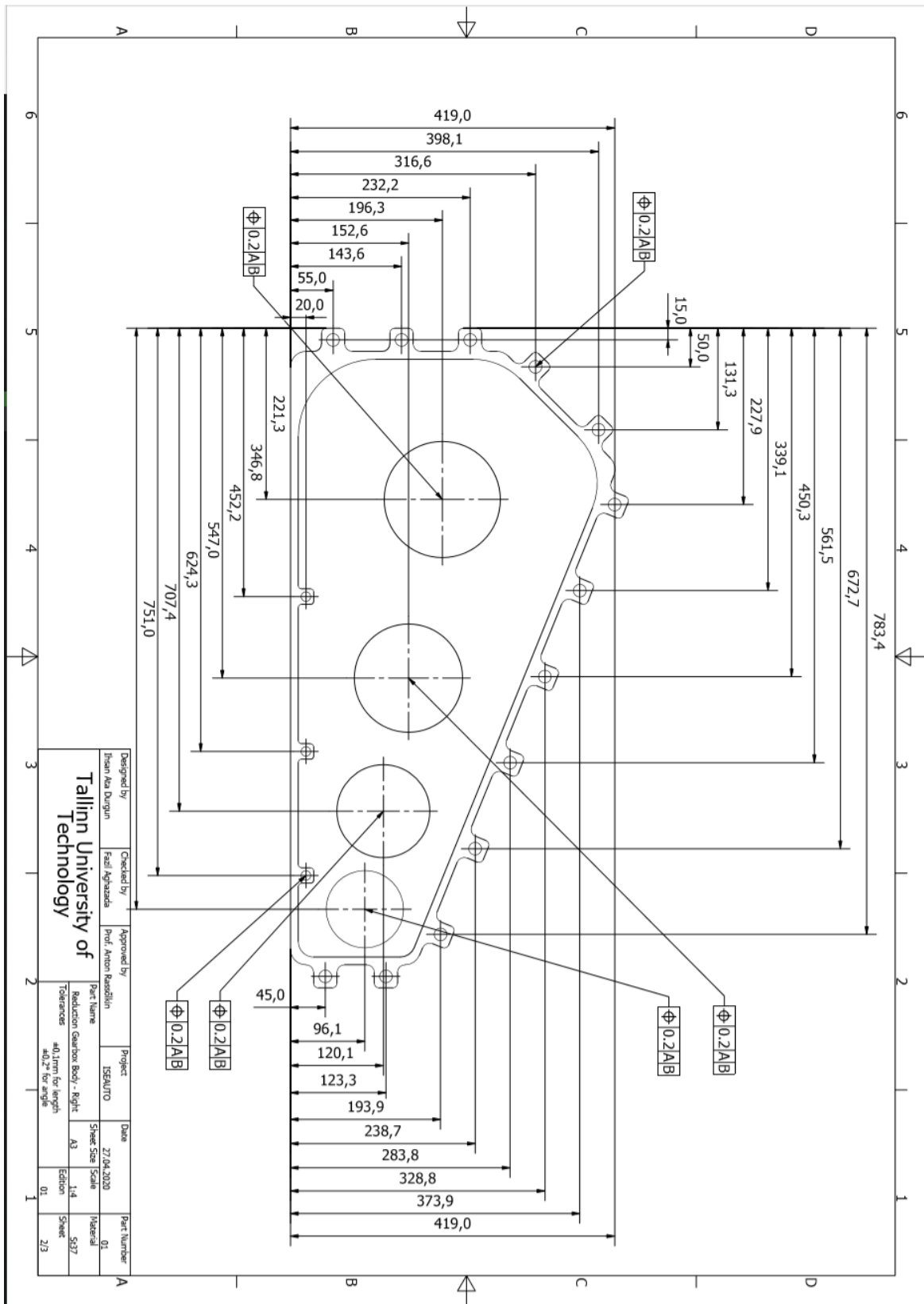
Part Number	Part Name	Quantity	Material
1	First Bearing (d=35mm, D=100mm)	2	SS304
2	Second Bearing (d=45mm, D=120mm)	2	SS304
3	Third Bearing (d=55mm, D=140mm)	2	SS304
4	Fourth Bearing (d=60mm, D=150mm)	2	SS304
5	Third Pinion	1	SS304
6	Body-Left Side	1	St37
7	Second Gear	1	SS420
8	Third Gear	1	SS420
9	Fourth Shaft	1	SS304
10	Third Shaft	1	SS304
11	Body-Right Side	1	St37
12	Plain Washer M16	13	SS304
13	Spring Washer M16	13	SS304
14	Hex Head M16x90mm	13	SS304
15	Plain Washer M12	3	SS304
16	Spring Washer M12	3	SS304
17	Hex Head Bolt M12x120mm	3	SS304
18	Second Shaft	1	SS304
19	First Shaft	1	SS304
20	Second Pinion	1	SS304
21	First Gear	1	SS420
22	First Pinion	1	SS304

Designed by İhsan Ata Durgun	Checked by Fazil Aghazada	Approved by Prof. Anton Rassölkin	Project ISEAUTO	Date 30.04.2020	Part Number -
Tallinn University of Technology			Part Name Reduction Gearbox	Sheet Size A4	Scale 1:9
			Tolerances -		Edition 01
					Material -
					Sheet 1/1

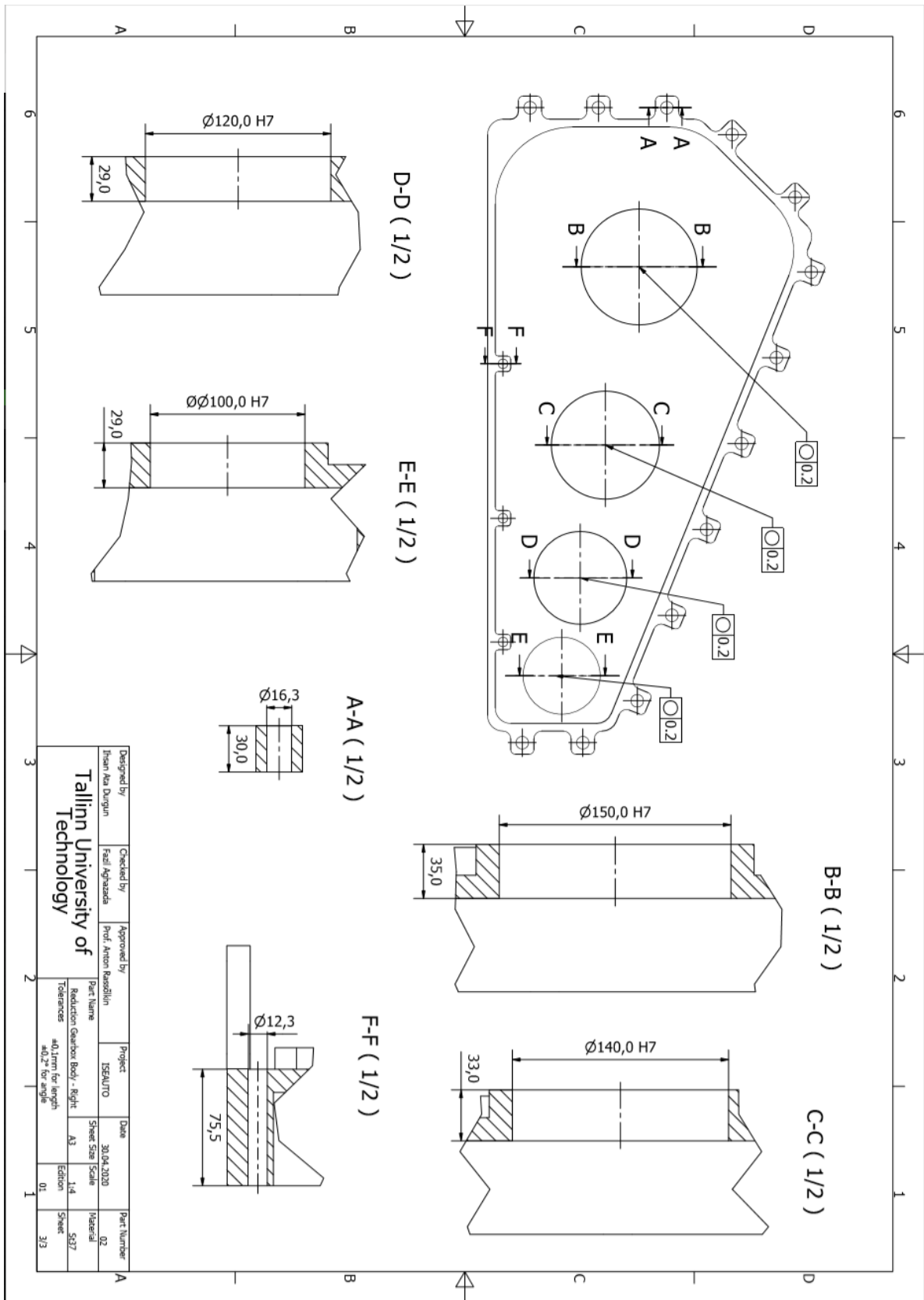
A.25. Technical Drawing of Right Body Part of the RG Page-1/3



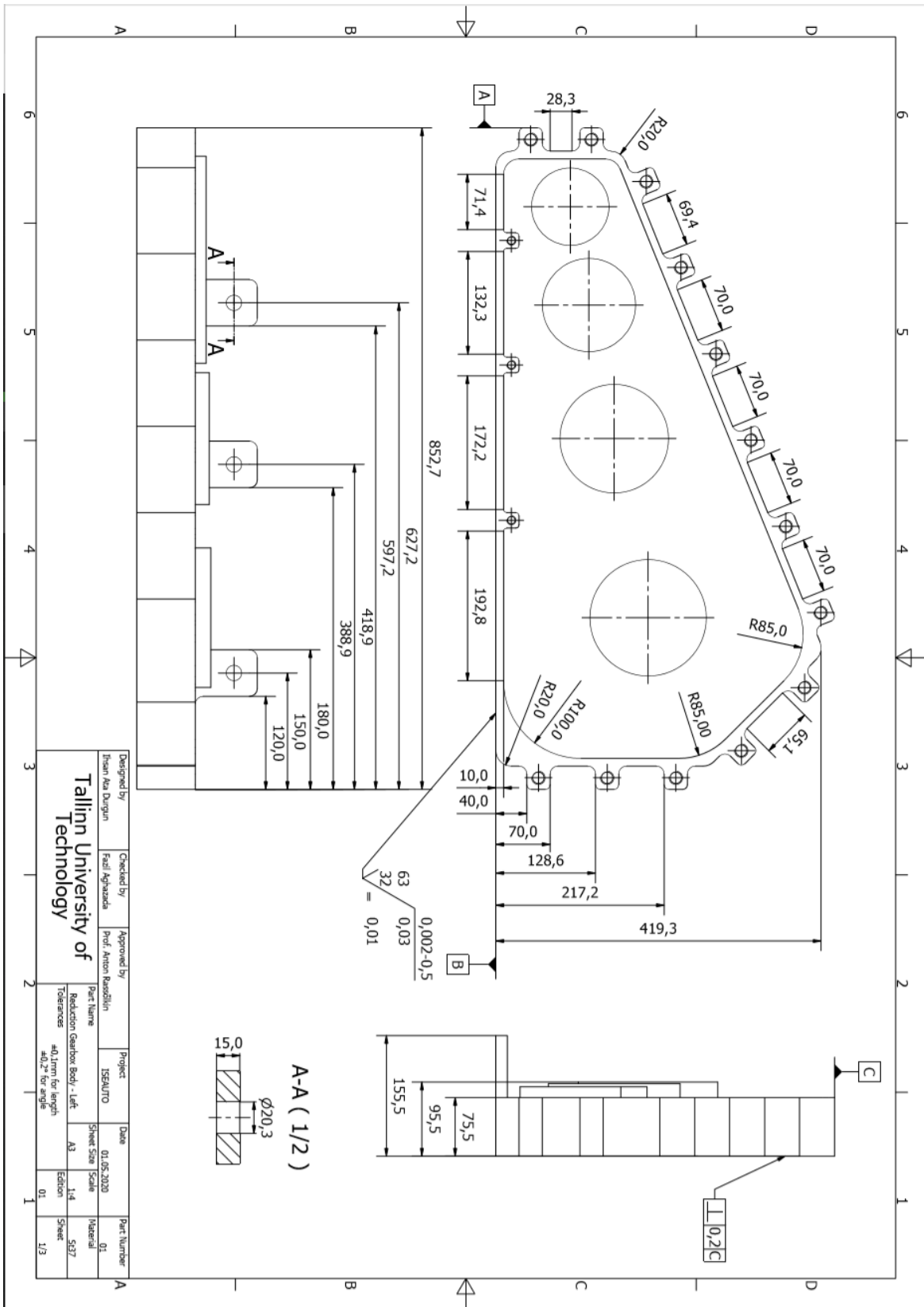
A.26. Technical Drawing of Right Body Part of the RG Page-2/3



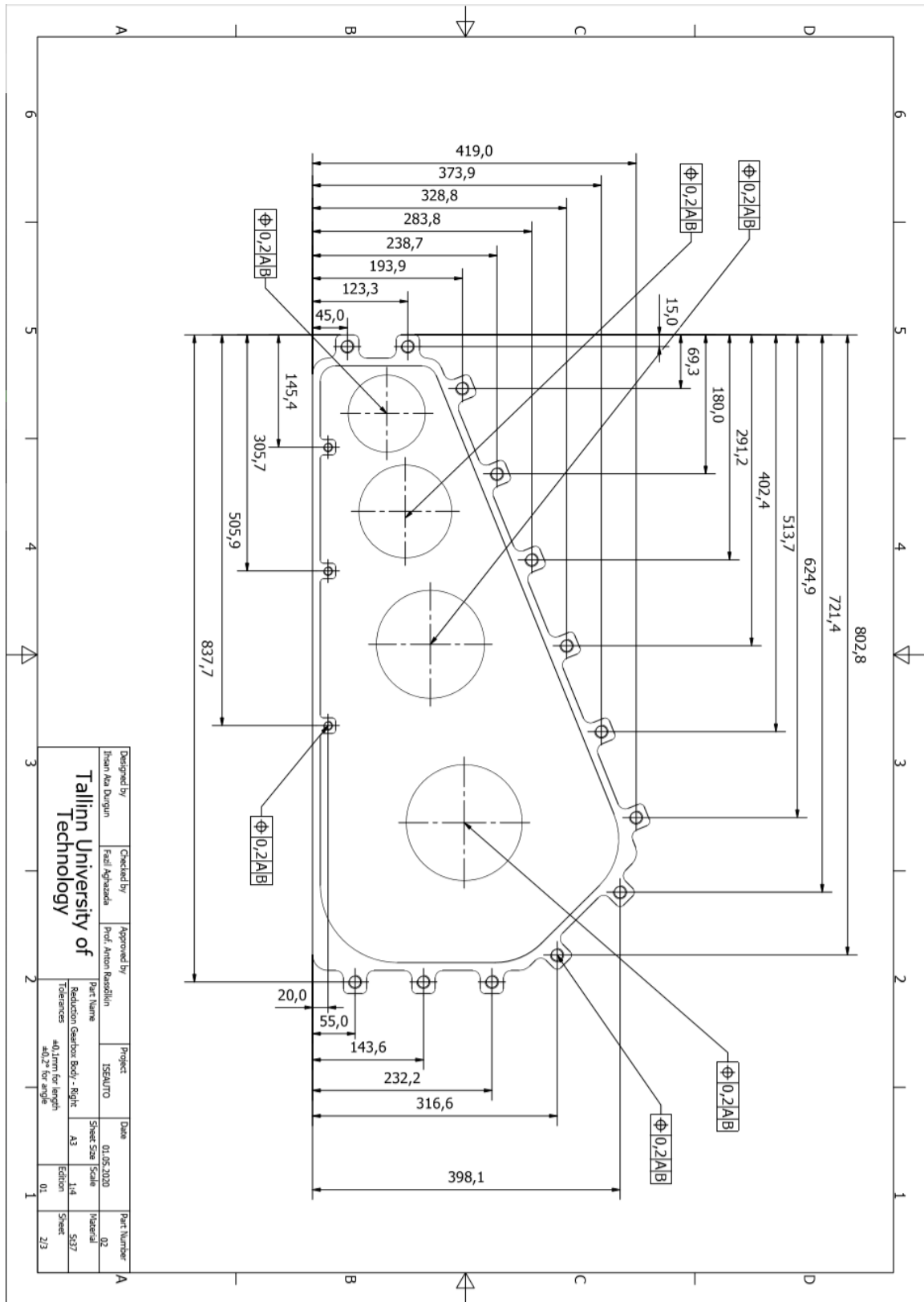
A.27. Technical Drawing of Right Body Part of the RG Page-3/3



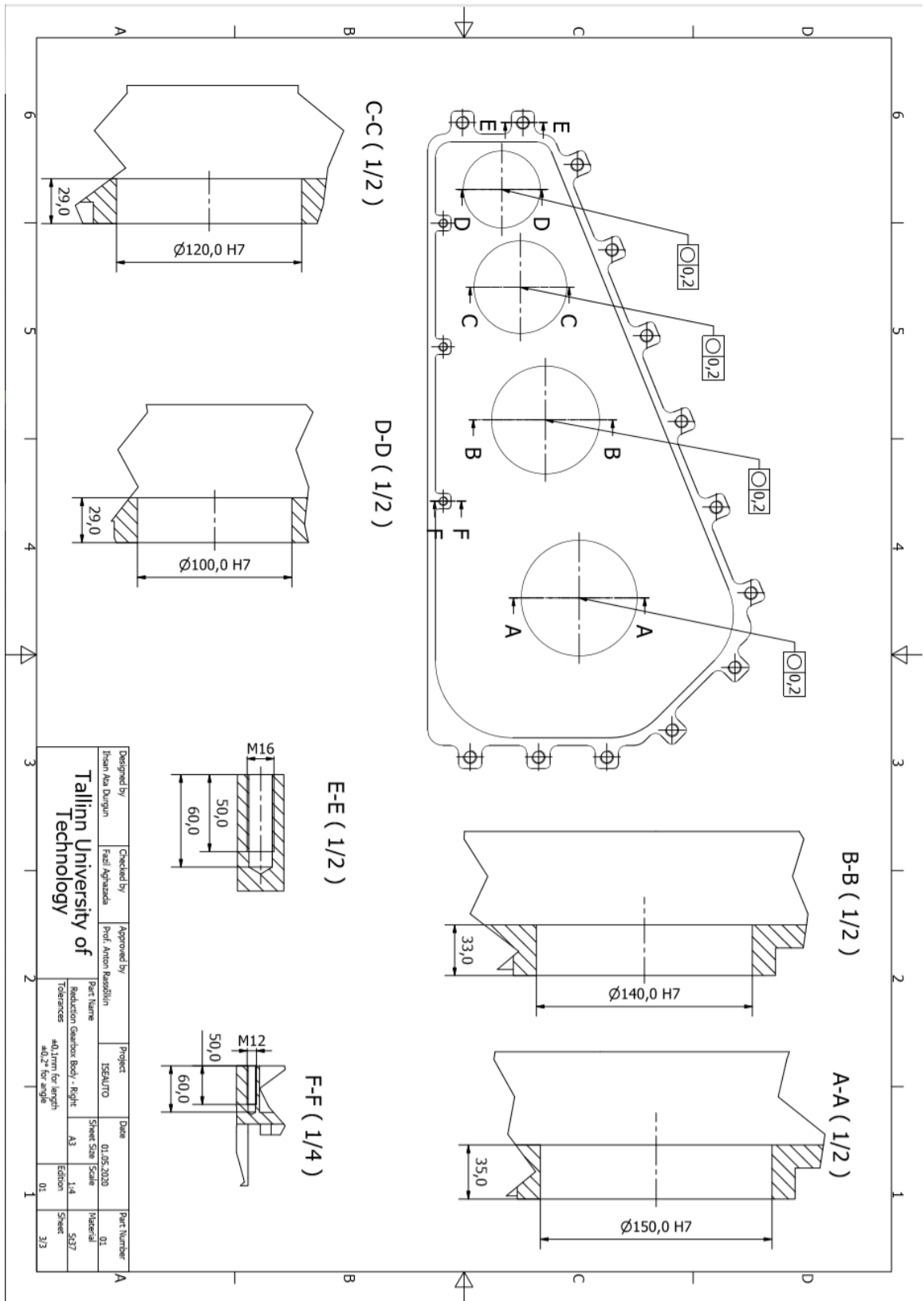
A.28. Technical Drawing of Left Body Part of the RG Page-1/3



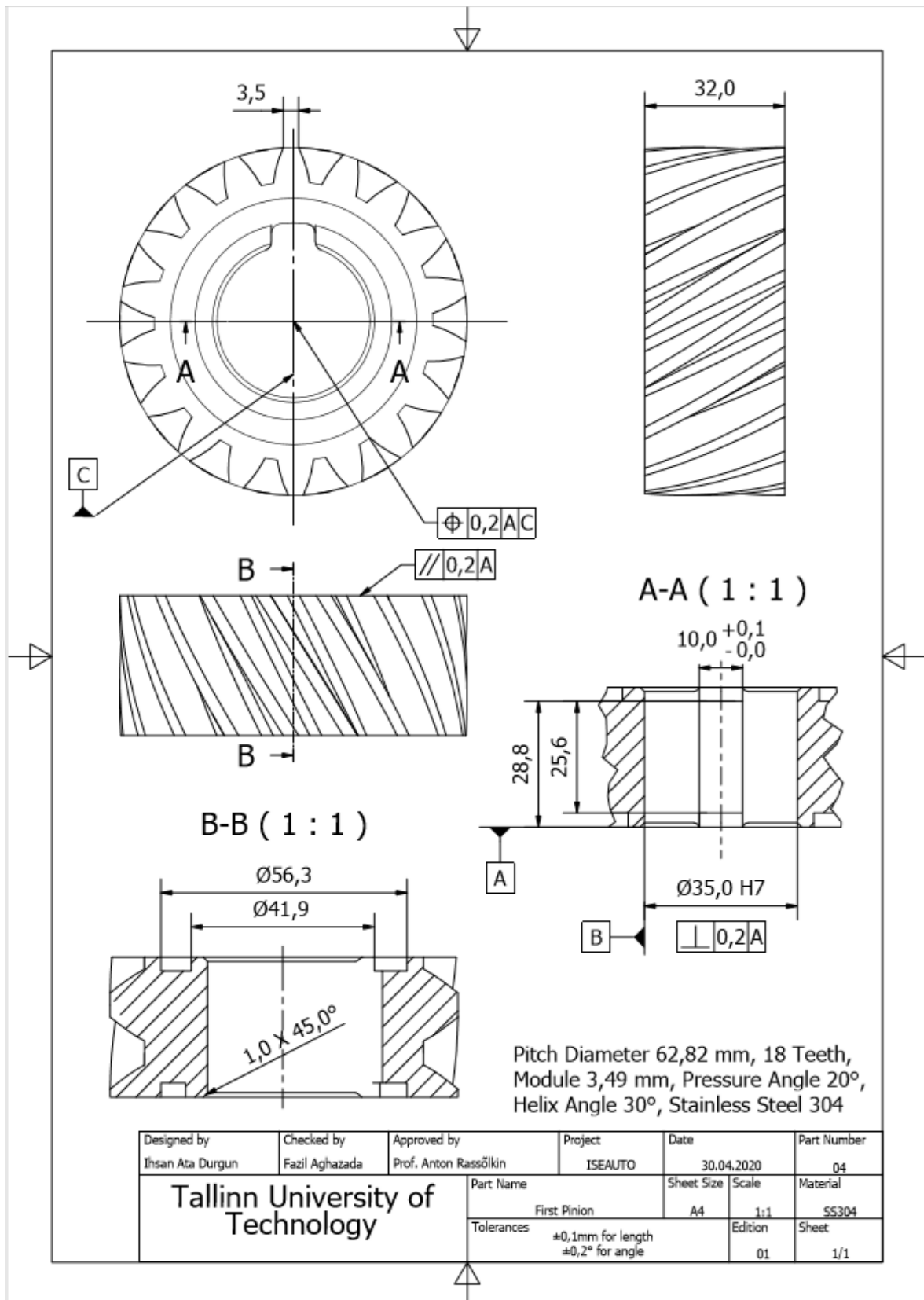
A.29. Technical Drawing of Left Body Part of the RG Page-2/3



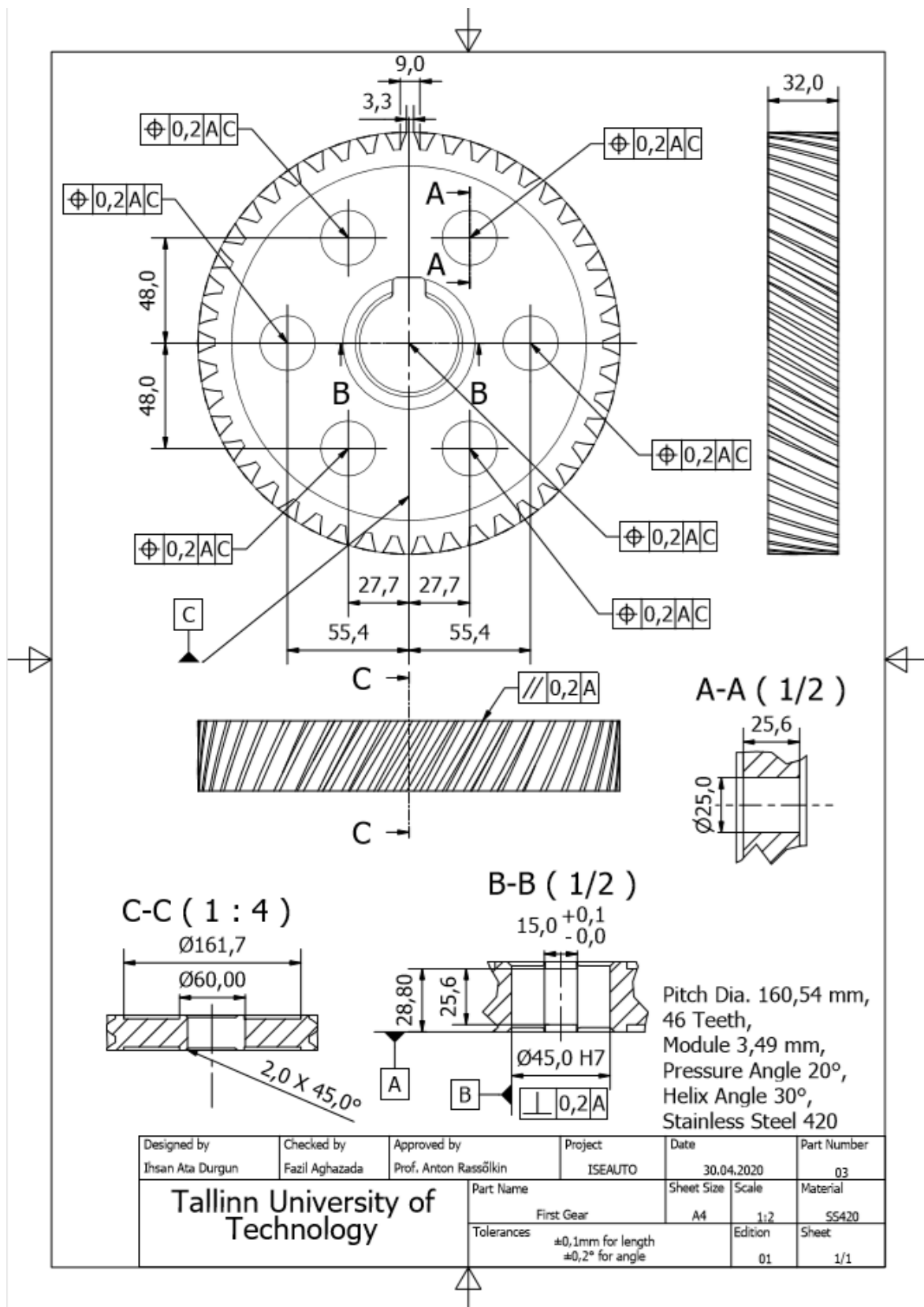
A.30. Technical Drawing of Left Body Part of the RG Page-3/3



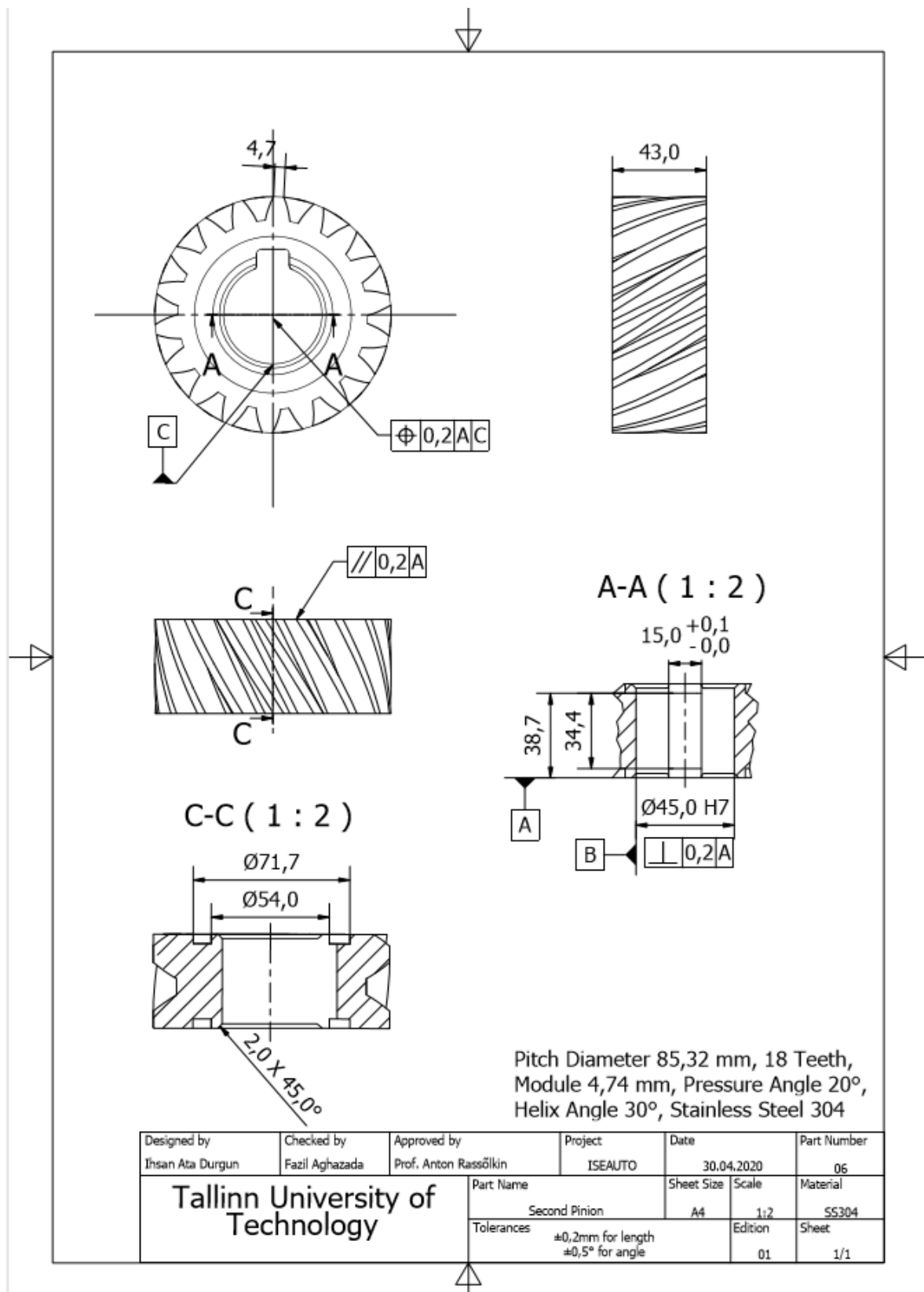
A.31. Technical Drawing of the First Pinion



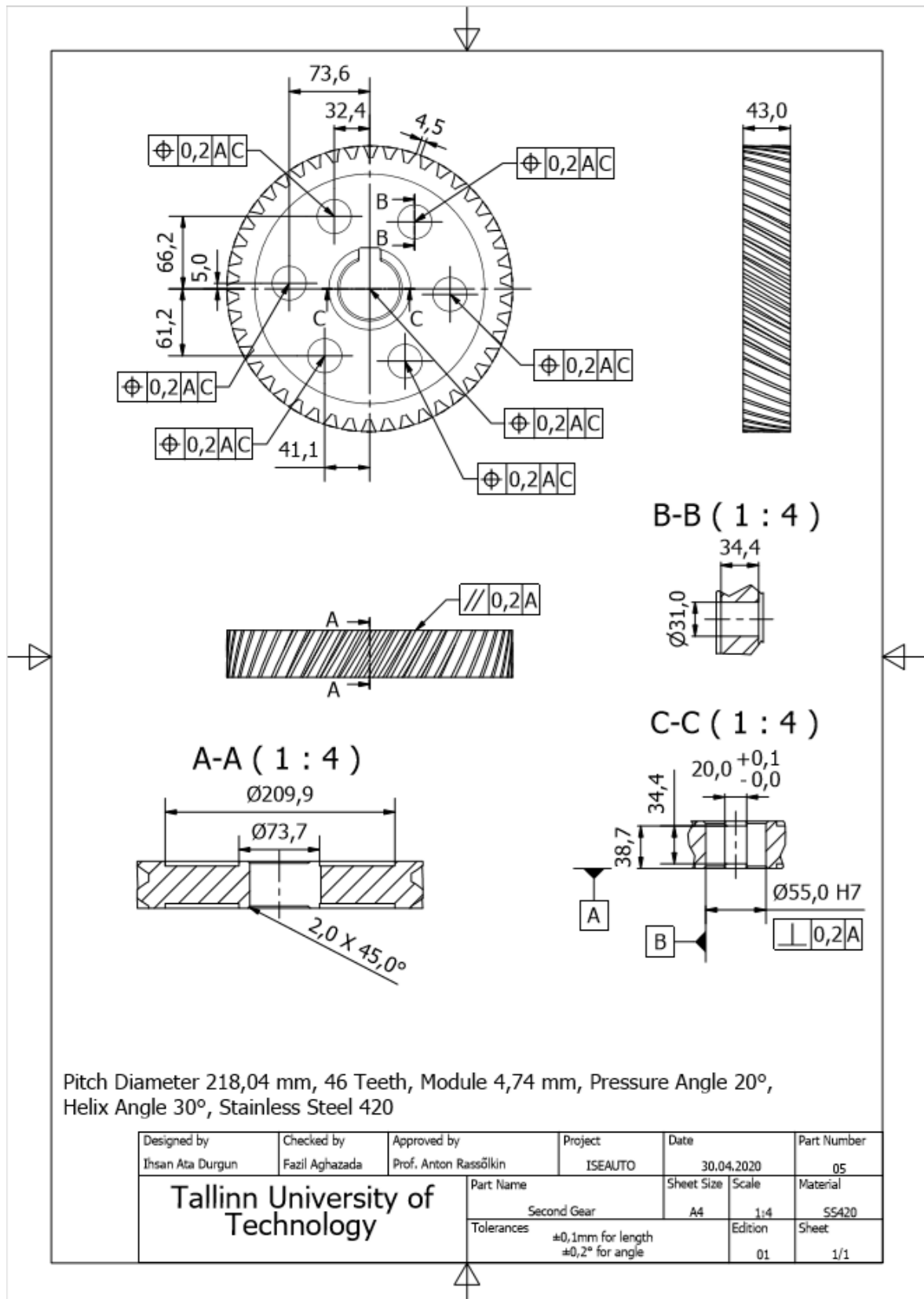
A.32. Technical Drawing of the First Gear



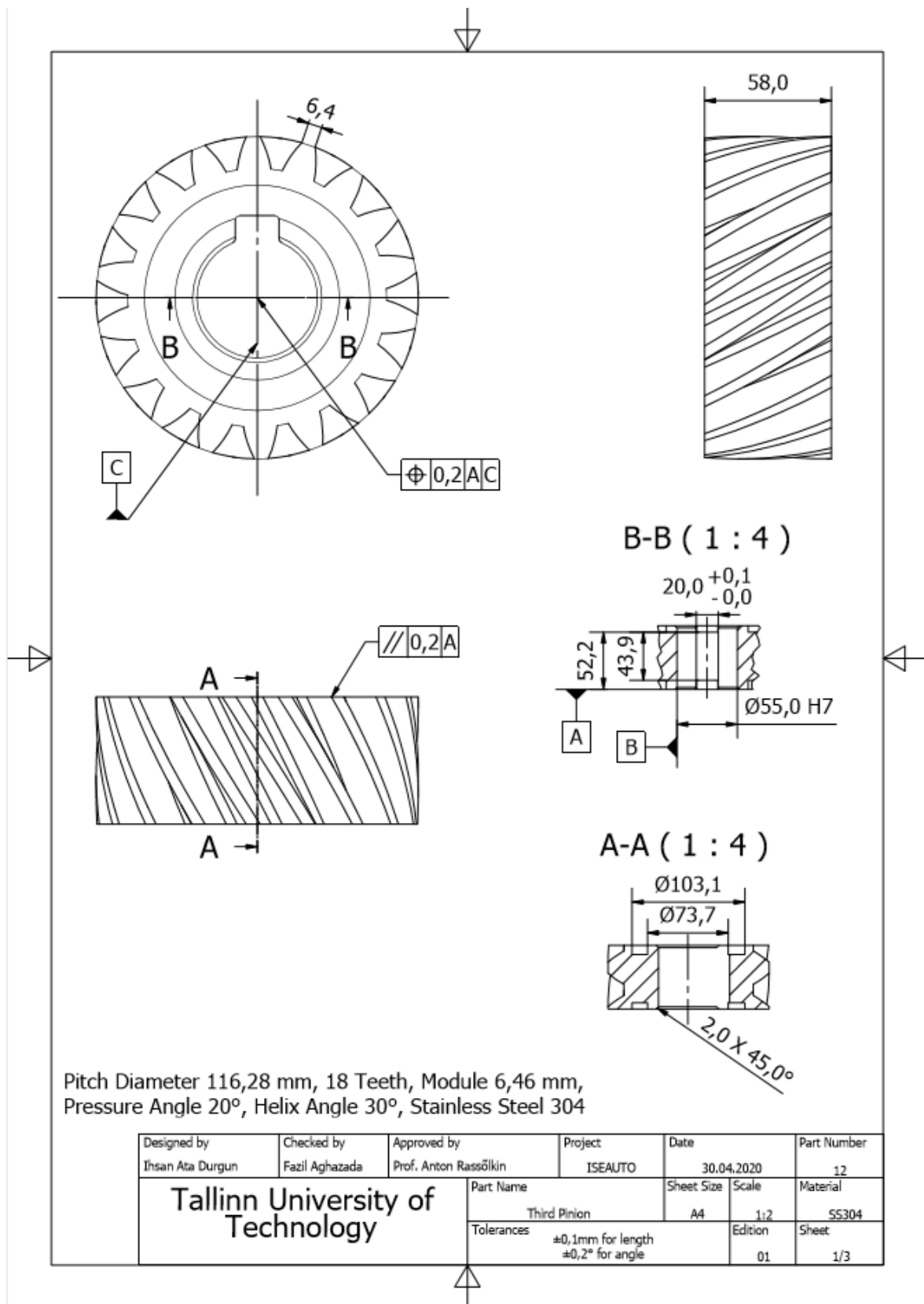
A.33. Technical Drawing of the Second Gear



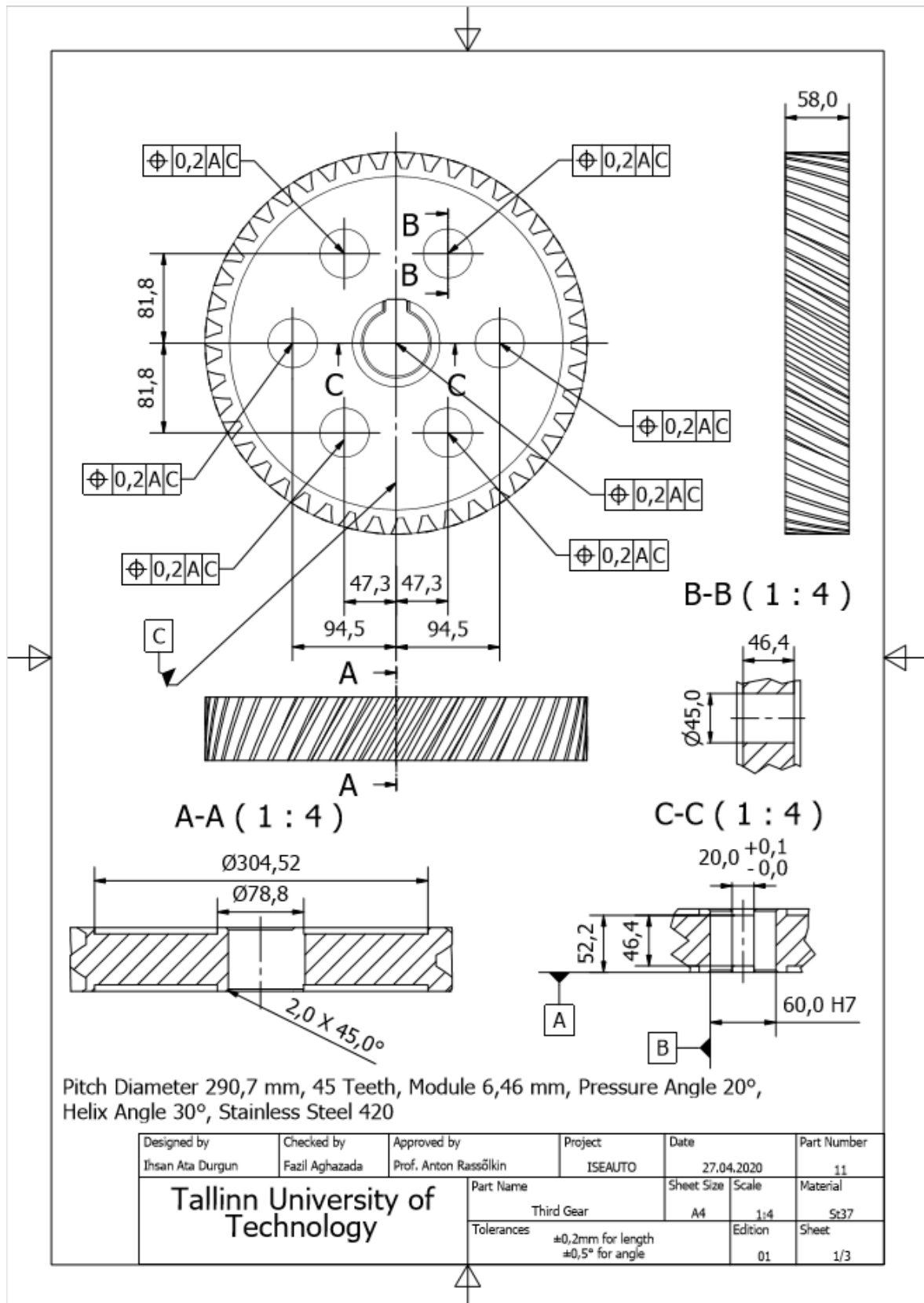
A.34. Technical Drawing of the Second Gear



A.35. Technical Drawing of the Third Pinion



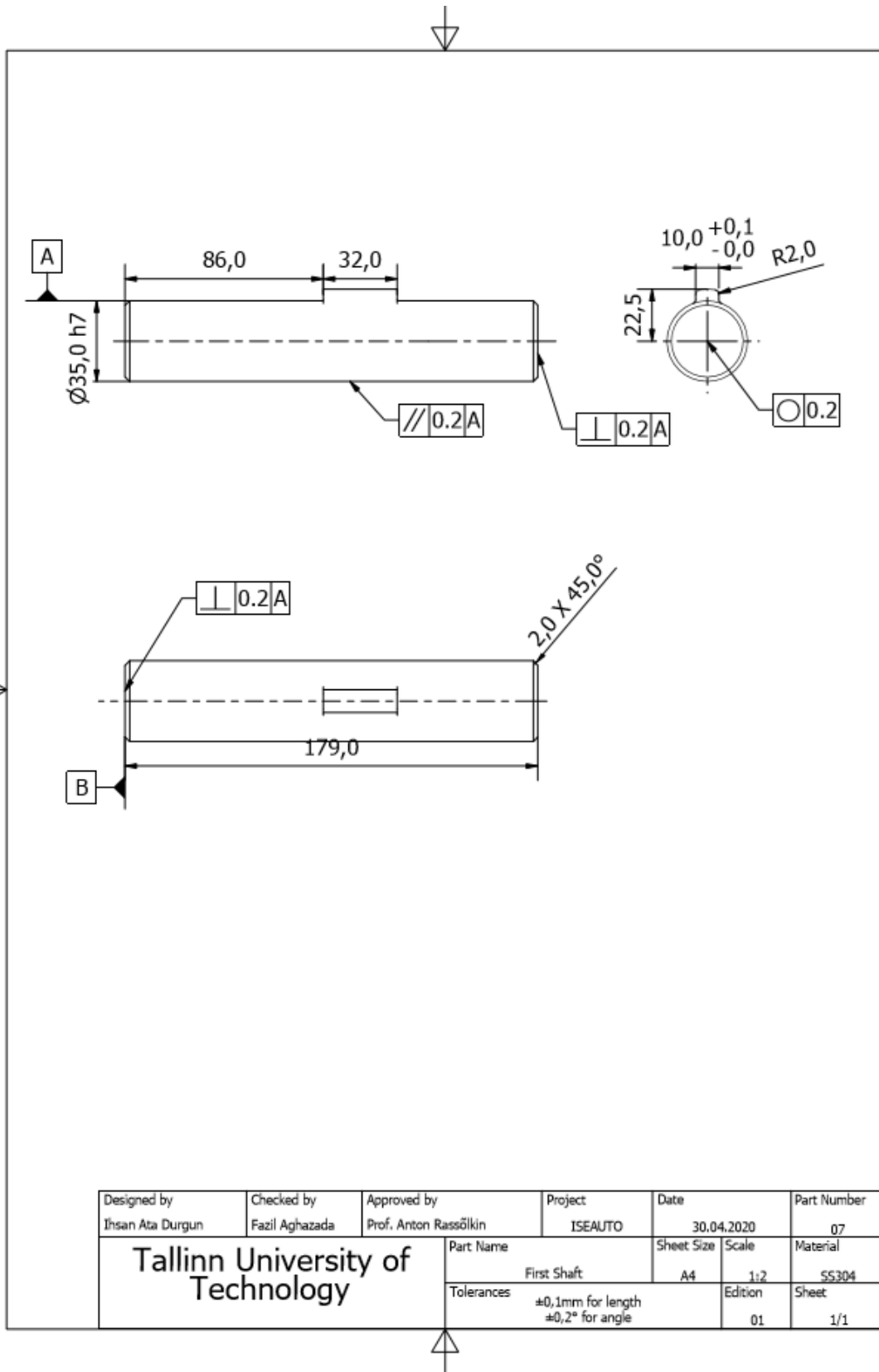
A.36. Technical Drawing of the Third Gear



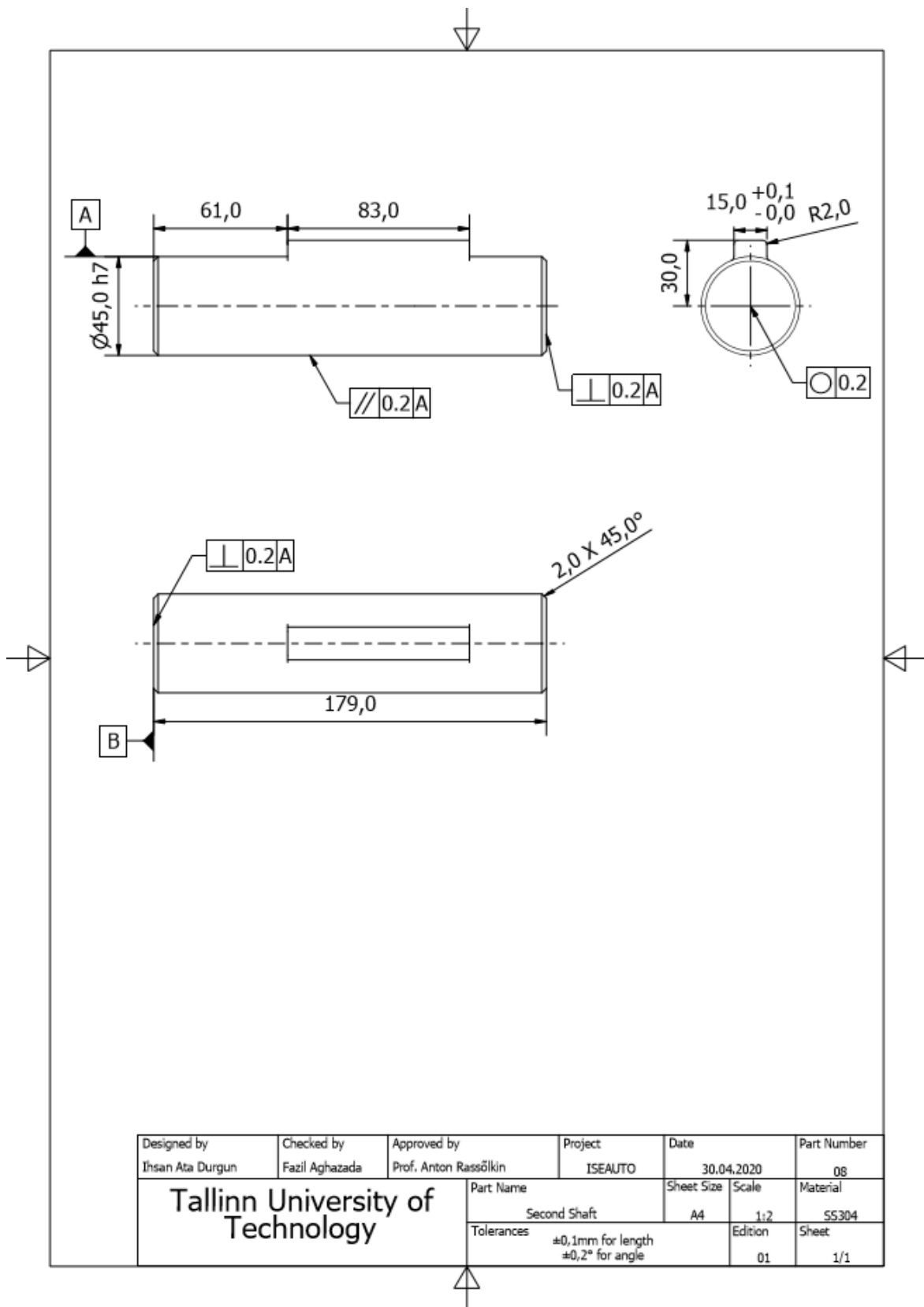
Pitch Diameter 290,7 mm, 45 Teeth, Module 6,46 mm, Pressure Angle 20° , Helix Angle 30° , Stainless Steel 420

Designed by İhsan Ata Durgun	Checked by Fazil Aghazada	Approved by Prof. Anton Rassõlkin	Project ISEAUTO	Date 27.04.2020	Part Number 11	
Tallinn University of Technology			Part Name Third Gear	Sheet Size A4	Scale 1:4	Material St37
			Tolerances $\pm 0,2$ mm for length $\pm 0,5^\circ$ for angle		Edition 01	Sheet 1/3

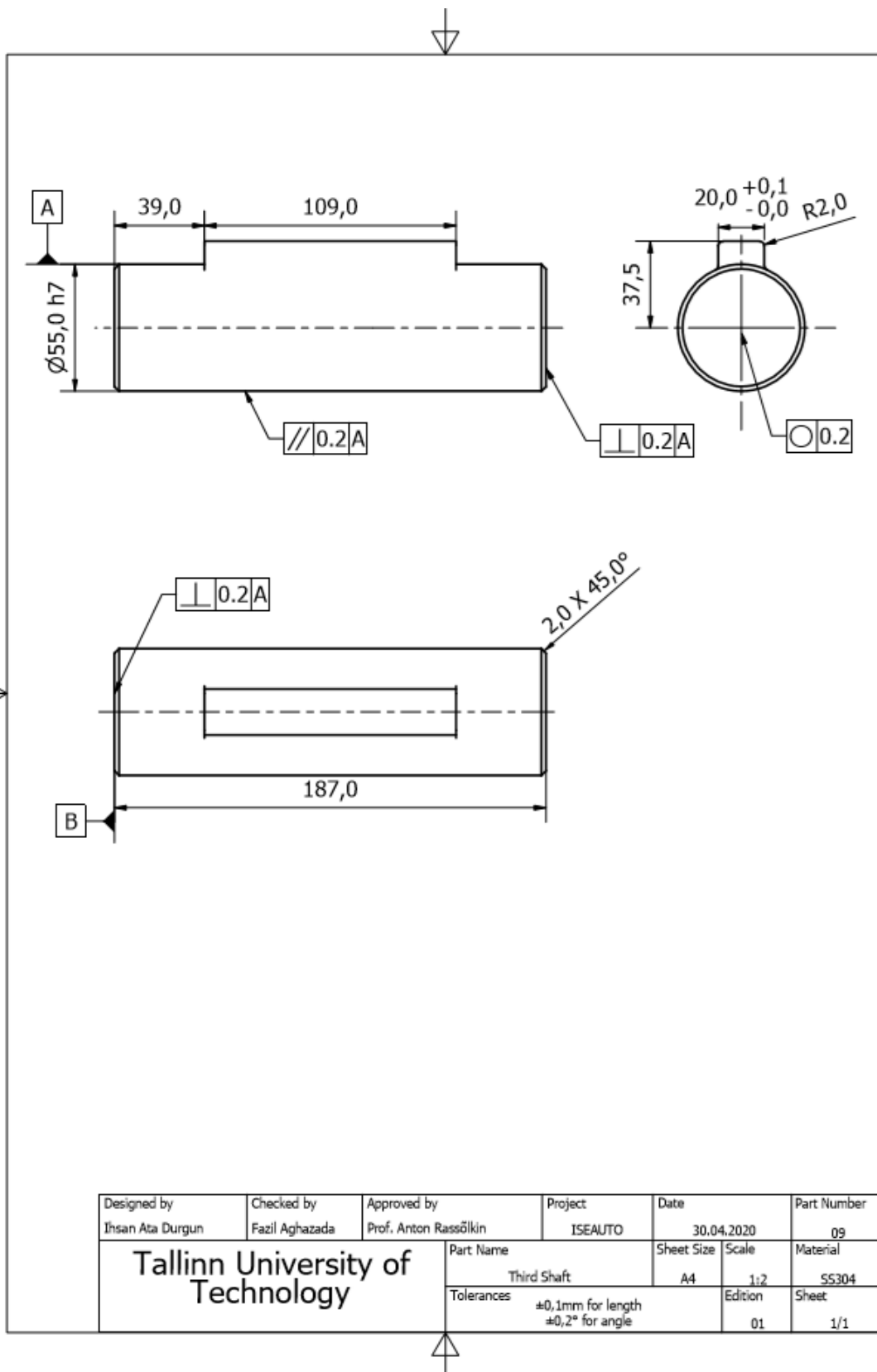
A.37. Technical Drawing of the First Shaft



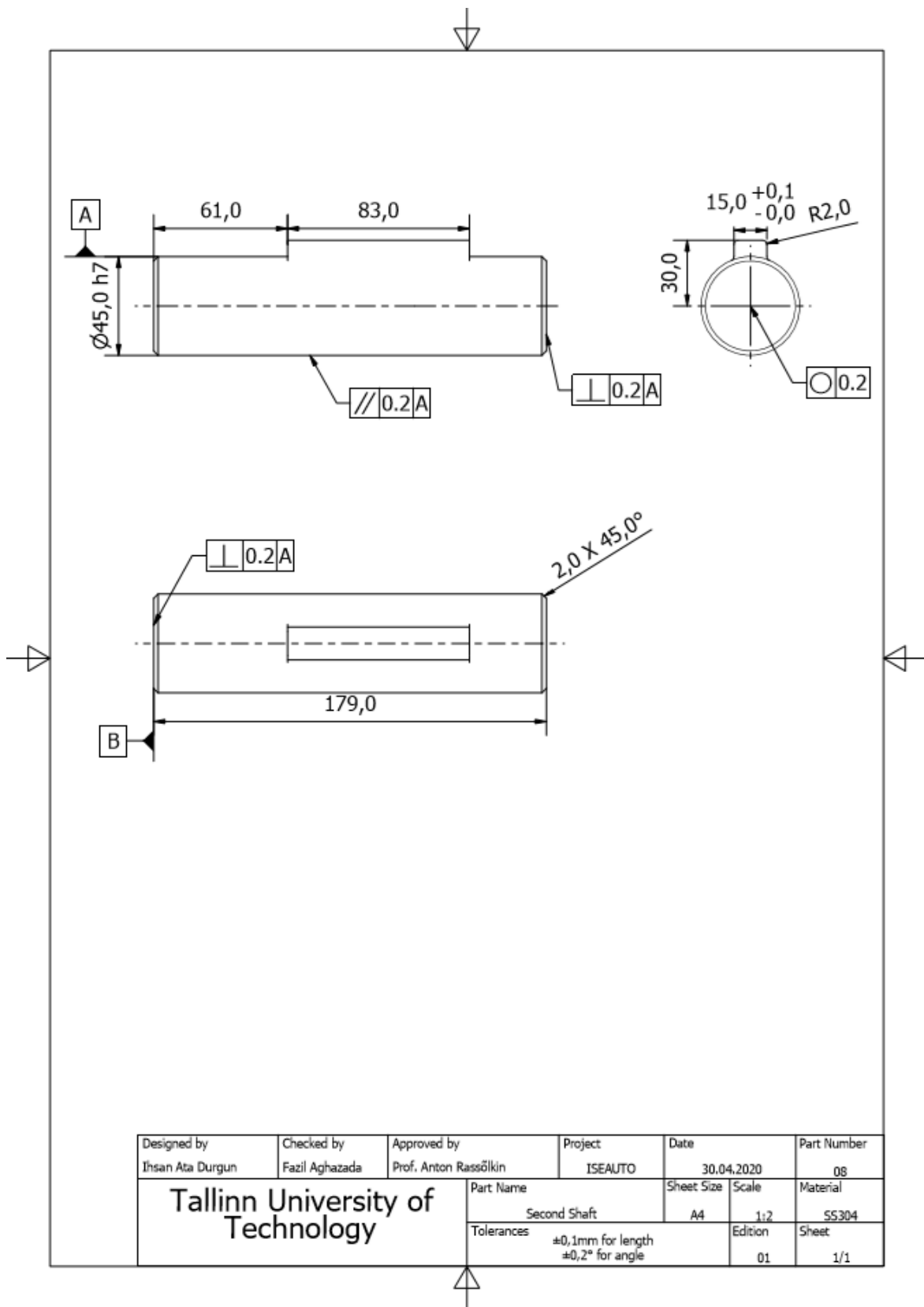
A.38. Technical Drawing of Second Shaft



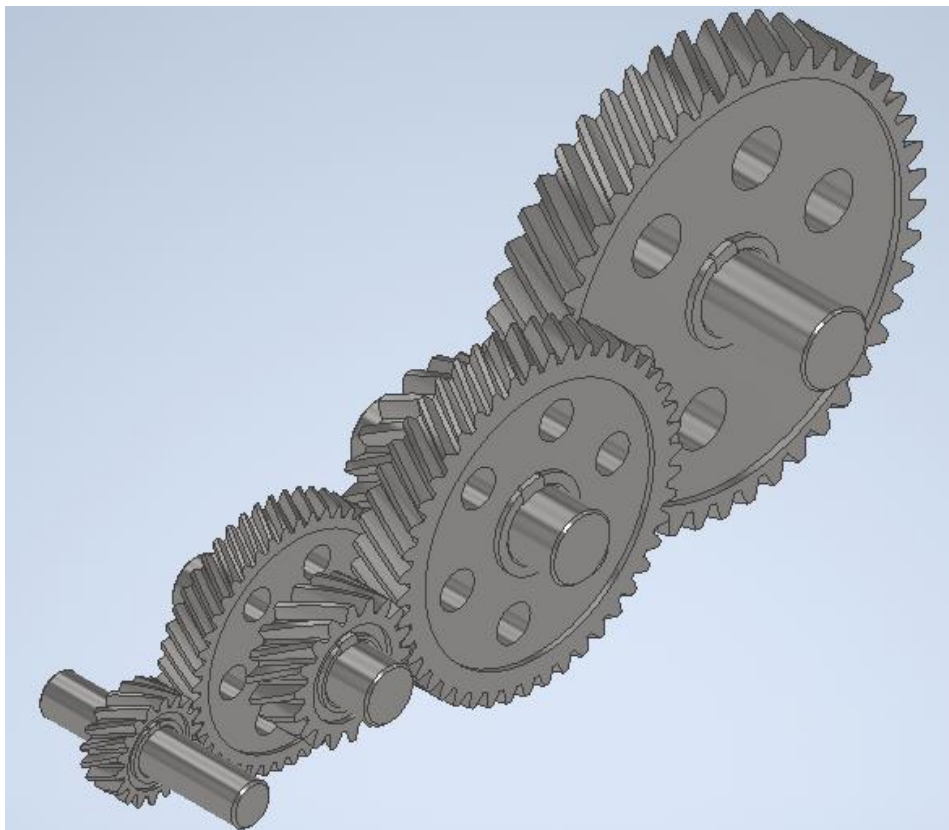
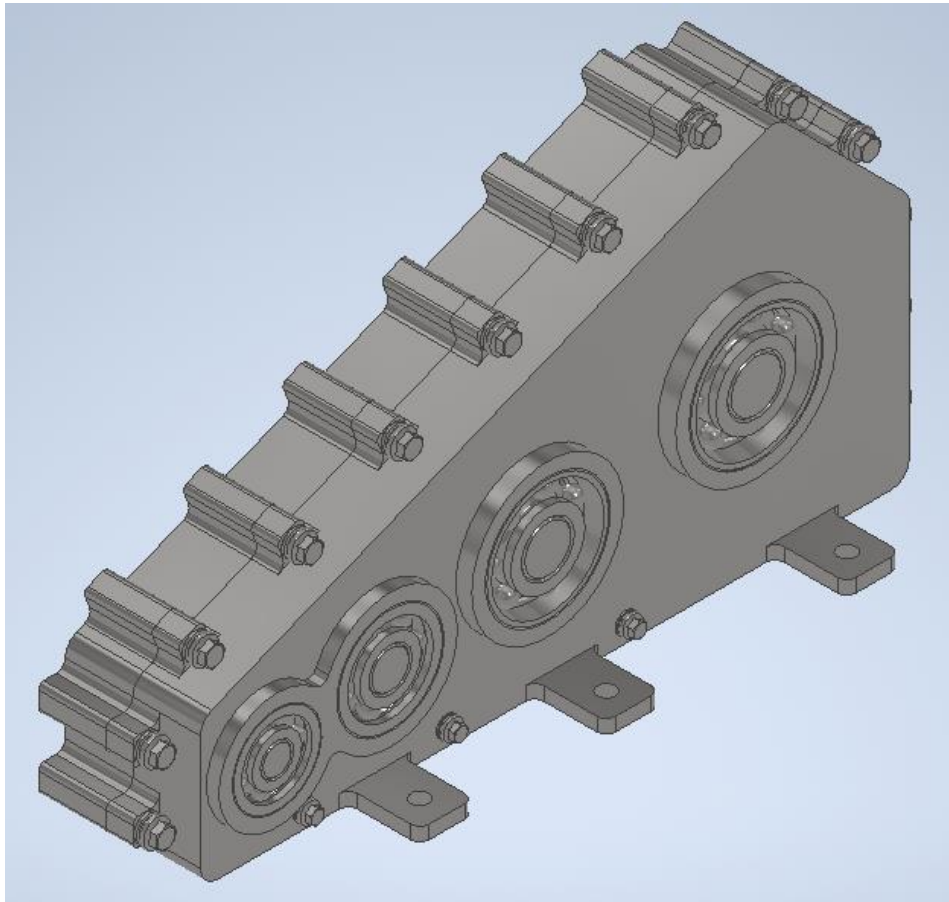
A.39. Technical Drawing of the Third Shaft



A.40. Technical Drawing of the Fourth Shaft

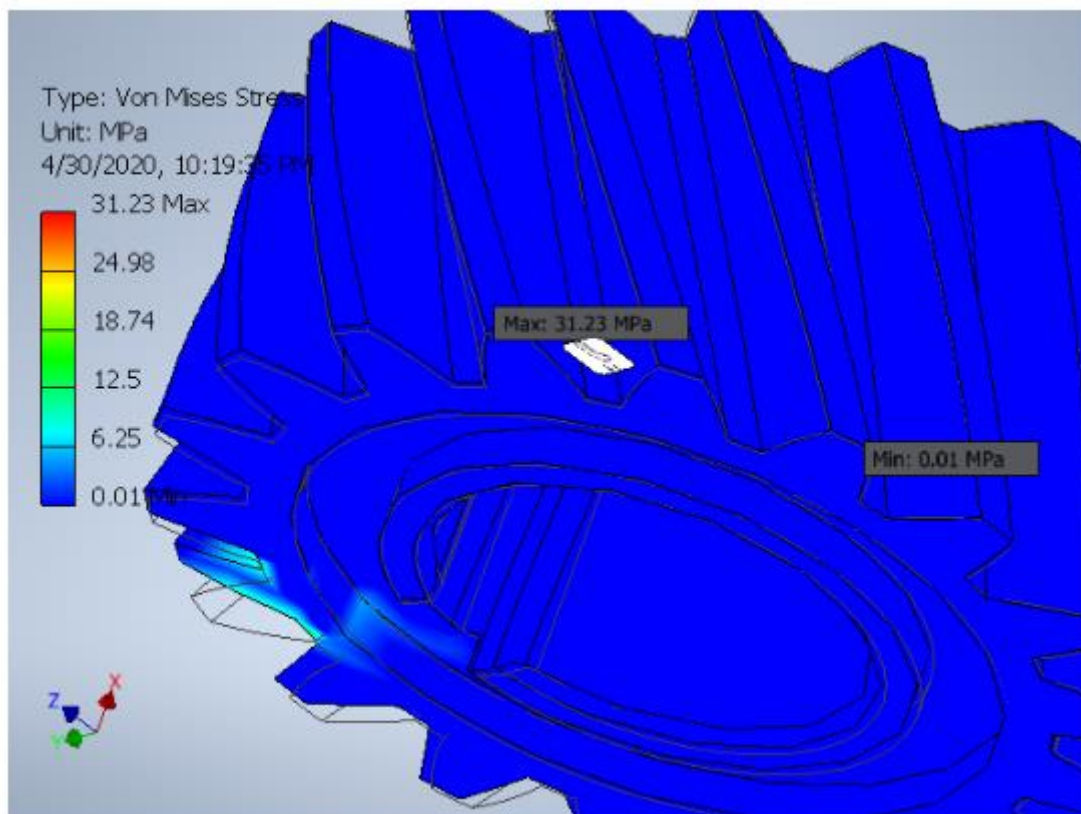
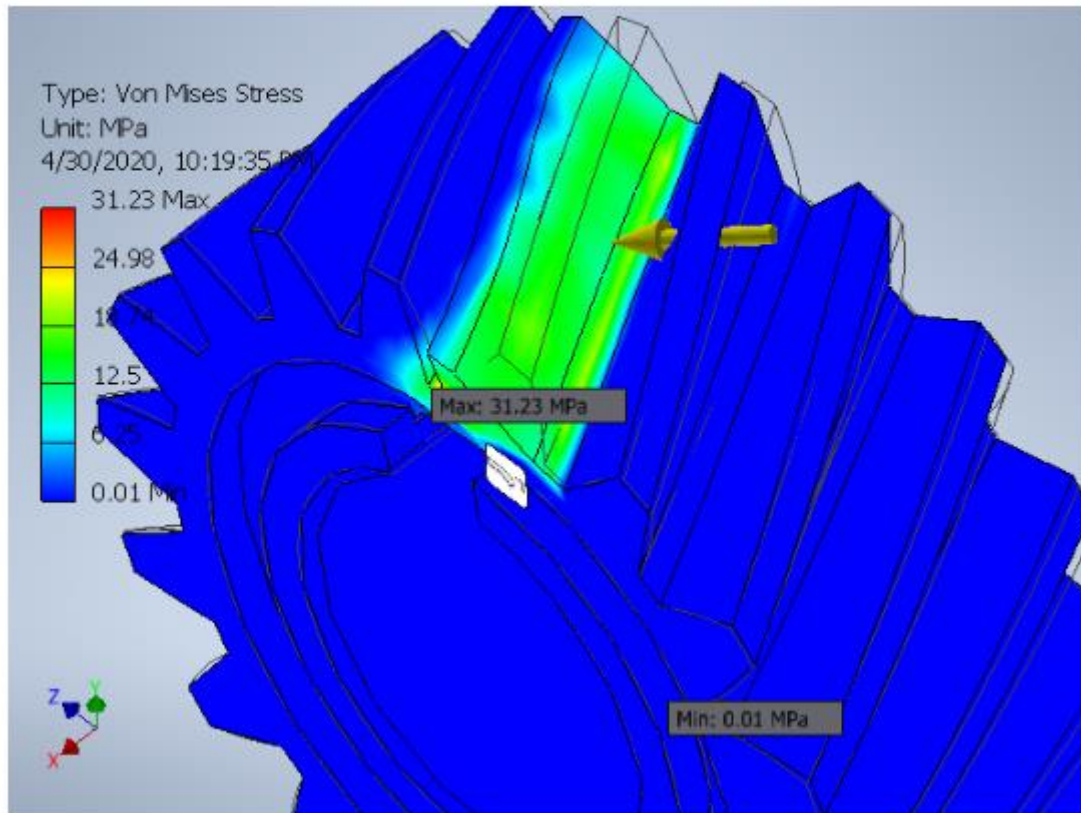


A.41. BOM Drawing of the RG



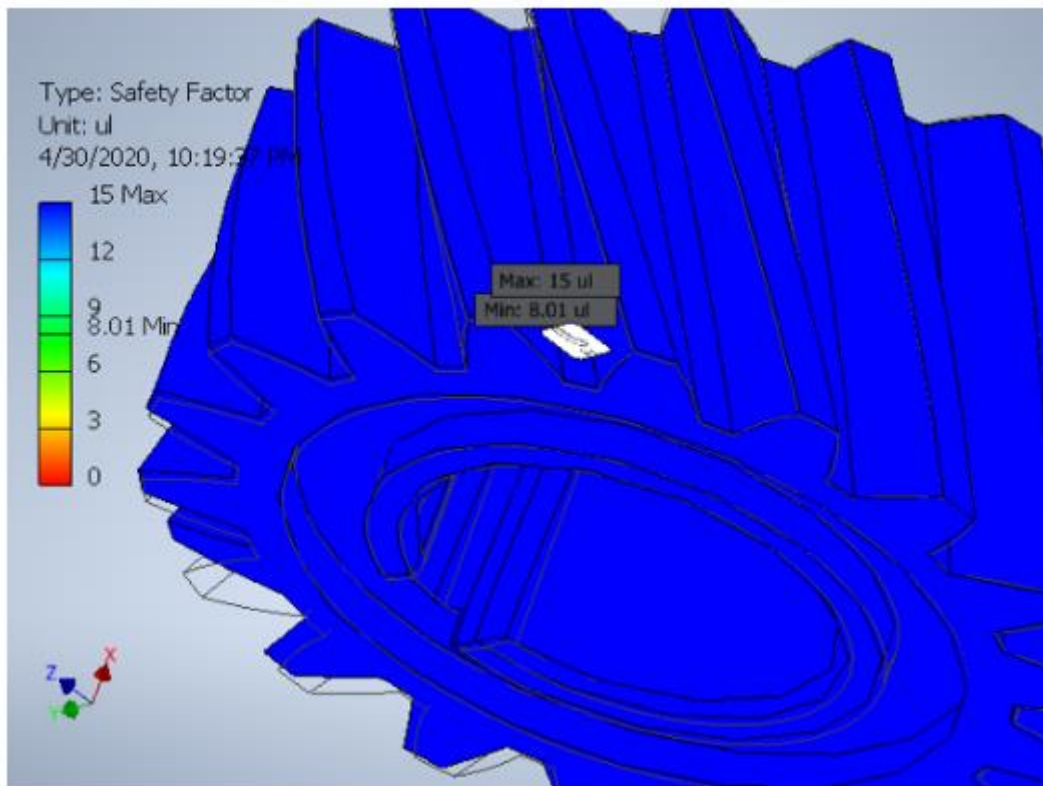
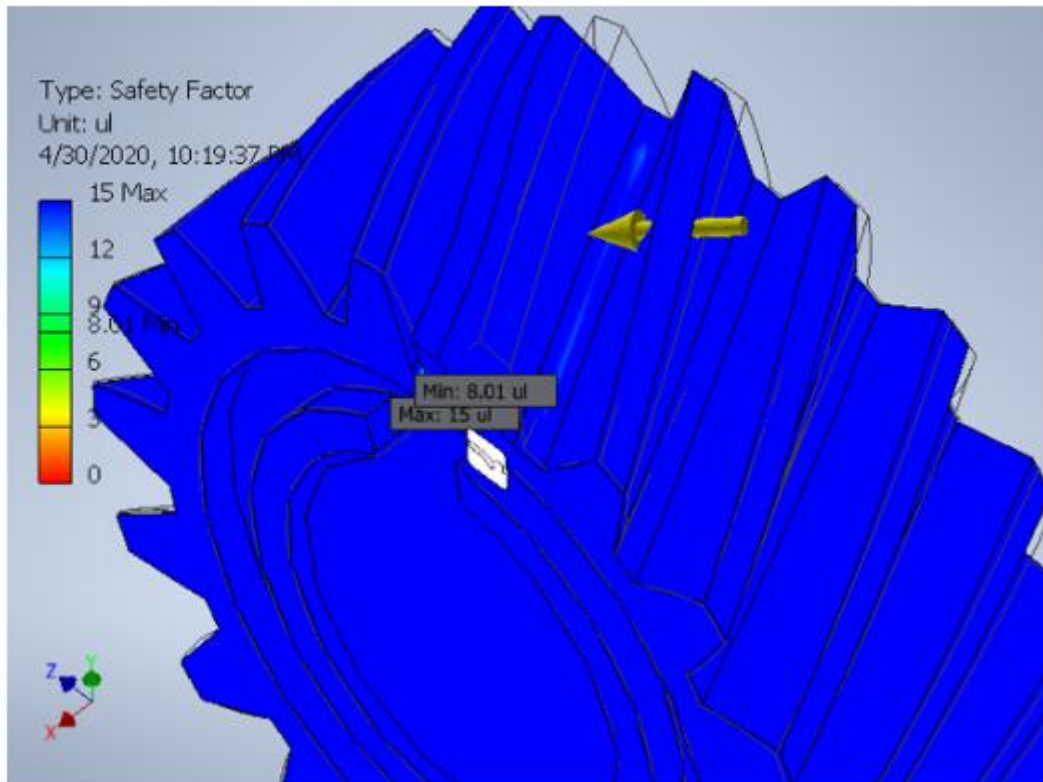
A.42. Stress Analyses of the First Pinion

☐ Von Mises Stress



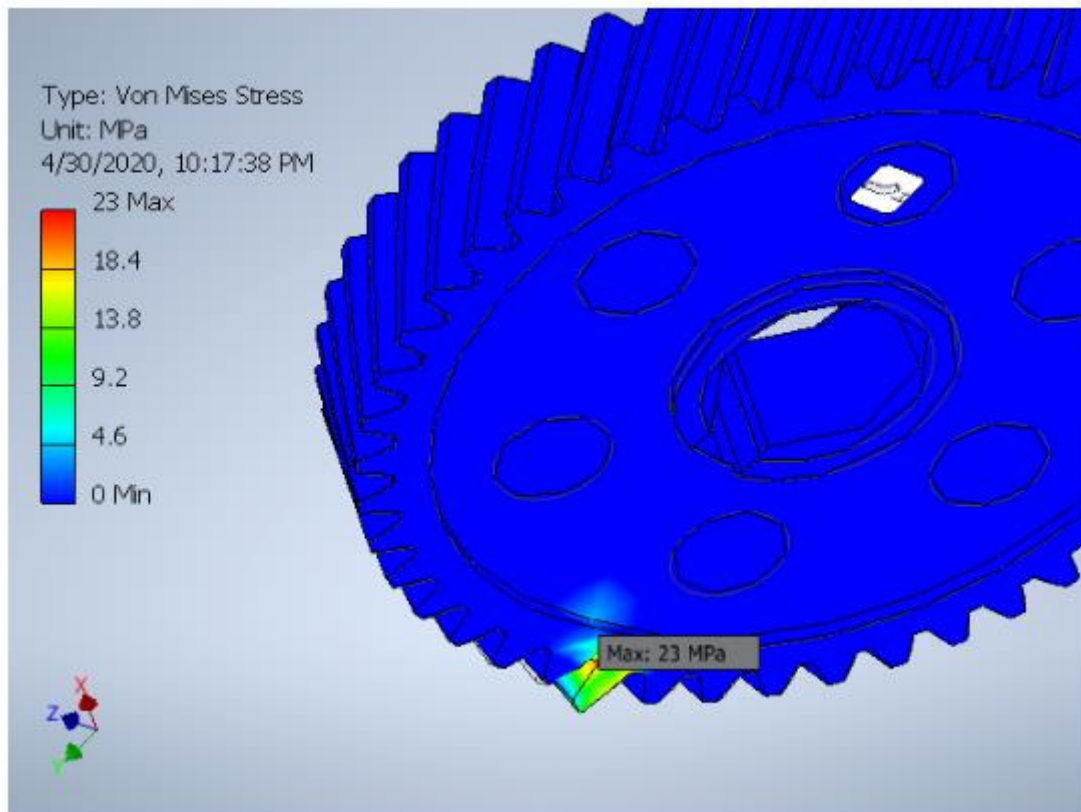
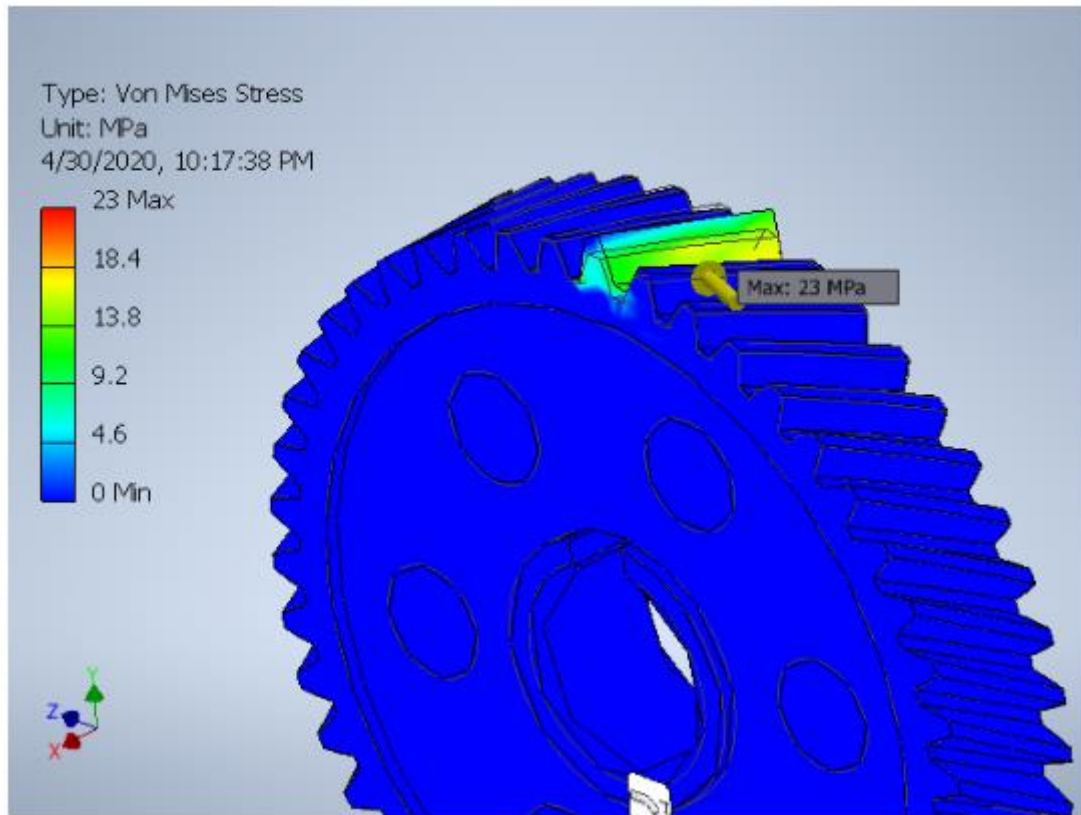
A.43. Safety Analyses of the First Pinion

☐ Safety Factor



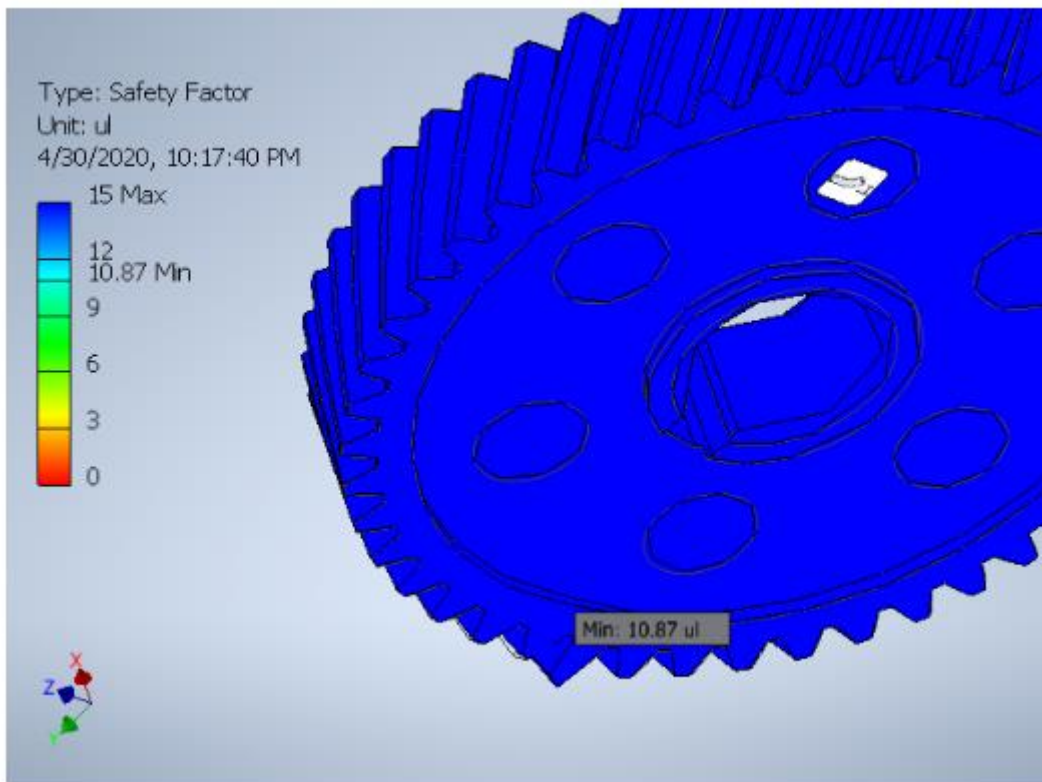
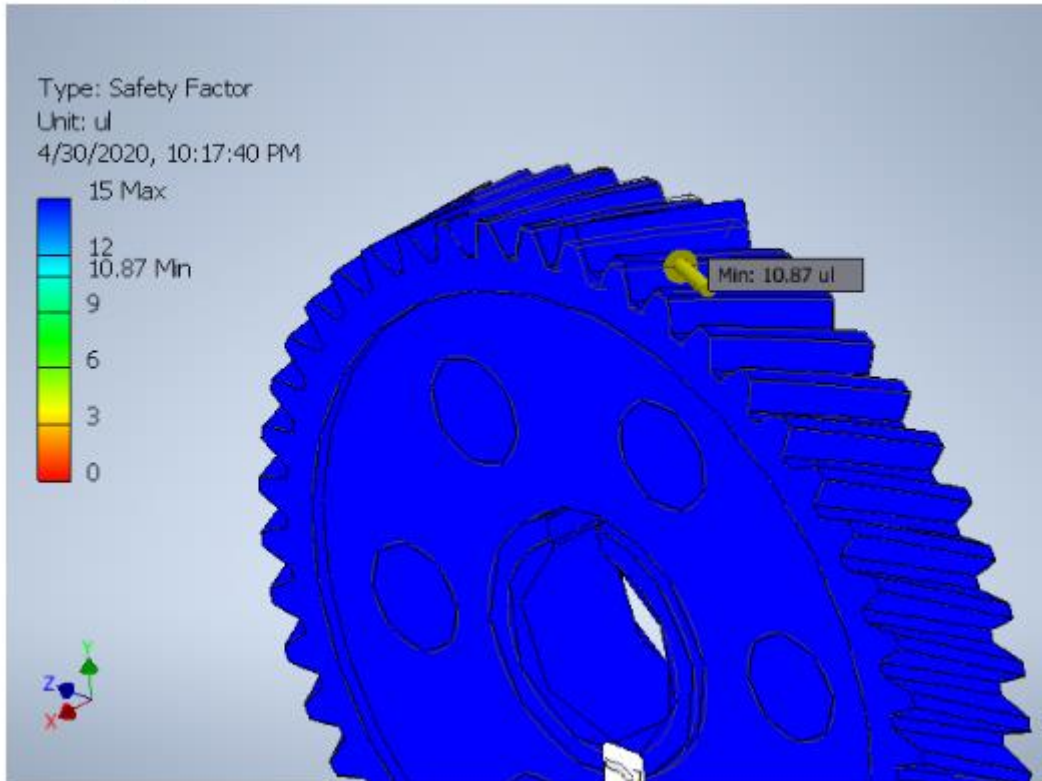
A.44. Stress Analyses of the First Gear

☐ Von Mises Stress



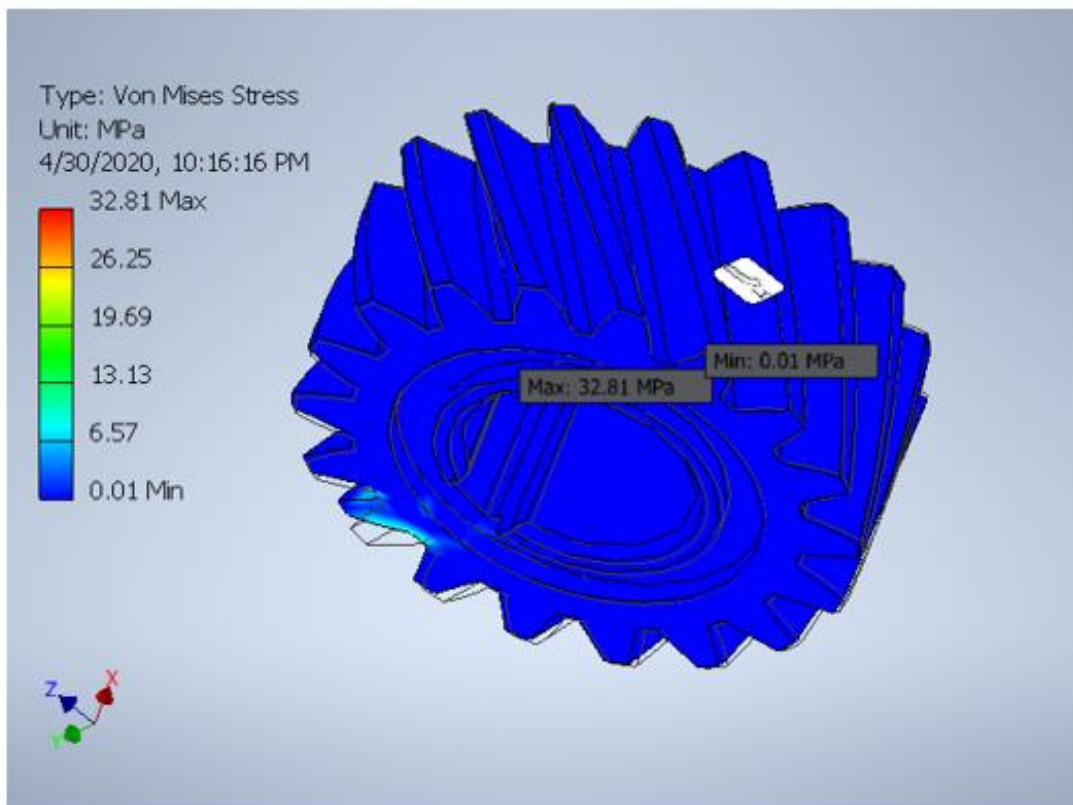
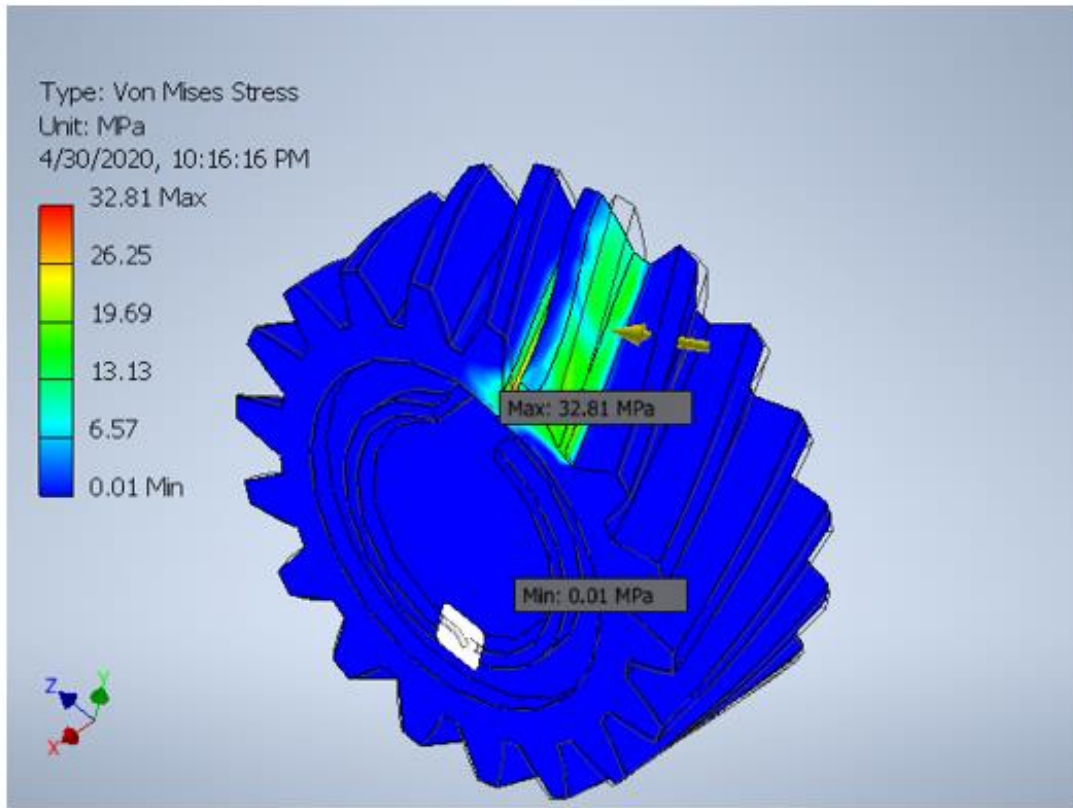
A.45. Safety Analyses of the First Gear

☐ Safety Factor



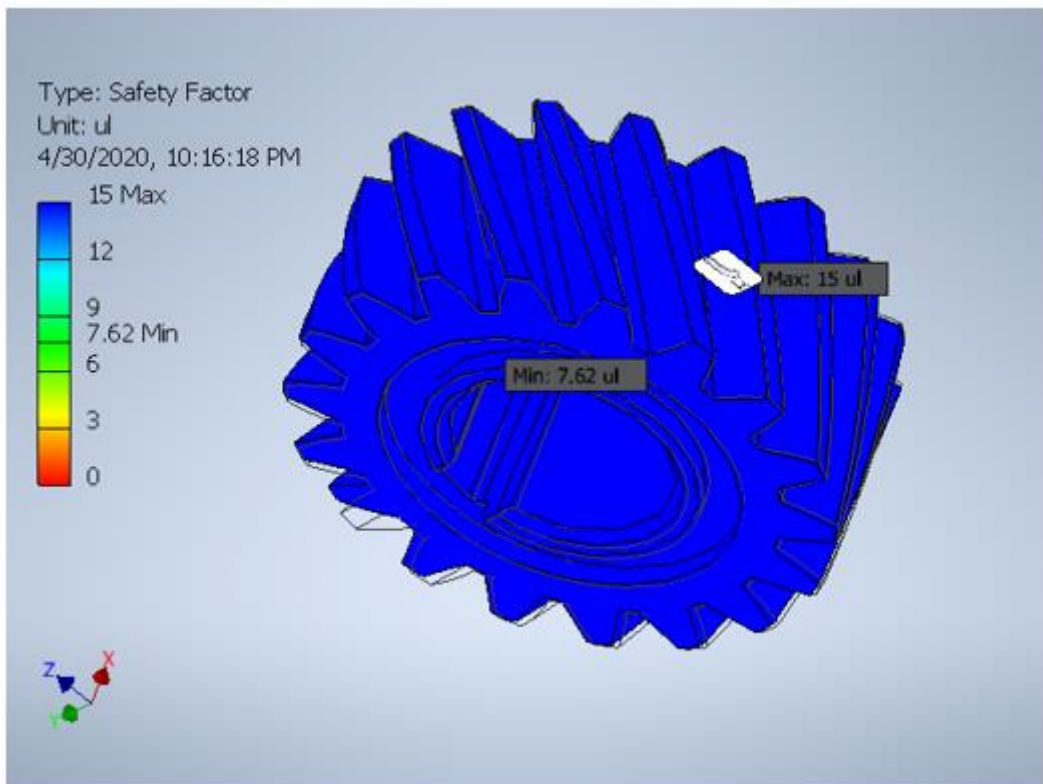
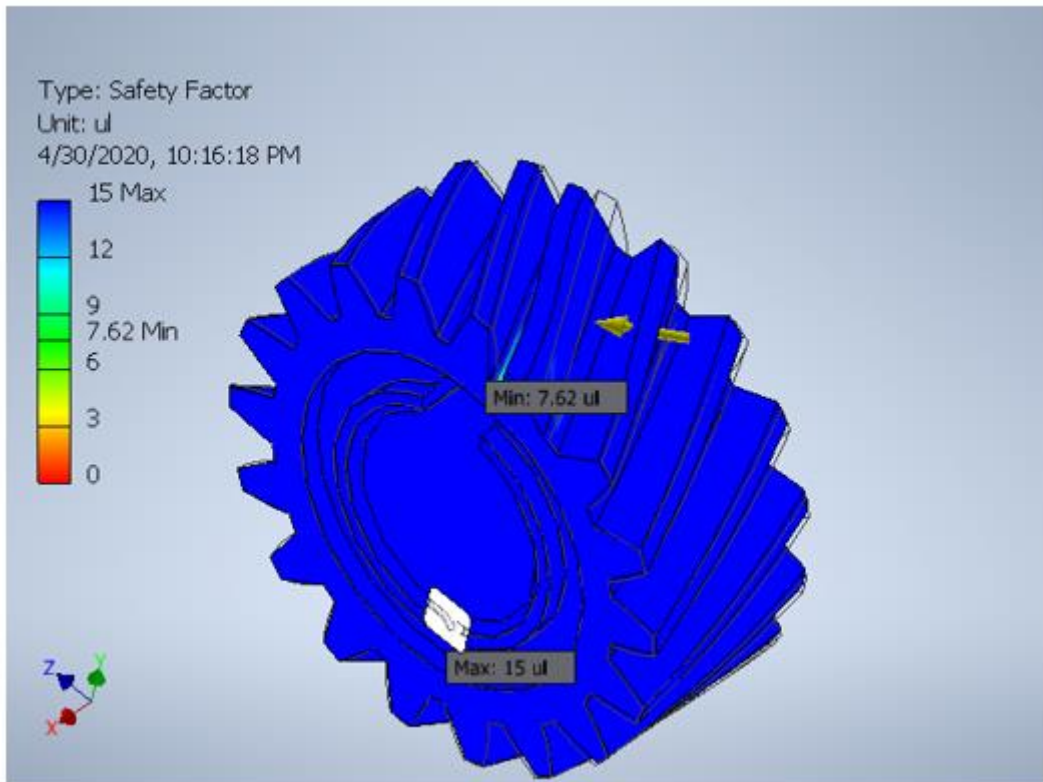
A.46. Stress Analyses of the Second Pinion

☐ Von Mises Stress



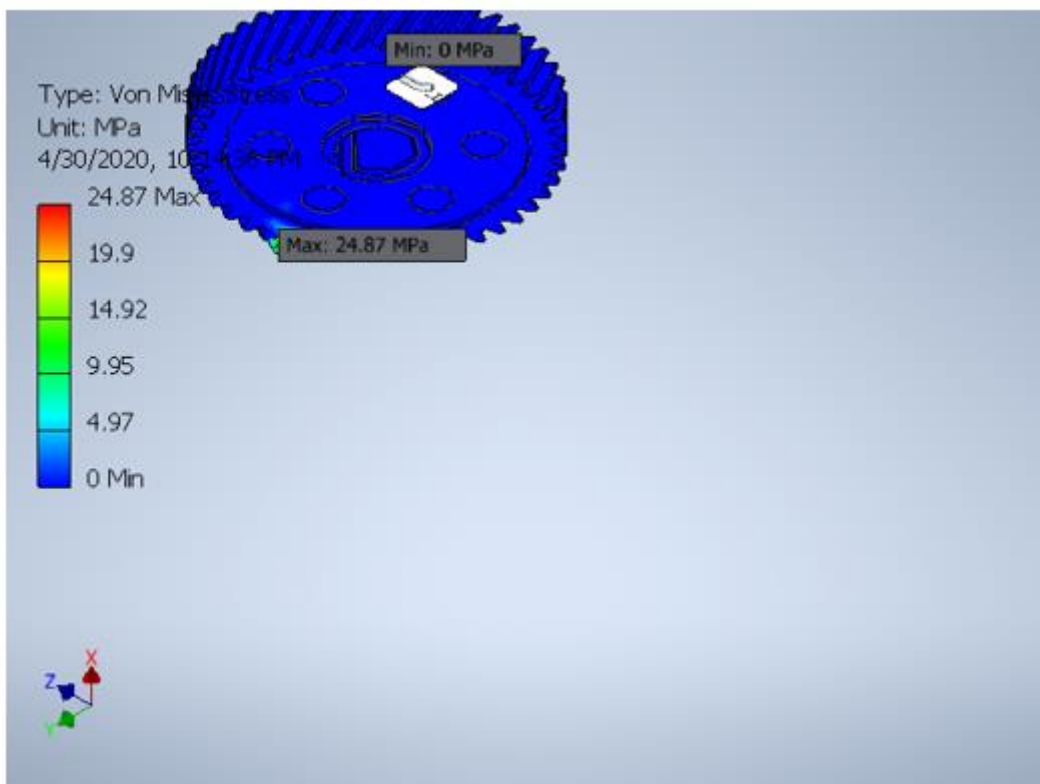
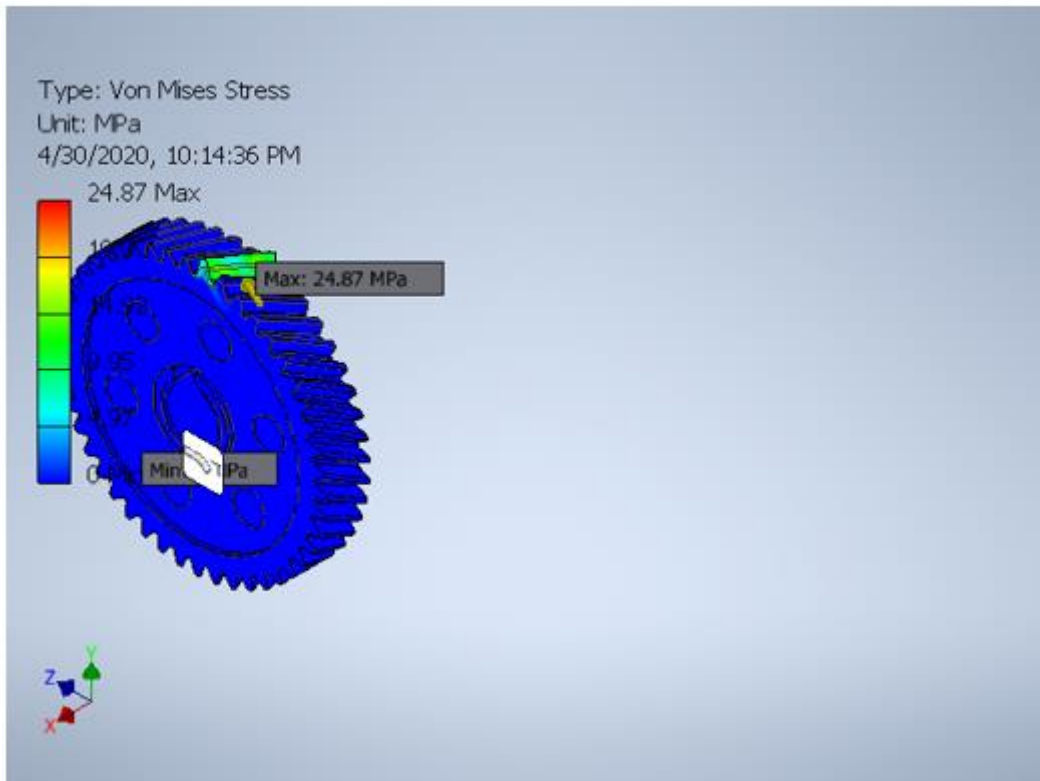
A.47. Safety Analyses of the Second Pinion

☐ Safety Factor



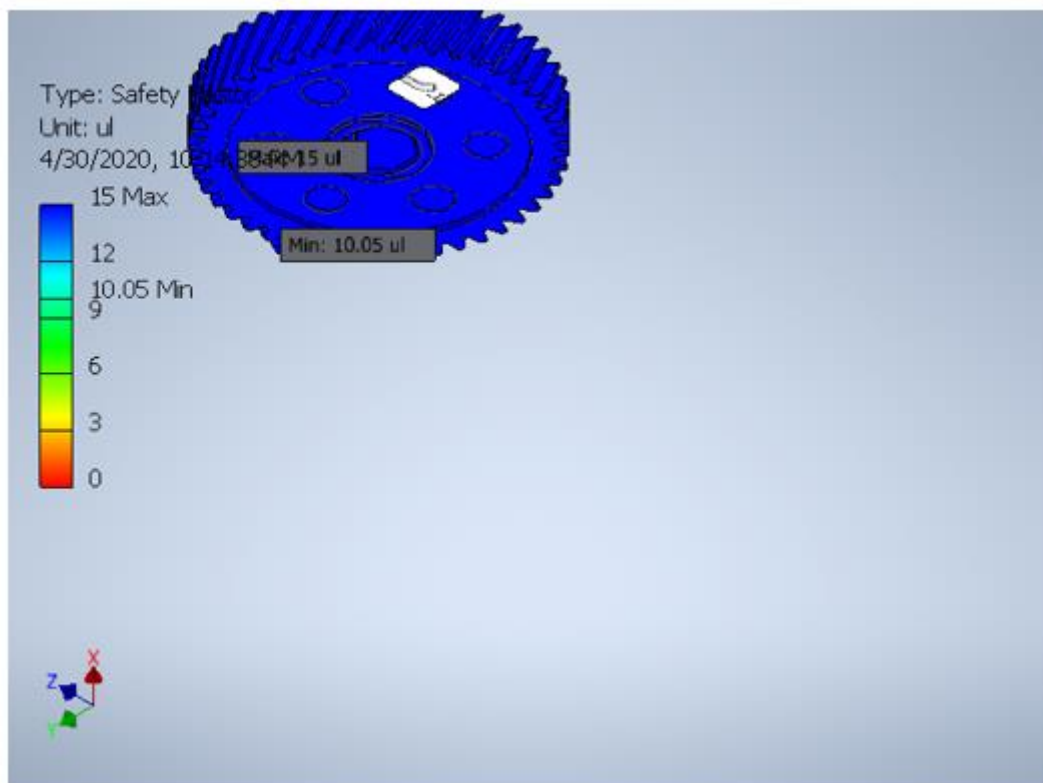
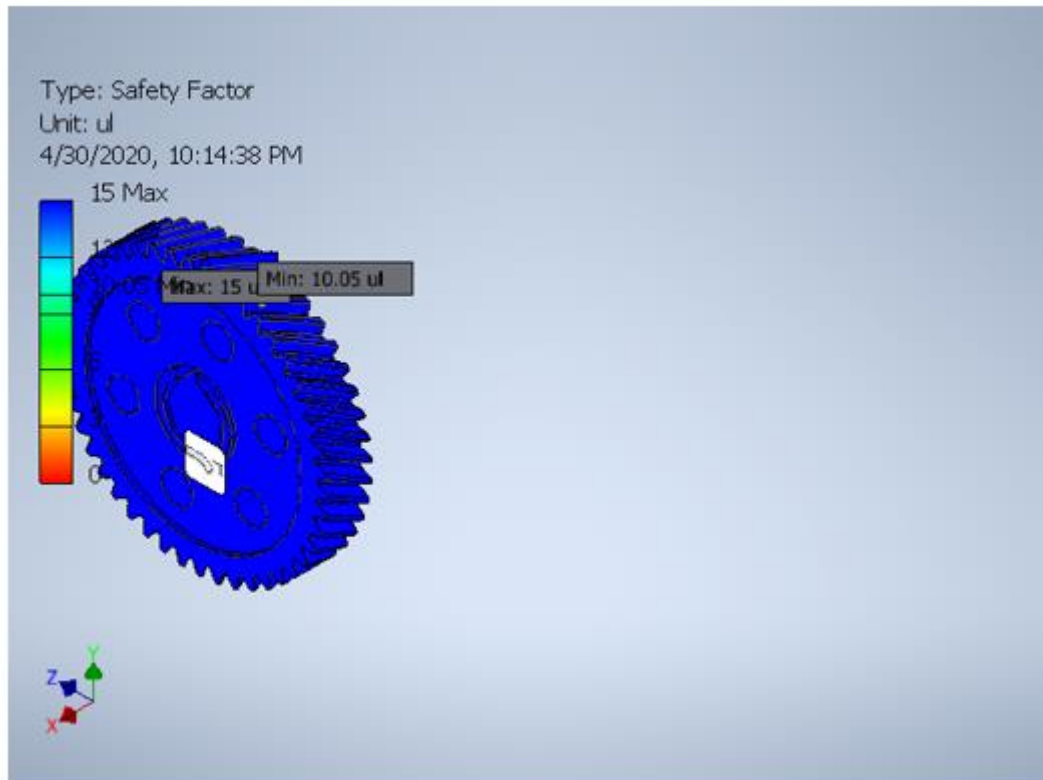
A.48. Stress Analyses of the Second Gear

☐ Von Mises Stress



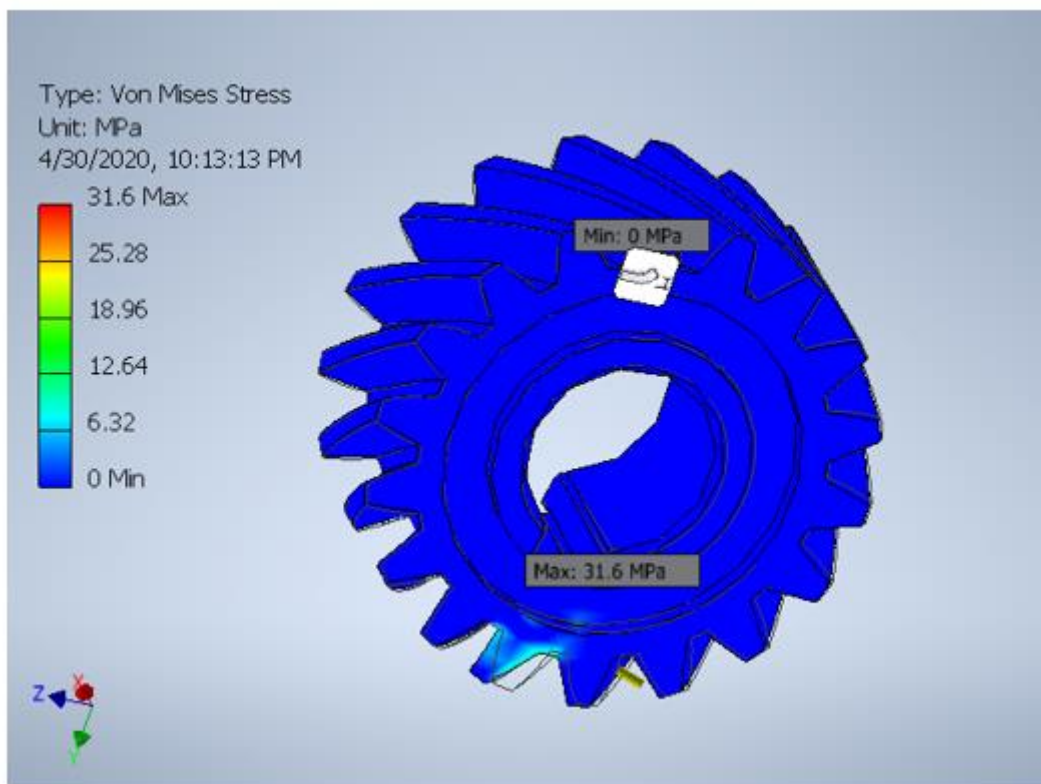
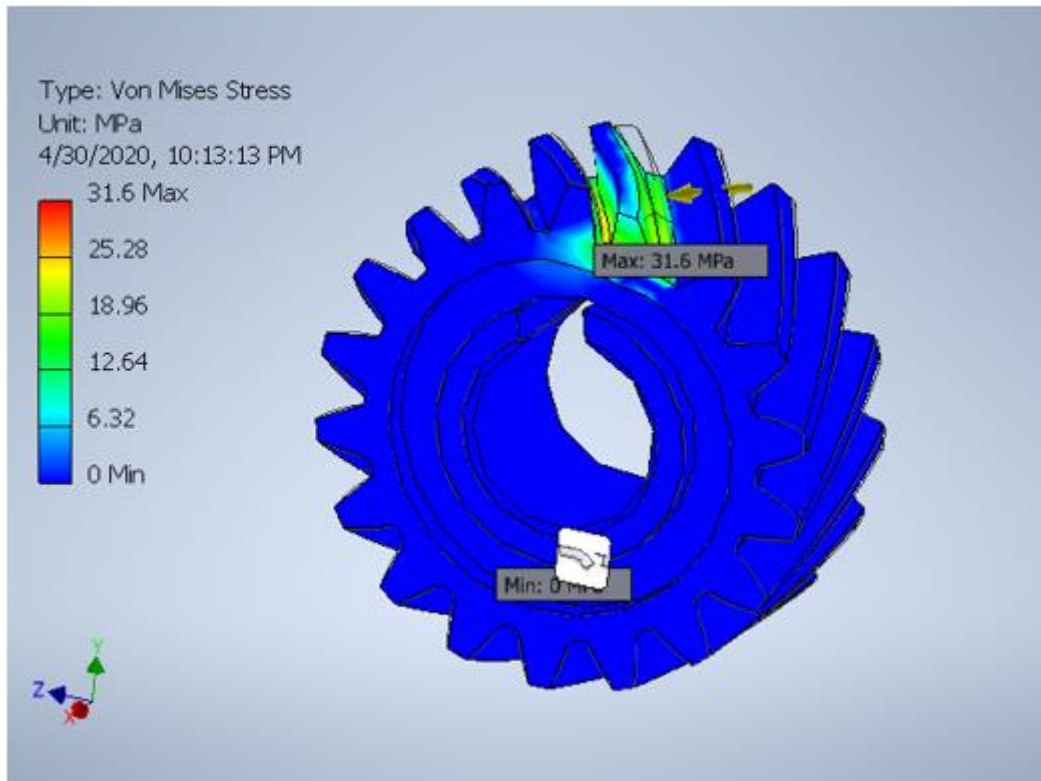
A.49. Safety Analyses of the Second Gear

☐ Safety Factor



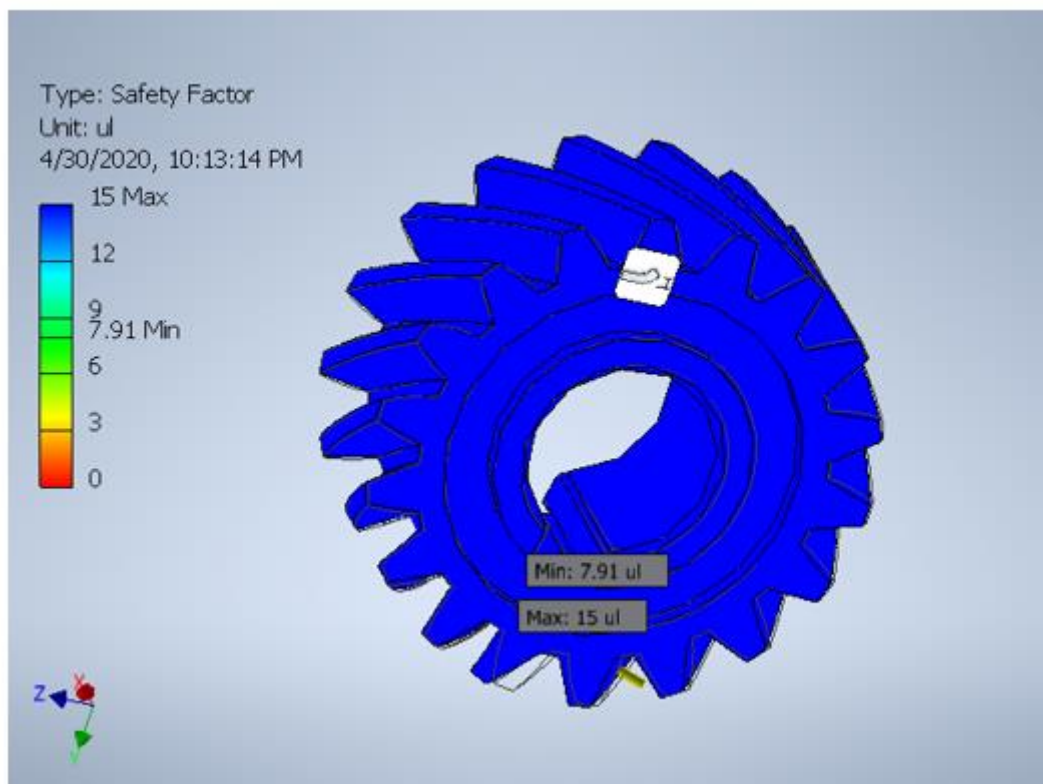
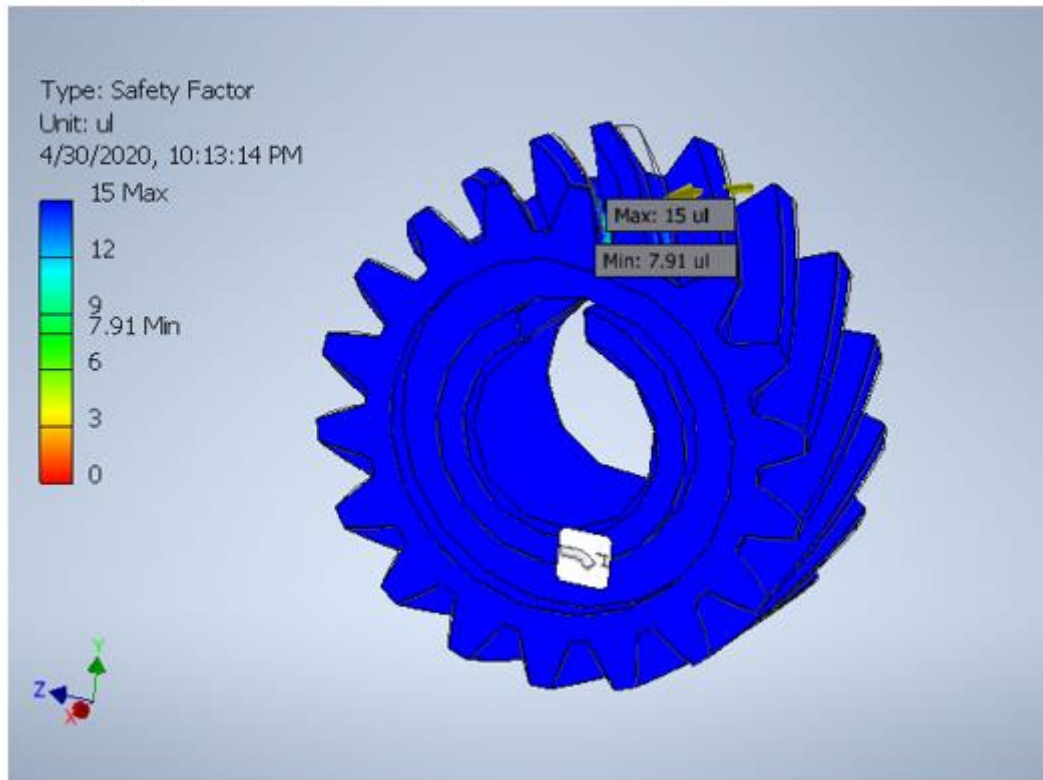
A.50. Stress Analyses of the Third Pinion

☐ Von Mises Stress



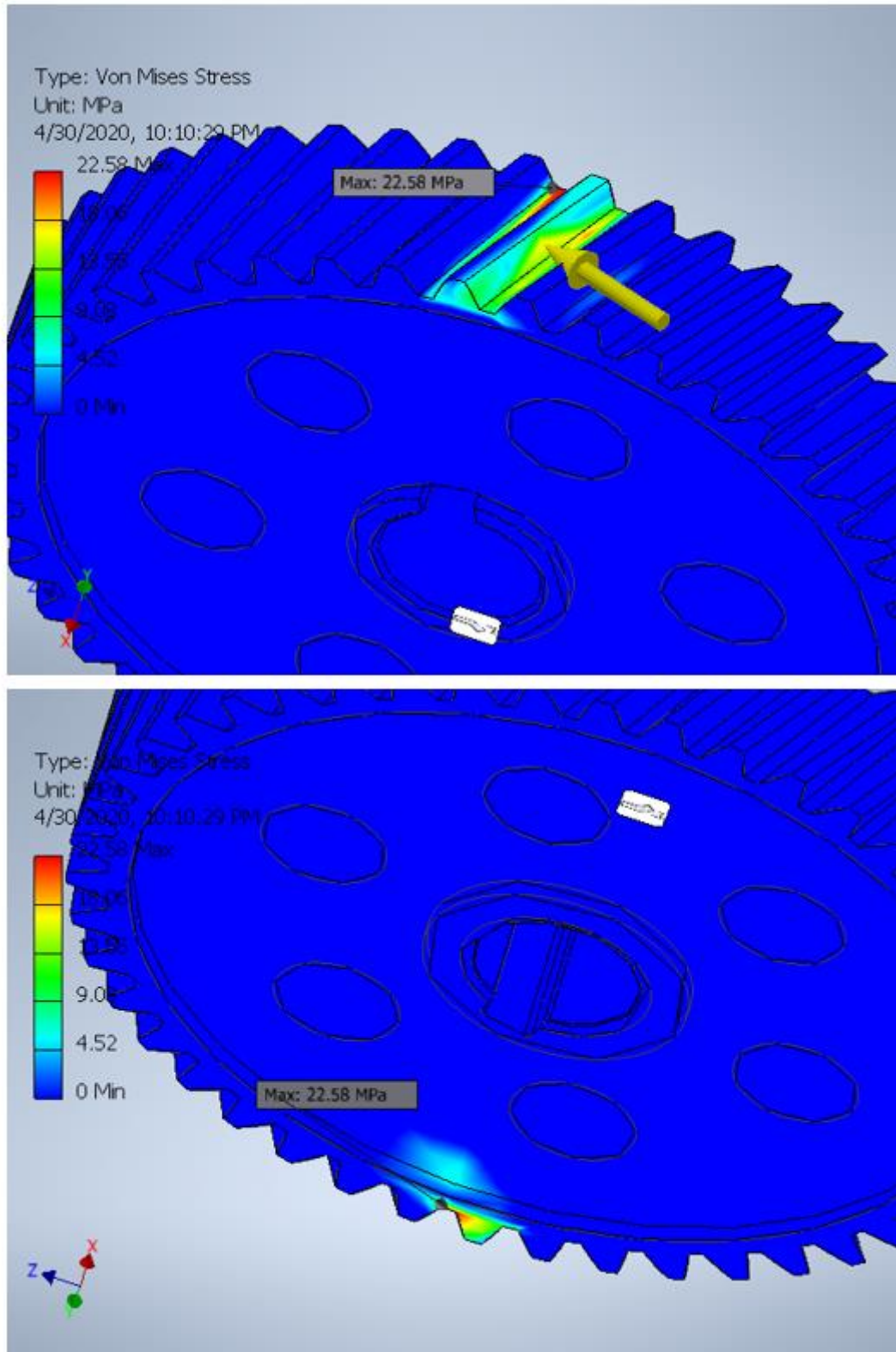
A.51. Safety Analyses of the Third Pinion

☐ Safety Factor



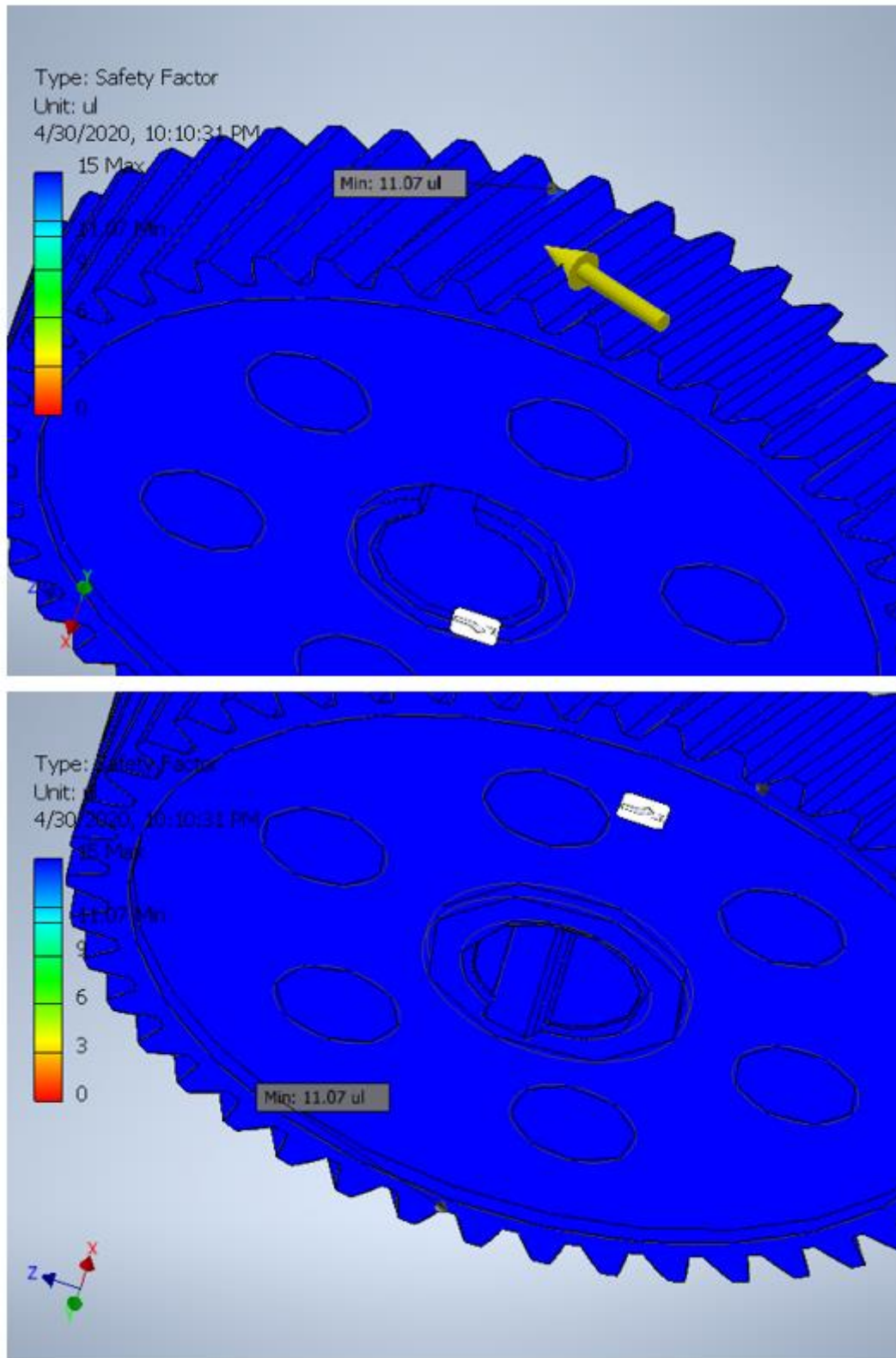
A.52. Stress Analyses of the Third Gear

☐ Von Mises Stress



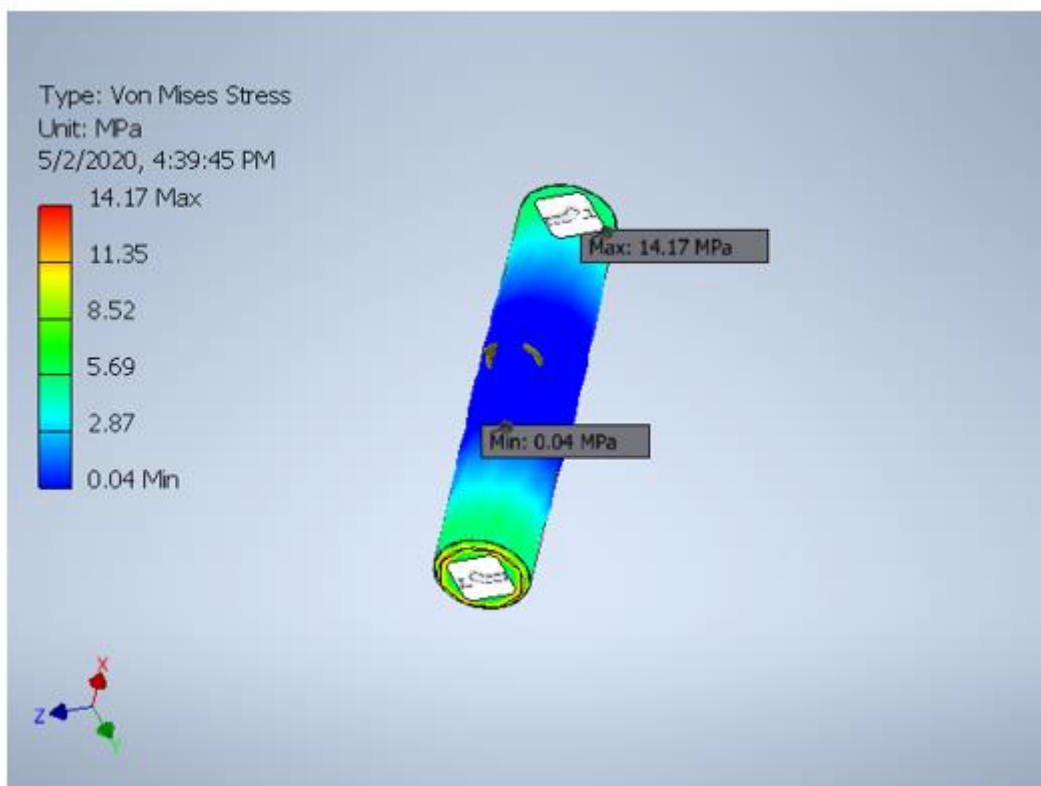
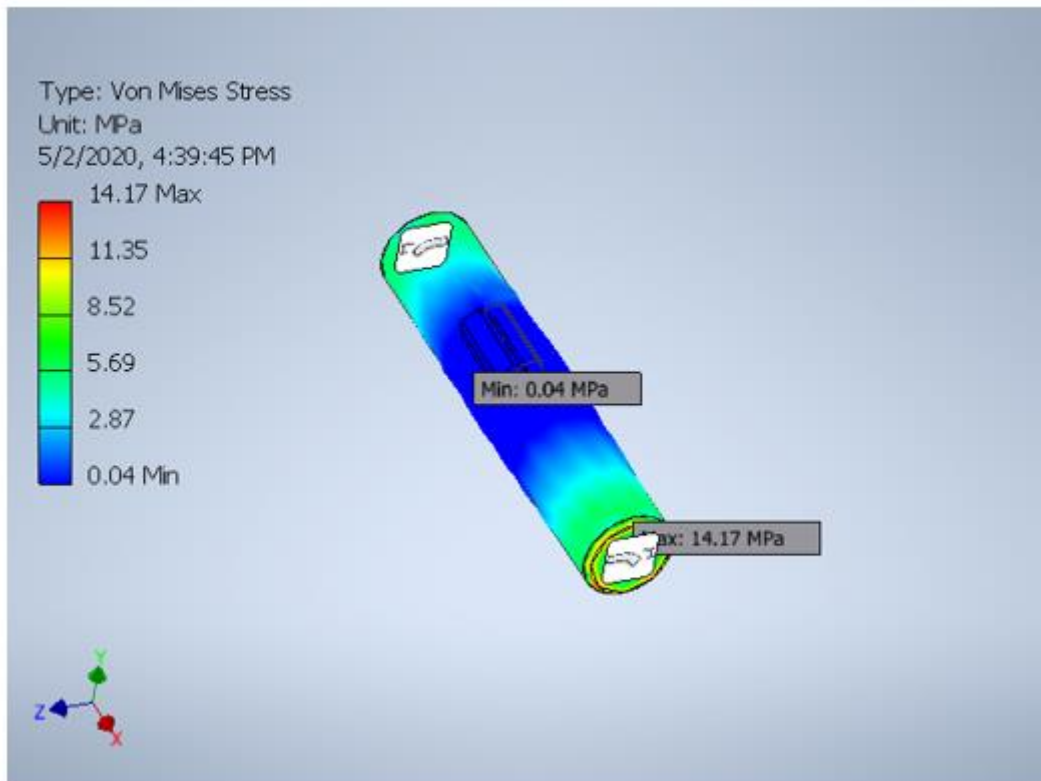
A.53. Safety Analyses of the Third Pinion

☐ Safety Factor



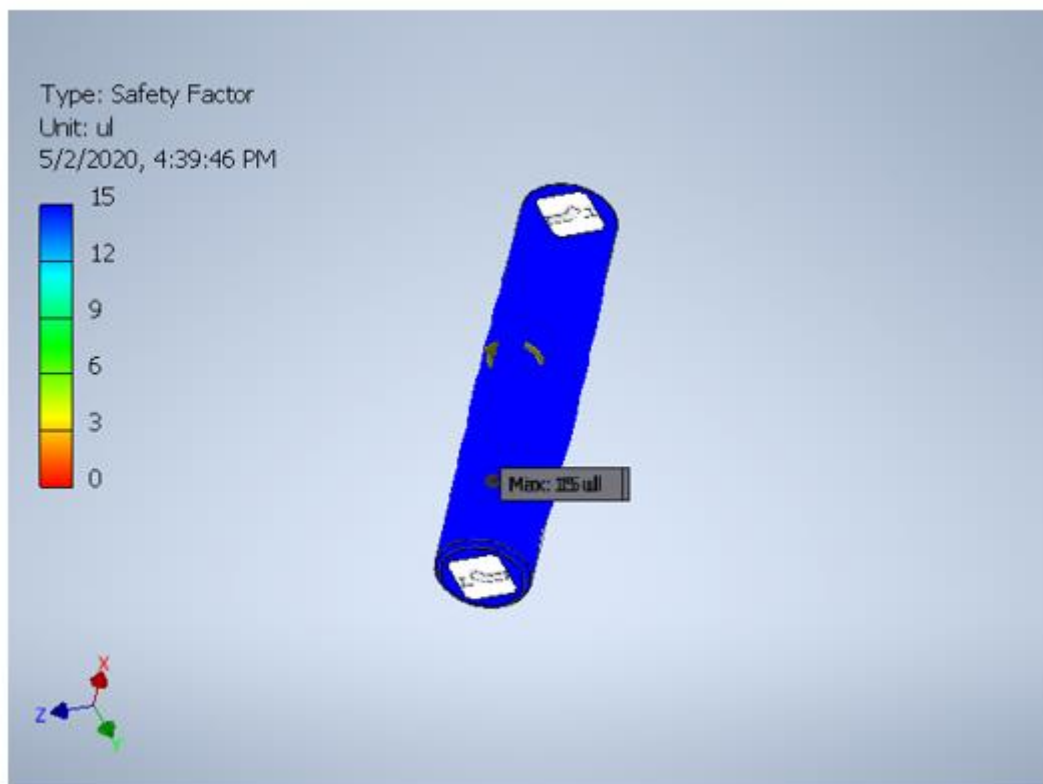
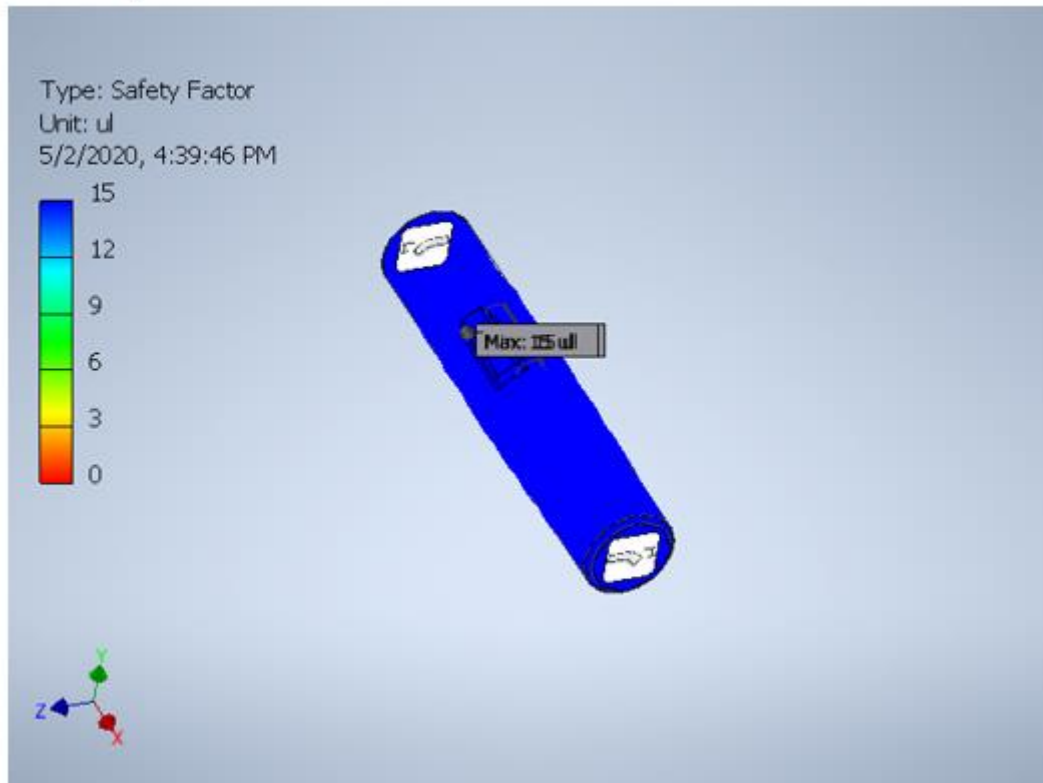
A.54. Stress Analyses of the First Shaft

☐ Von Mises Stress



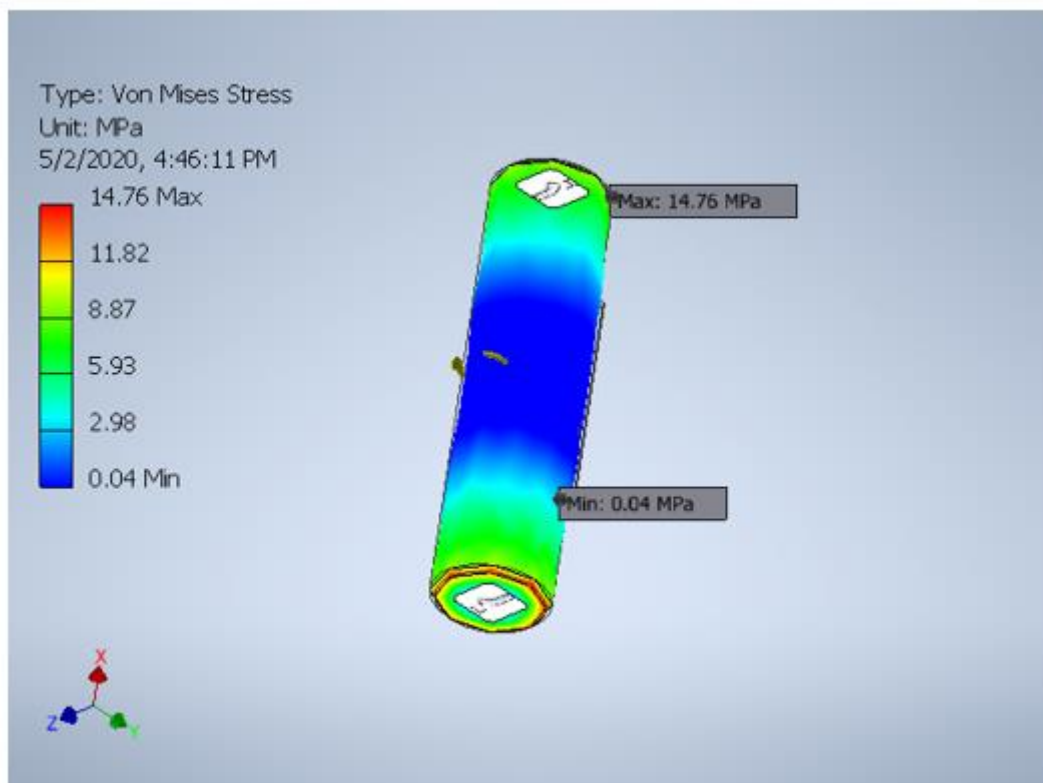
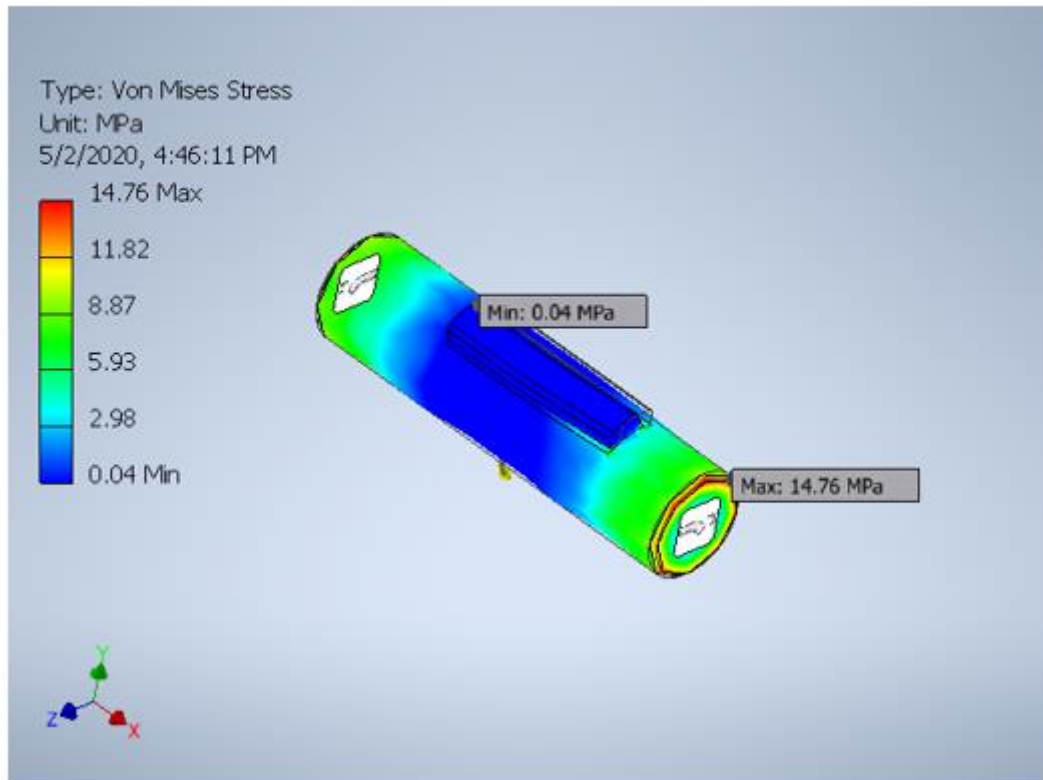
A.55. Safety Analyses of the First Shaft

☐ Safety Factor



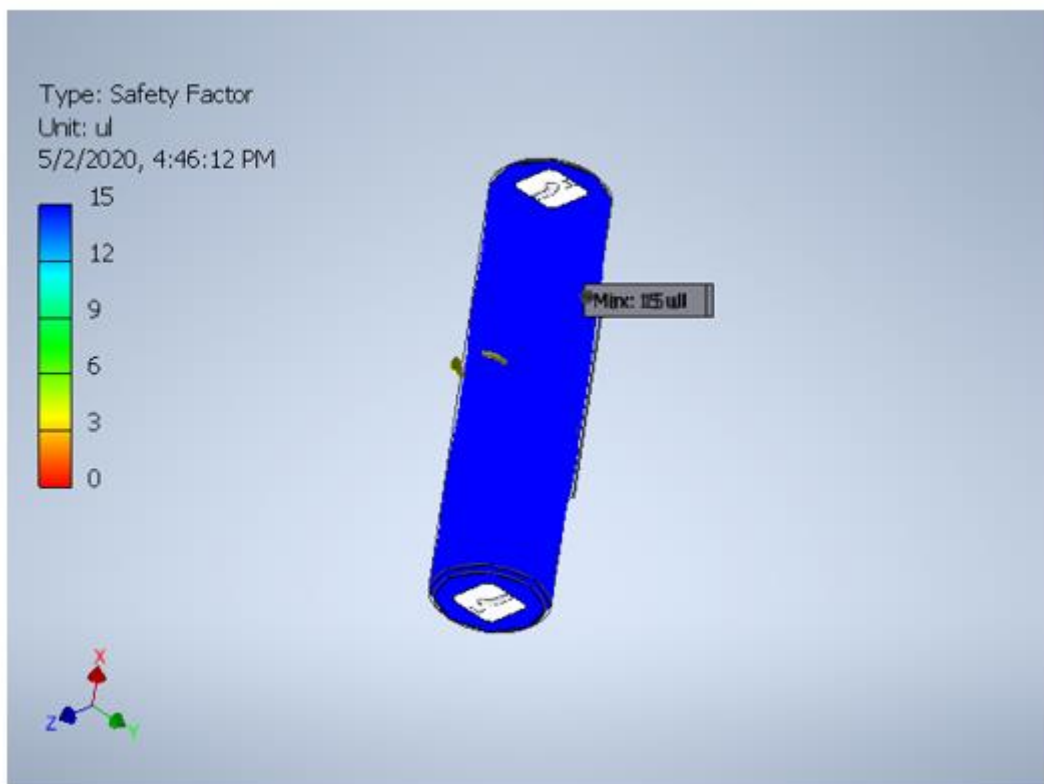
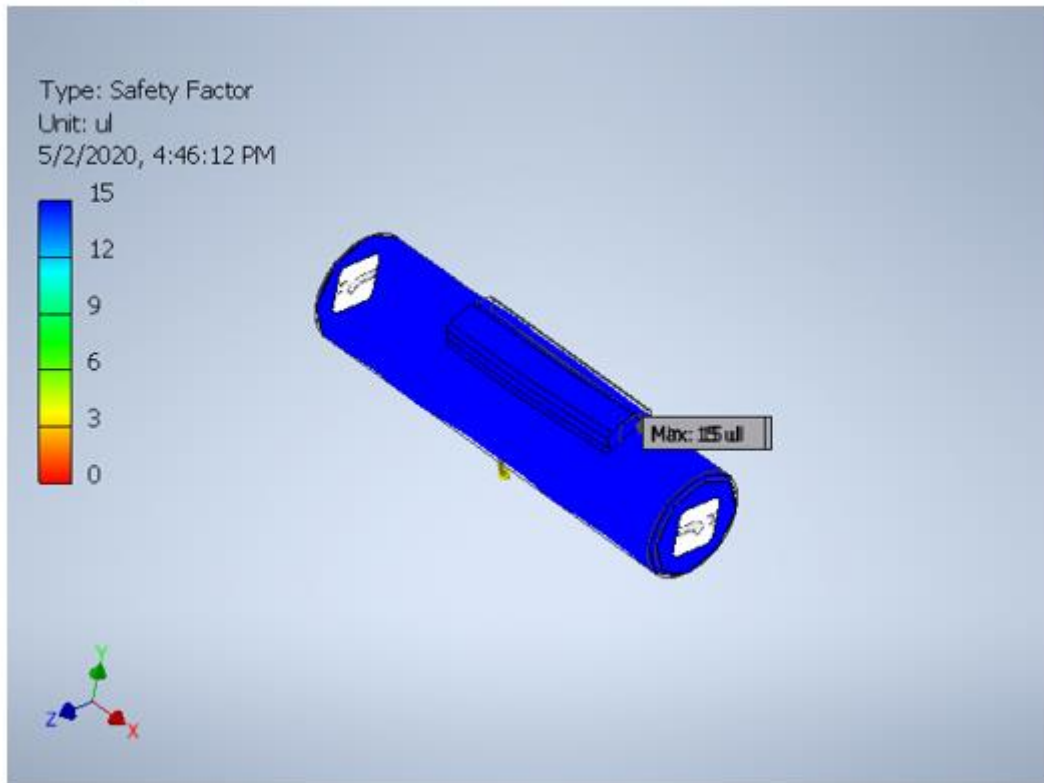
A.56. Stress Analyses of the Second Shaft

☐ Von Mises Stress



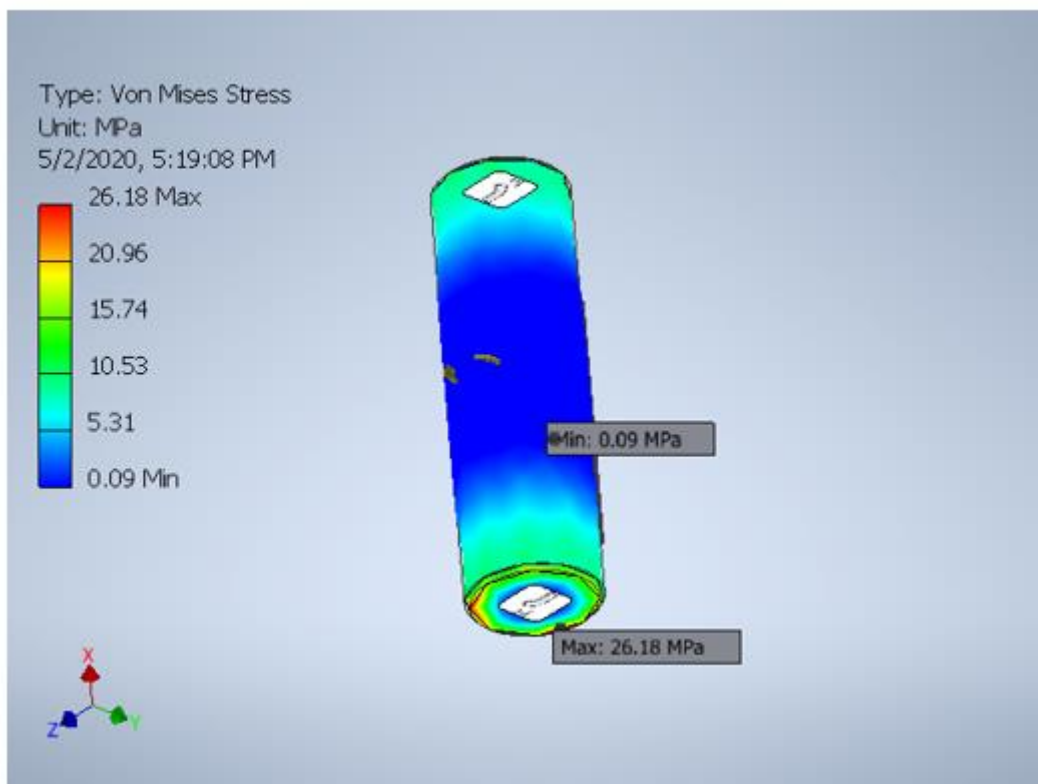
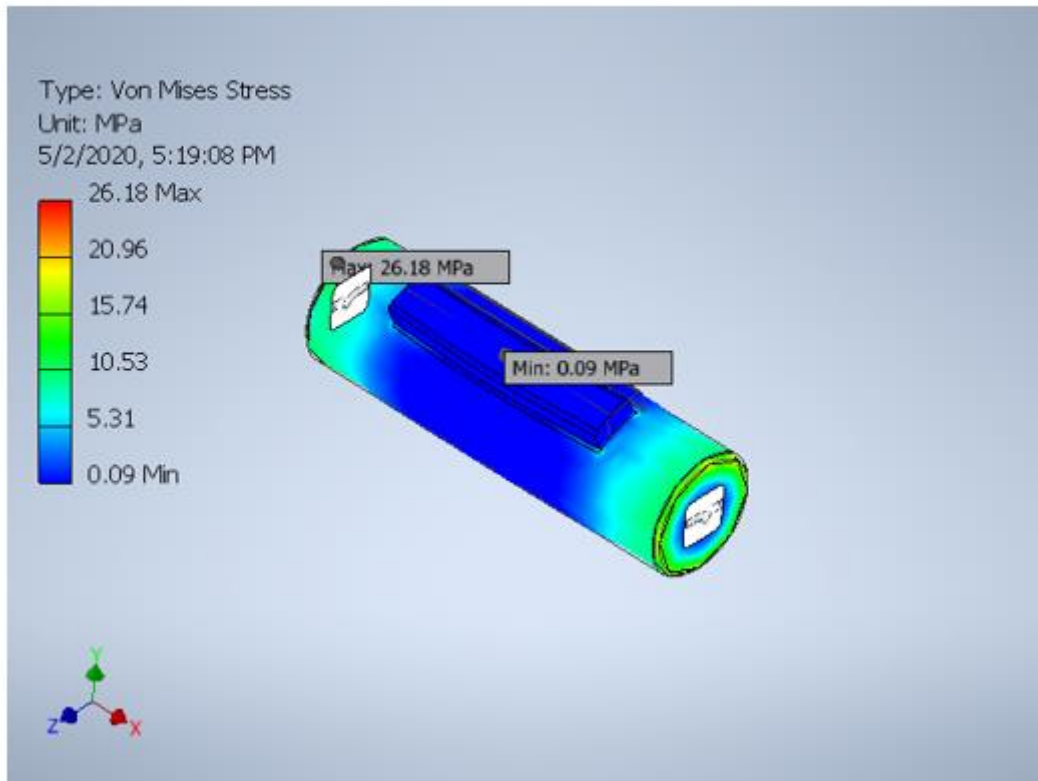
A.57. Safety Analyses of the Second Shaft

☐ Safety Factor



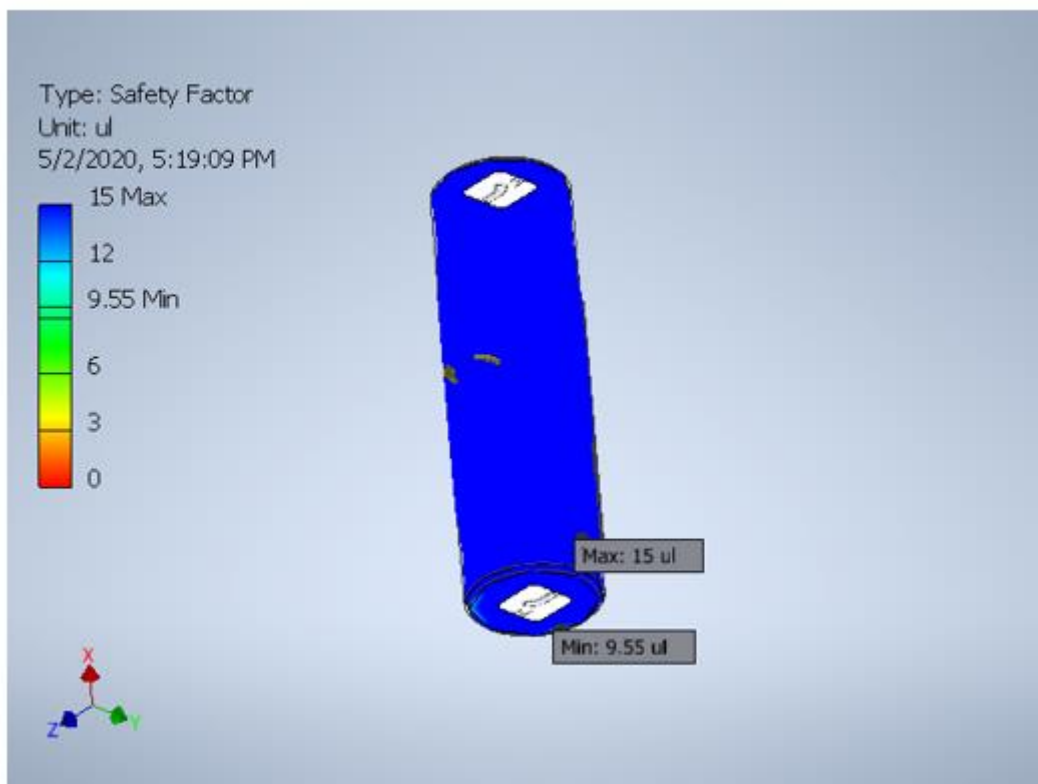
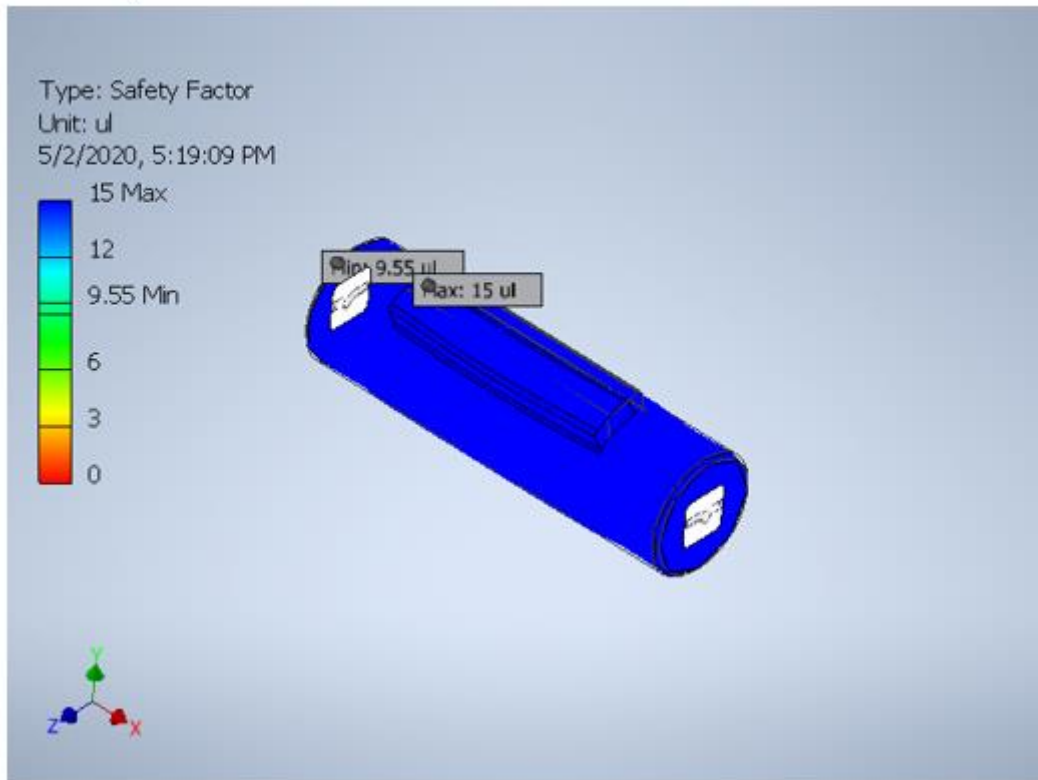
A.58. Stress Analyses of the Third Shaft

☐ Von Mises Stress



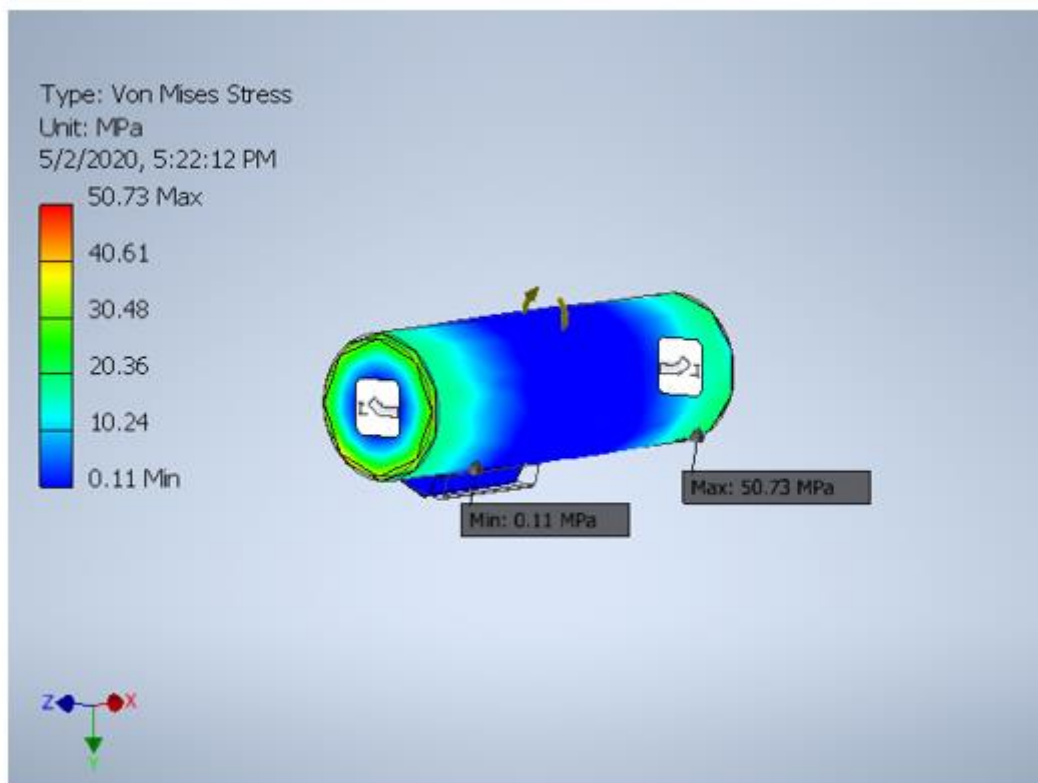
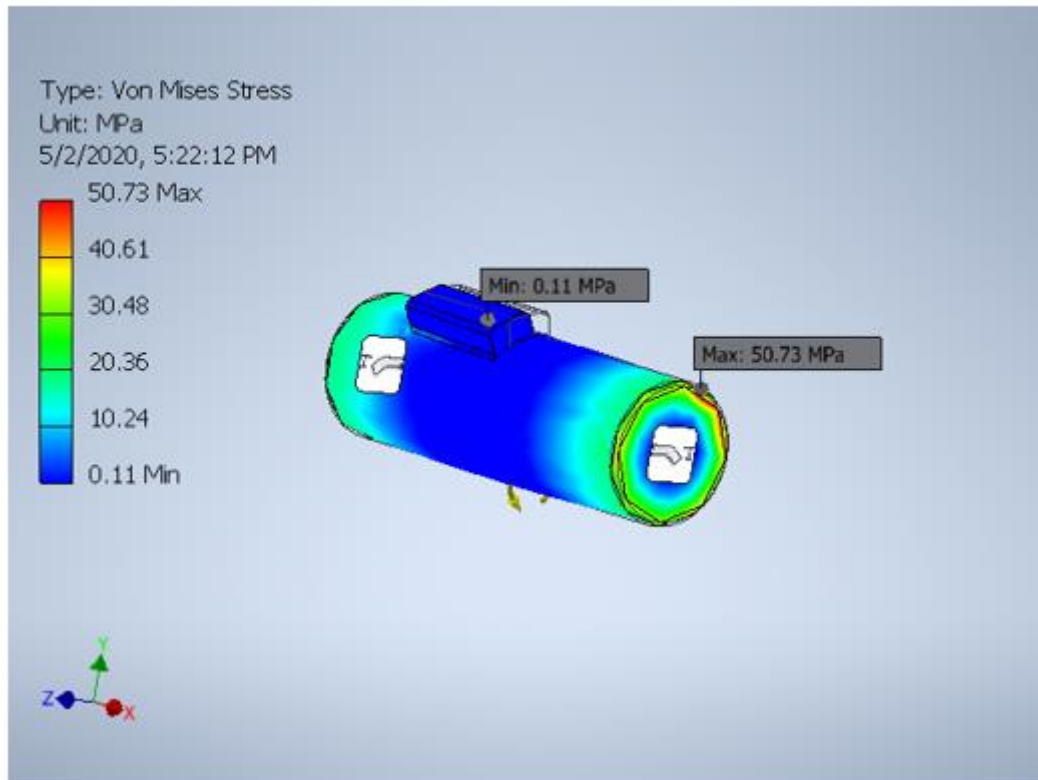
A.59. Safety Analyses of the Third Shaft

☐ Safety Factor



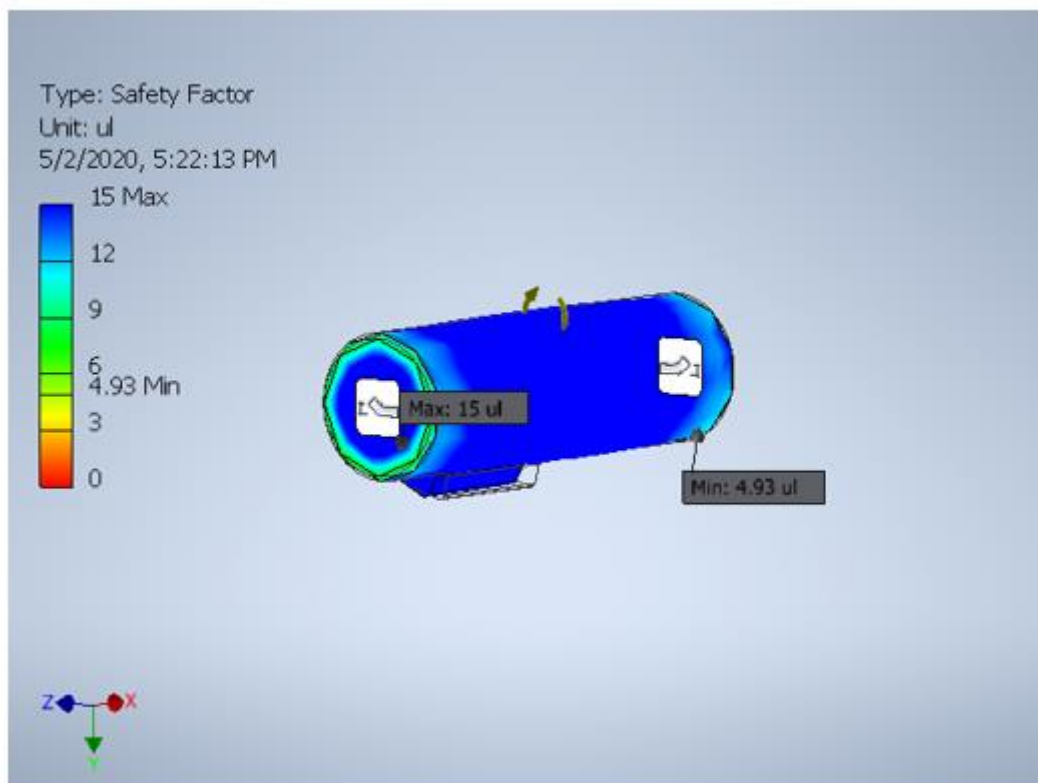
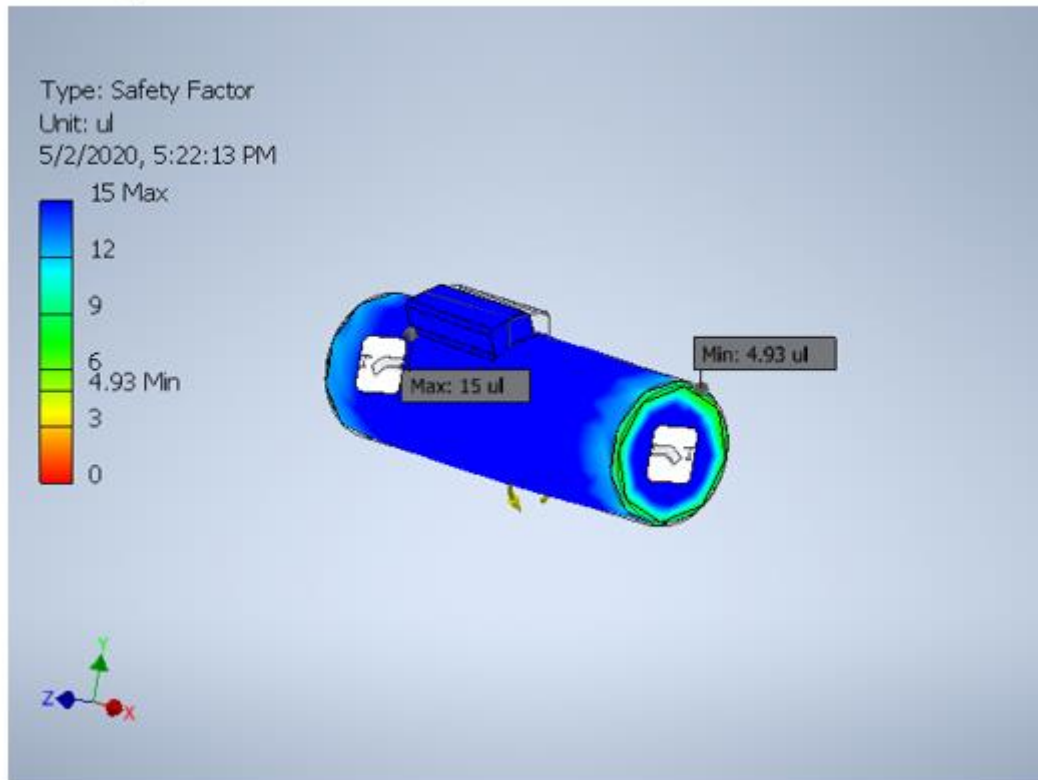
A.60. Stress Analyses of the Fourth Shaft

☐ Von Mises Stress



A.61. Safety Analyses of the Fourth Shaft

☐ Safety Factor

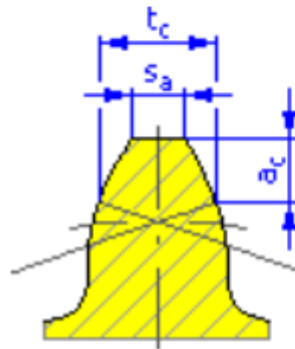
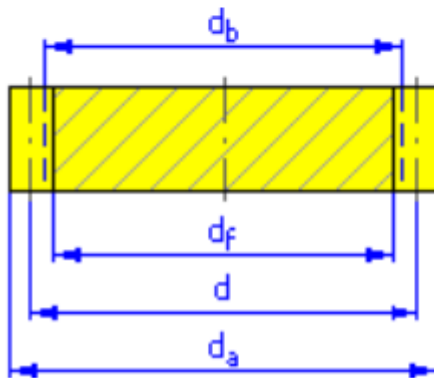


A.62. Parameters of the First Gear Pair

Gear Ratio	i	2.5556 ul
Desired Gear Ratio	i_{in}	2.5500 ul
Module	m	3.490 mm
Helix Angle	β	30.0000 deg
Pressure Angle	α	20.0000 deg
Center Distance	a_w	128.957 mm
Product Center Distance	a	128.957 mm
Total Unit Correction	Σx	0.0000 ul
Circular Pitch	p	10.964 mm
Base Circular Pitch	p_{tb}	11.671 mm
Operating Pressure Angle	α_w	20.0000 deg
Tangential Pressure Angle	α_t	22.7959 deg
Tangential Operating Pressure Angle	α_{tw}	22.7959 deg
Base Helix Angle	β_b	28.0243 deg
Tangential Module	m_t	4.030 mm
Tangential Circular Pitch	p_t	12.660 mm
Contact Ratio	ε	2.8039 ul
Transverse Contact Ratio	ε_α	1.3446 ul
Overlap Ratio	ε_β	1.4593 ul
Limit Deviation of Axis Parallelity	f_x	0.0120 mm
Limit Deviation of Axis Parallelity	f_y	0.0060 mm

		Gear 1	Gear 2
Type of model		Component	Component
Number of Teeth	z	18 ul	46 ul
Unit Correction	x	0.0000 ul	0.0000 ul
Pitch Diameter	d	72.538 mm	185.376 mm
Outside Diameter	d_a	79.518 mm	192.356 mm
Root Diameter	d_f	63.813 mm	176.651 mm
Base Circle Diameter	d_b	66.872 mm	170.896 mm
Work Pitch Diameter	d_w	72.538 mm	185.376 mm
Facewidth	b	32.000 mm	32.000 mm
Facewidth Ratio	b_r	0.4411 ul	0.1726 ul
Addendum	a^*	1.0000 ul	1.0000 ul
Clearance	c^*	0.2500 ul	0.2500 ul
Root Fillet	r_f^*	0.3500 ul	0.3500 ul
Tooth Thickness	s	5.482 mm	5.482 mm
Tangential Tooth Thickness	s_t	6.330 mm	6.330 mm
Chordal Thickness	t_c	4.841 mm	4.841 mm
Chordal Addendum	a_c	2.609 mm	2.609 mm
Chordal Dimension	W	37.383 mm	80.653 mm
Chordal Dimension Teeth	z_w	4.000 ul	8.000 ul
Dimension Over (Between) Wires	M	80.831 mm	193.772 mm
Wire Diameter	d_M	6.000 mm	6.000 mm
Limit Deviation of Helix Angle	F_β	0.0120 mm	0.0130 mm
Limit Circumferential Run-out	F_r	0.0210 mm	0.0280 mm
Limit Deviation of Axial Pitch	f_{pt}	0.0085 mm	0.0090 mm
Limit Deviation of Basic Pitch	f_{pb}	0.0080 mm	0.0085 mm
Virtual Number of Teeth	z_v	26.673 ul	68.164 ul

Virtual Pitch Diameter	d_n	93.088 mm	237.891 mm
Virtual Outside Diameter	d_{an}	100.068 mm	244.871 mm
Virtual Base Circle Diameter	d_{bn}	87.474 mm	223.545 mm
Unit Correction without Tapering	x_z	0.4442 ul	-0.5519 ul
Unit Correction without Undercut	x_p	-0.5404 ul	-2.9671 ul
Unit Correction Allowed Undercut	x_d	-0.7103 ul	-3.1371 ul
Addendum Truncation	k	0.0000 ul	0.0000 ul
Unit Outside Tooth Thickness	s_a	0.6995 ul	0.7790 ul
Tip Pressure Angle	α_a	30.9955 deg	25.0966 deg

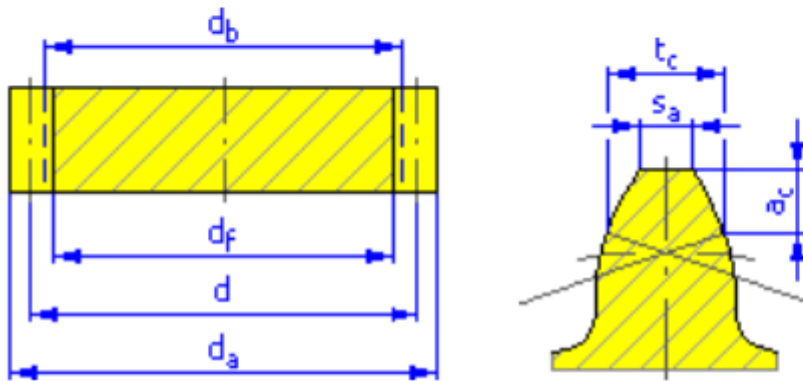


A.63. Parameters of the Second Gear Pair

Gear Ratio	i	2.5556 ul
Desired Gear Ratio	i_{in}	2.5300 ul
Module	m	4.740 mm
Helix Angle	β	30.0000 deg
Pressure Angle	α	20.0000 deg
Center Distance	a_w	175.145 mm
Product Center Distance	a	175.145 mm
Total Unit Correction	Σx	0.0000 ul
Circular Pitch	p	14.891 mm
Base Circular Pitch	p_{tb}	15.852 mm
Operating Pressure Angle	α_w	20.0000 deg
Tangential Pressure Angle	α_t	22.7959 deg
Tangential Operating Pressure Angle	α_{tw}	22.7959 deg
Base Helix Angle	β_b	28.0243 deg
Tangential Module	m_t	5.473 mm
Tangential Circular Pitch	p_t	17.195 mm
Contact Ratio	ε	2.7885 ul
Transverse Contact Ratio	ε_α	1.3446 ul
Overlap Ratio	ε_β	1.4438 ul
Limit Deviation of Axis Parallelity	f_x	0.0140 mm
Limit Deviation of Axis Parallelity	f_y	0.0070 mm

		Gear 1	Gear 2
Type of model		Component	Component
Number of Teeth	z	18 ul	46 ul
Unit Correction	x	0.0000 ul	0.0000 ul
Pitch Diameter	d	98.519 mm	251.771 mm
Outside Diameter	d_a	107.999 mm	261.251 mm
Root Diameter	d_f	86.669 mm	239.921 mm
Base Circle Diameter	d_b	90.824 mm	232.105 mm
Work Pitch Diameter	d_w	98.519 mm	251.771 mm
Facewidth	b	43.000 mm	43.000 mm
Facewidth Ratio	b_r	0.4365 ul	0.1708 ul
Addendum	a^*	1.0000 ul	1.0000 ul
Clearance	c^*	0.2500 ul	0.2500 ul
Root Fillet	r_f^*	0.3500 ul	0.3500 ul
Tooth Thickness	s	7.446 mm	7.446 mm
Tangential Tooth Thickness	s_t	8.597 mm	8.597 mm
Chordal Thickness	t_c	6.575 mm	6.575 mm
Chordal Addendum	a_c	3.544 mm	3.544 mm
Chordal Dimension	W	50.773 mm	109.541 mm
Chordal Dimension Teeth	z_w	4.000 ul	8.000 ul
Dimension Over (Between) Wires	M	112.701 mm	266.304 mm
Wire Diameter	d_M	9.000 mm	9.000 mm
Limit Deviation of Helix Angle	F_β	0.0140 mm	0.0150 mm
Limit Circumferential Run-out	F_r	0.0220 mm	0.0290 mm
Limit Deviation of Axial Pitch	f_{pt}	0.0090 mm	0.0100 mm
Limit Deviation of Basic Pitch	f_{pb}	0.0085 mm	0.0095 mm
Virtual Number of Teeth	z_v	26.673 ul	68.164 ul

Virtual Pitch Diameter	d_n	126.429 mm	323.096 mm
Virtual Outside Diameter	d_{an}	135.909 mm	332.576 mm
Virtual Base Circle Diameter	d_{bn}	118.804 mm	303.611 mm
Unit Correction without Tapering	x_z	0.4442 ul	-0.5519 ul
Unit Correction without Undercut	x_p	-0.5404 ul	-2.9671 ul
Unit Correction Allowed Undercut	x_d	-0.7103 ul	-3.1371 ul
Addendum Truncation	k	0.0000 ul	0.0000 ul
Unit Outside Tooth Thickness	s_a	0.6995 ul	0.7790 ul
Tip Pressure Angle	α_a	30.9955 deg	25.0966 deg

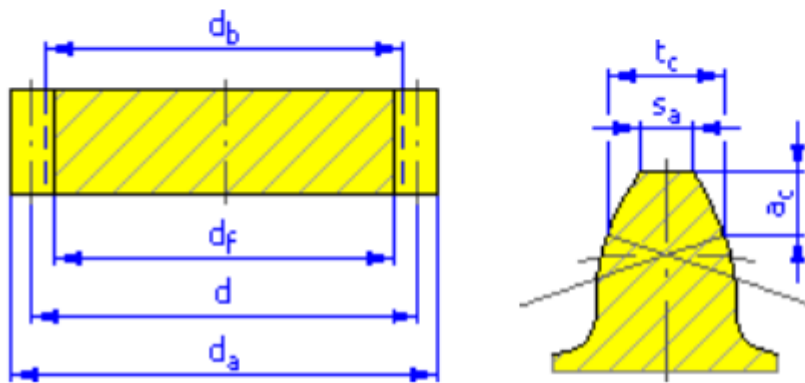


A.64. Parameters of the Third Gear Pair

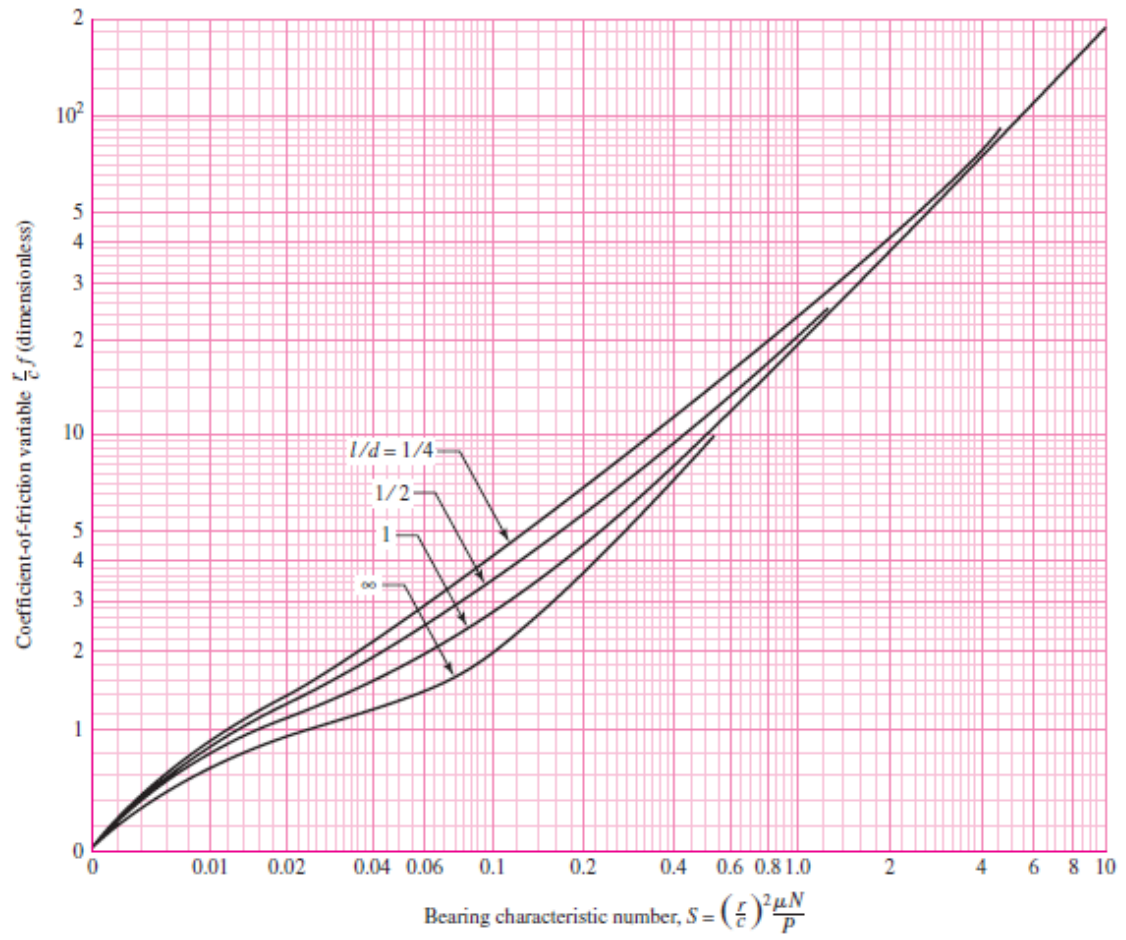
Gear Ratio	i	2.5000 ul
Desired Gear Ratio	i_{in}	2.5000 ul
Module	m	6.460 mm
Helix Angle	β	30.0000 deg
Pressure Angle	α	20.0000 deg
Center Distance	a_w	234.970 mm
Product Center Distance	a	234.970 mm
Total Unit Correction	Σx	0.0000 ul
Circular Pitch	p	20.295 mm
Base Circular Pitch	p_{tb}	21.604 mm
Operating Pressure Angle	α_w	20.0000 deg
Tangential Pressure Angle	α_t	22.7959 deg
Tangential Operating Pressure Angle	α_{tw}	22.7959 deg
Base Helix Angle	β_b	28.0243 deg
Tangential Module	m_t	7.459 mm
Tangential Circular Pitch	p_t	23.434 mm
Contact Ratio	ϵ	2.7724 ul
Transverse Contact Ratio	ϵ_a	1.3435 ul
Overlap Ratio	ϵ_β	1.4289 ul
Limit Deviation of Axis Parallelity	f_x	0.0150 mm
Limit Deviation of Axis Parallelity	f_y	0.0075 mm

		Gear 1	Gear 2
Type of model		Component	Component
Number of Teeth	z	18 ul	45 ul
Unit Correction	x	0.0000 ul	0.0000 ul
Pitch Diameter	d	134.269 mm	335.671 mm
Outside Diameter	d_a	147.189 mm	348.591 mm
Root Diameter	d_f	118.119 mm	319.521 mm
Base Circle Diameter	d_b	123.781 mm	309.452 mm
Work Pitch Diameter	d_w	134.269 mm	335.671 mm
Facewidth	b	58.000 mm	58.000 mm
Facewidth Ratio	b_r	0.4320 ul	0.1728 ul
Addendum	a^*	1.0000 ul	1.0000 ul
Clearance	c^*	0.2500 ul	0.2500 ul
Root Fillet	r_f^*	0.3500 ul	0.3500 ul
Tooth Thickness	s	10.147 mm	10.147 mm
Tangential Tooth Thickness	s_t	11.717 mm	11.717 mm
Chordal Thickness	t_c	8.960 mm	8.960 mm
Chordal Addendum	a_c	4.829 mm	4.829 mm
Chordal Dimension	W	69.197 mm	149.153 mm
Chordal Dimension Teeth	z_w	4.000 ul	8.000 ul
Dimension Over (Between) Wires	M	149.243 mm	350.814 mm
Wire Diameter	d_M	11.000 mm	11.000 mm
Limit Deviation of Helix Angle	F_β	0.0150 mm	0.0150 mm
Limit Circumferential Run-out	F_r	0.0300 mm	0.0390 mm
Limit Deviation of Axial Pitch	f_{pt}	0.0110 mm	0.0120 mm
Limit Deviation of Basic Pitch	f_{pb}	0.0100 mm	0.0110 mm
Virtual Number of Teeth	z_v	26.673 ul	66.682 ul

Virtual Pitch Diameter	d_n	172.306 mm	430.765 mm
Virtual Outside Diameter	d_{an}	185.226 mm	443.685 mm
Virtual Base Circle Diameter	d_{bn}	161.915 mm	404.787 mm
Unit Correction without Tapering	x_z	0.4442 ul	-0.5168 ul
Unit Correction without Undercut	x_p	-0.5404 ul	-2.8804 ul
Unit Correction Allowed Undercut	x_d	-0.7103 ul	-3.0504 ul
Addendum Truncation	k	0.0000 ul	0.0000 ul
Unit Outside Tooth Thickness	s_a	0.6995 ul	0.7777 ul
Tip Pressure Angle	α_a	30.9955 deg	25.1950 deg



A.65. Sommerfeld number – Coefficient of Friction Graph



A.66. Graphs, Tables, and Parameter Calculations for RG Efficiency Calculation

A.66.1 Table for rolling frictional variable (G_{rr}) and sliding frictional variable (G_{sl}) [30]

Geometric and load dependent variables for rolling and sliding frictional moments – radial bearings		
Bearing type	Rolling frictional variable G _{rr}	Sliding frictional variable G _{sl}
Deep groove ball bearings	when $F_a = 0$ $G_{rr} = R_1 d_m^{1.96} F_r^{0.54}$	when $F_a = 0$ $G_{sl} = S_1 d_m^{-0.26} F_r^{5/3}$
	when $F_a > 0$ $G_{rr} = R_1 d_m^{1.96} \left(F_r + \frac{R_2}{\sin \alpha_F} F_a \right)^{0.54}$	when $F_a > 0$ $G_{sl} = S_1 d_m^{-0.145} \left(F_r^{1.5} + \frac{S_2 d_m^{1.5}}{\sin \alpha_F} F_a^4 \right)^{1/3}$
	$\alpha_F = 24,6 (F_a/C_0)^{0.28} [^\circ]$	
Angular contact ball bearings ¹⁾	$G_{rr} = R_1 d_m^{1.97} [F_r + F_q + R_2 F_a]^{0.54}$ $F_q = R_3 d_m^4 n^2$	$G_{sl} = S_1 d_m^{0.26} [(F_r + F_q)^{4/3} + S_2 F_a^{4/3}]$ $F_q = S_3 d_m^4 n^2$
Four-point contact ball bearings	$G_{rr} = R_1 d_m^{1.97} [F_r + F_q + R_2 F_a]^{0.54}$ $F_q = R_3 d_m^4 n^2$	$G_{sl} = S_1 d_m^{0.26} [(F_r + F_q)^{4/3} + S_2 F_a^{4/3}]$ $F_q = S_3 d_m^4 n^2$
Self-aligning ball bearings	$G_{rr} = R_1 d_m^2 [F_r + F_q + R_2 F_a]^{0.54}$ $F_q = R_3 d_m^{3.5} n^2$	$G_{sl} = S_1 d_m^{-0.12} [(F_r + F_q)^{4/3} + S_2 F_a^{4/3}]$ $F_q = S_3 d_m^{3.5} n^2$
Cylindrical roller bearings	$G_{rr} = R_1 d_m^{2.41} F_r^{0.31}$	$G_{sl} = S_1 d_m^{0.9} F_a + S_2 d_m F_r$
Tapered roller bearings ¹⁾	$G_{rr} = R_1 d_m^{2.38} (F_r + R_2 Y F_a)^{0.31}$	$G_{sl} = S_1 d_m^{0.82} (F_r + S_2 Y F_a)$
For the axial load factor Y for single row bearings → product tables		
Spherical roller bearings	$G_{rr,e} = R_1 d_m^{1.85} (F_r + R_2 F_a)^{0.54}$	$G_{sl,e} = S_1 d_m^{0.25} (F_r^4 + S_2 F_a^4)^{1/3}$
	$G_{rr,l} = R_3 d_m^{2.3} (F_r + R_4 F_a)^{0.31}$	$G_{sl,l} = S_3 d_m^{0.94} (F_r^3 + S_4 F_a^3)^{1/3}$
	when $G_{rr,e} < G_{rr,l}$ $G_{rr} = G_{rr,e}$	when $G_{sl,e} < G_{sl,l}$ $G_{sl} = G_{sl,e}$
	otherwise $G_{rr} = G_{rr,l}$	otherwise $G_{sl} = G_{sl,l}$
CARB toroidal roller bearings	when $F_r < (R_2^{1.85} d_m^{0.78} / R_1^{1.85})^{2.35}$ $G_{rr} = R_1 d_m^{1.97} F_r^{0.54}$	when $F_r < (S_2 d_m^{1.24} / S_1)^{1.5}$ $G_{sl} = S_1 d_m^{-0.19} F_r^{5/3}$
	otherwise $G_{rr} = R_2 d_m^{2.37} F_r^{0.31}$	otherwise $G_{sl} = S_2 d_m^{1.05} F_r$

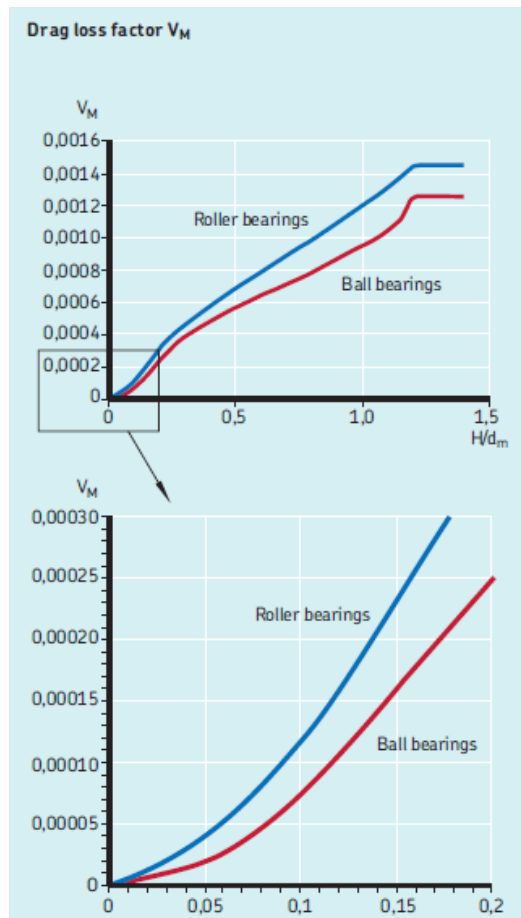
A.66.2 Table for geometric constants (K_z & K_L) [30]

Geometric constants K_z and K_L		
Bearing type	Geometric constants	
	K_z	K_L
Deep groove ball bearings – single and double row	3,1	–
Angular contact ball bearings – single row	4,4	–
– double row	3,1	–
– four-point contact	3,1	–
Self-aligning ball bearings	4,8	–
Cylindrical roller bearings – with a cage	5,1	0,65
– full complement	6,2	0,7
Tapered roller bearings	6	0,7
Spherical roller bearings	5,5	0,8
CARB toroidal roller bearings – with a cage	5,3	0,8
– full complement	6	0,75
Thrust ball bearings	3,8	–
Cylindrical roller thrust bearings	4,4	0,43
Spherical roller thrust bearings	5,6	0,58 ¹⁾

A.66.3 Table for seal counterface diameter (d_s), exponent (β), and constant (K_{S2}) [30]

Seal frictional moment: Exponent and constants						
Seal type Bearing type	Bearing outside diameter [mm]		Exponent and constants			Seal counterface diameter $d_s^{1)}$
	D over	incl.	β	K_{S1}	K_{S2}	
RSL seals						
Deep groove ball bearings	– 25	25 52	0 2,25	0 0,0018	0 0	d_2 d_2
RSH seals						
Deep groove ball bearings	–	52	2,25	0,028	2	d_2
RS1 seals						
Deep groove ball bearings	– 62 80 100	62 80 100	2,25 2,25 2,25 2,25	0,023 0,018 0,018 0,018	2 20 15 0	d_1, d_2 d_1, d_2 d_1, d_2 d_1, d_2
Angular contact ball bearings	30	120	2	0,014	10	d_1
Self-aligning ball bearings	30	125	2	0,014	10	d_2
LS seals						
Cylindrical roller bearings	42	360	2	0,032	50	E
CS, CS2 and CS5 seals						
Spherical roller bearings	62	300	2	0,057	50	d_2
CARB toroidal roller bearings	42	340	2	0,057	50	d_2

A.66.4 Graph for drag loss factor (V_M) [30]



A.66.5 Table of Sliding Frictional Moments (S_1 & S_2) [30]

Geometric constants for rolling and sliding frictional moments of deep groove ball bearings				
Bearing series	Geometric constants for rolling frictional moments		sliding frictional moments	
	R_1	R_2	S_1	S_2
2, 3	$4,4 \times 10^{-7}$	1,7	$2,00 \times 10^{-3}$	100
42, 43	$5,4 \times 10^{-7}$	0,96	$3,00 \times 10^{-3}$	40
60, 630	$4,1 \times 10^{-7}$	1,7	$3,73 \times 10^{-3}$	14,6
62, 622	$3,9 \times 10^{-7}$	1,7	$3,23 \times 10^{-3}$	36,5
63, 623	$3,7 \times 10^{-7}$	1,7	$2,84 \times 10^{-3}$	92,8
64	$3,6 \times 10^{-7}$	1,7	$2,43 \times 10^{-3}$	198
160, 161	$4,3 \times 10^{-7}$	1,7	$4,63 \times 10^{-3}$	4,25
617, 618, 628, 637, 638	$4,7 \times 10^{-7}$	1,7	$6,50 \times 10^{-3}$	0,78
619, 639	$4,3 \times 10^{-7}$	1,7	$4,75 \times 10^{-3}$	3,6

A.66.6 Table for Parameters & Results of Tooth Friction Losses

Parameter (Symbol, Unit)	1 st -Stage	2 nd -Stage	3 rd -Stage
Base helix angle (β_b , rad)	0,49	0,49	0,49
Transverse contact ratio, constant ($\epsilon_{\alpha t}$, constant)	1,35	1,35	1,35
Gear ratio (n, constant)	2,56	2,56	2,5
The number of teeth of the pinion (Z_1 , constant)	18	18	18

Gear geometry factor (k_0 , constant)	0,33	0,33	0,33
Gear loss factor (H_v , constant)	1,74	1,74	1,72
Efficiency parameter ($\Lambda(\mu)$, constant)	0,56	0,56	0,56
Transverse pressure angle (α_t , rad)	0,13	0,13	0,13
Input power (P_{in} , W)	25000	22297,18	19842,74
Average coefficient of friction (μ_{mZ} , constant)	0,16	0,16	0,16
Tooth friction (P_{VZP} , W)	2702,82	2454,44	2159,15

A.66.7 Table for Parameters & Results of Bearing Losses

Parameter (Symbol, Unit)	1 st -Bearing	2 nd -Bearing	3 rd -Bearing	4 th -Bearing
Rotational speed (N, rpm)	3000	1177	465	186
Actual operating viscosity of the oil (ν , mm ² /s)	32	32	32	32
Variable depending on the bearing type (G_{rr} , constant)	0,27	0,55	1,03	1,21
Inlet shear heating reduction factor (ϕ_{ish} , constant)	0,91	0,88	0,99	1
Kinematic replenishment/starvation reduction factor (ϕ_{rs} , constant)	0,89	0,96	0,98	0,99
Rolling frictional moment (M_{rr} , Nmm)	213,38	258,63	318,61	220,40
Variable depending on the bearing type (G_{sl})	816,97	1914,75	5408,2	5479,32
Sliding frictional coef. (μ_{sl} , constant)	0,02	0,02	0,03	0,06
Weight factor (ϕ_{bl} , constant)	0,013	0,035	0,11	0,367
Sliding frictional moment (M_{sl} , Nmm)	16,34	38,3	162,25	328,76
Constant depending the seal type (K_{s1} , constant)	0,0018	0,0018	0,028	0,028
Seal counter-face diameter (d_s , mm)	100	120	140	160
Constant depending the seal type (K_{s2} , constant)	0	0	2	2
Exponent depending on the seal type (β , constant)	2,25	2,25	2,25	2,25
Frictional moment of seals (M_{seal} , Nmm)	569,21	857,89	1889,76	2551,34
Drag loss factor (V_m , constant)	0,0008	0,0008	0,0008	0,0008
The bearing mean diameter (d_m , mm)	62,5	82,5	97,5	105
The rolling element related constant (K_{ball} , constant)	$45,07 * 10^{-12}$	$47,74 * 10^{-12}$	$44,54 * 10^{-12}$	$50,63 * 10^{-12}$
R_s (constant)	308768	502041	695079	840792
f_A (constant)	0,32	0,34	0,36	0,36
f_t (constant)	1	1	1	1
T (deg)	218,94	204,48	202,72	211,32
Frictional moment of drag losses (M_{drag} , Nmm)	1700,49	1614,42	1269,04	872,93
Total frictional moment (M, Nmm)	2499,42	2769,24	3639,66	3973,43

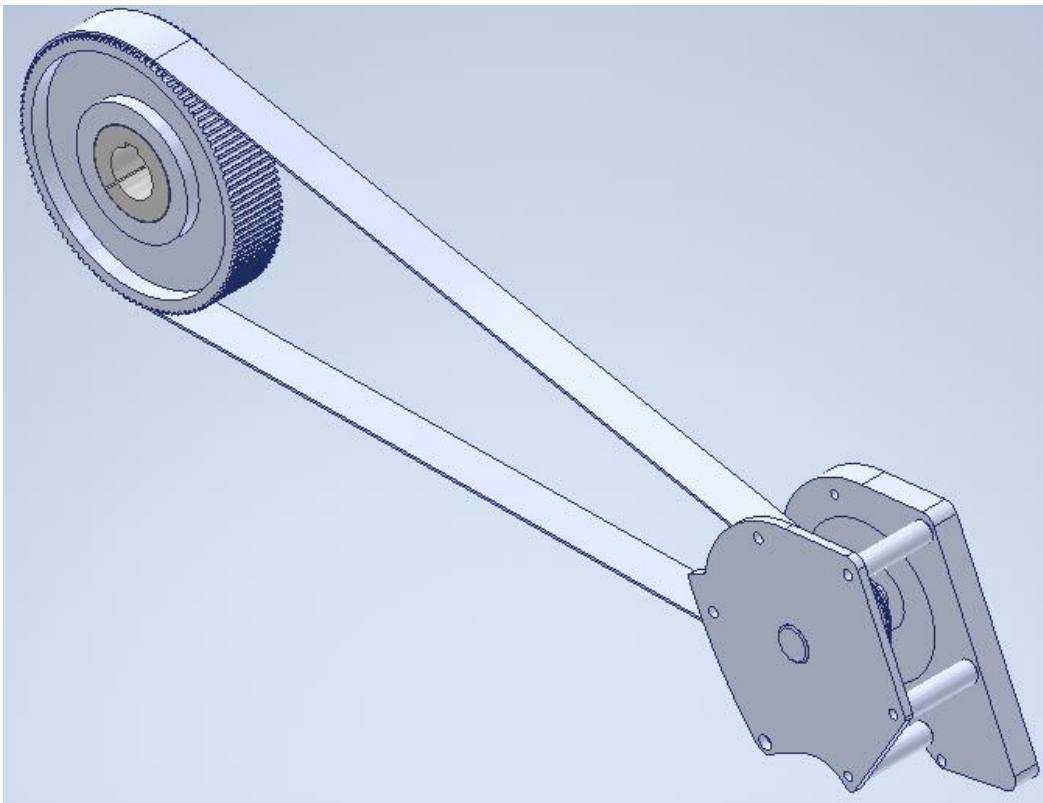
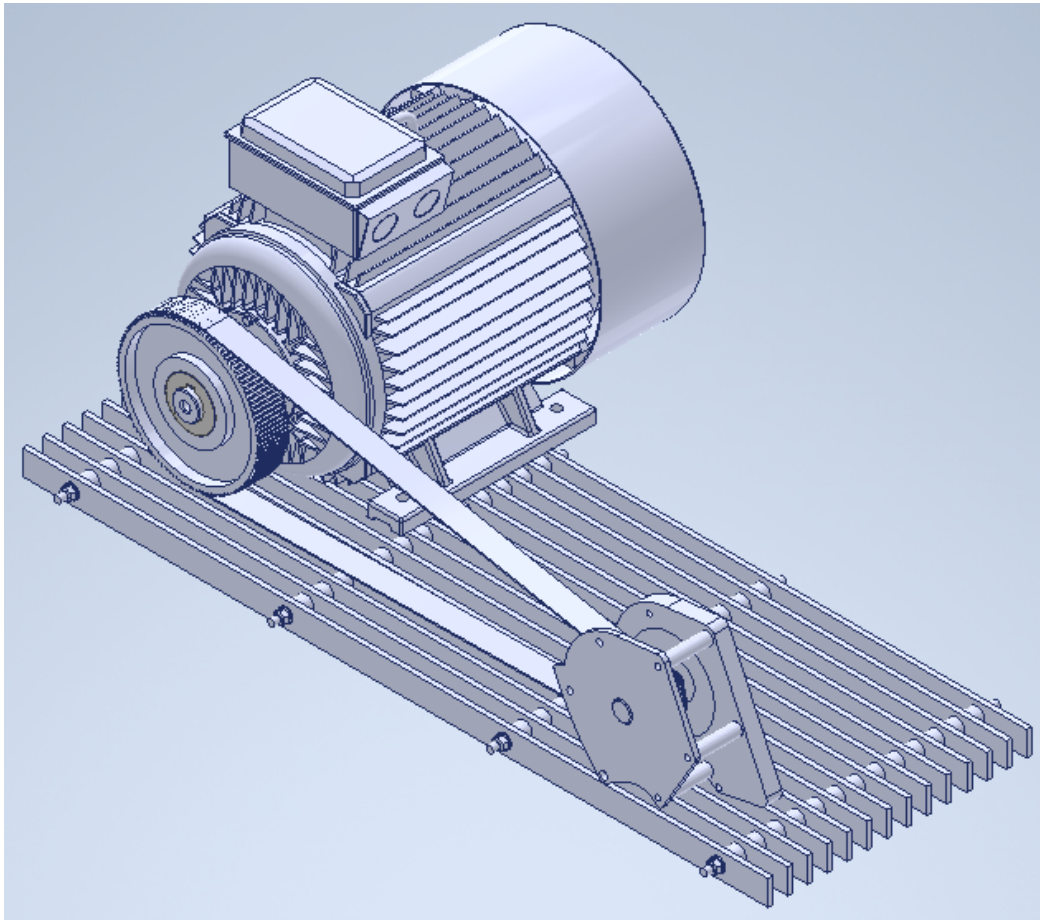
A.66.8 Table for Parameters & Results of Lubricant Losses

Constant depending the seal type (Ks1, constant)	0,0018	0,0018	0,028	0,028
Seal counter-face diameter (ds, mm)	100	120	140	160
Constant depending the seal type (Ks2, constant)	0	0	2	2
Exponent depending on the seal type (β , constant)	2,25	2,25	2,25	2,25
Frictional moment of seals (Mseal, Nmm)	569,21	857,89	1889,76	2551,34
Drag loss factor (Vm, constant)	0,0008	0,0008	0,0008	0,0008
The bearing mean diameter (dm, mm)	62,5	82,5	97,5	105
The rolling element related constant (Kball, constant)	$45,07 * 10^{-12}$	$47,74 * 10^{-12}$	$44,54 * 10^{-12}$	$50,63 * 10^{-12}$
Rs (constant)	308768	502041	695079	840792
fA (constant)	0,32	0,34	0,36	0,36
ft (constant)	1	1	1	1
T (deg)	218,94	204,48	202,72	211,32
Frictional moment of drag losses (Mdrag, Nmm)	1700,49	1614,42	1269,04	872,93

A.66.9 Table for Parameters & Results of Shaft Sealing Losses

Parameter (Symbol, Unit)	1 st -Shaft	2 nd -Shaft	3 rd -Shaft	4 th -Shaft
Rotational speed (N, rpm)	3000	1177	465	186
Shaft diameter (D, mm)	35	45	55	65
Shaft sealing power loss (Pj, W)	28,26	18,33	10,82	6,04

A.67. 3D-Model of the Clutch System



A.68. Photograph of the TB

